4.3-μm CO_2 LASER

by

© THOMAS ARVID ZNOTINS, B.Sc., M.Sc.

A Thesis

Submitted to the School of Graduate Studies

in Partial Fulfilment of the Requirements

for the Degree

Doctor of Philosophy

McMaster University

1981

4.3-μm CO_2 LASER

DOCTOR OF PHILOSOPHY (1981)
(Physics)

McMASTER UNIVERSITY
Hamilton, Ontario

TITLE: 4.3-μm CO_2 Laser

AUTHOR: Thomas Arvid Znotins, B.Sc. (University of Windsor)
M.Sc. (McMaster University)

SUPERVISORS: Professor B.K. Garside, Professor E.A. Ballik

NUMBER OF PAGES: xii, 143

ABSTRACT

The work described in this thesis concerns the investigation of the properties of a new type of CO_2 laser, one which operates in the wavelength region near 4.3 μm rather than in the 9-11-μm region where most CO_2 lasers operate. Lasing at 4.3 μm is achieved by using a 10-μm sequence CO_2 laser to optically pump CO_2 molecules which have been excited in an electrical discharge. The laser is based on existing CO_2 laser technology, and therefore it is potentially a very useful source of coherent radiation in a spectral region where there are presently few lasers suitable for widespread use.

Preliminary experiments are described which serve to identify the various physical processes involved in 4.3-μm laser action. Efficient optical pumping is demonstrated and peak output powers of 1 kW are observed. A theoretical model of the laser is developed. The model can accurately predict the observed 4.3-μm output and it is shown that the lifetime of the upper laser level is the critical factor in determining the gain dynamics of the laser system.

Two principal operating regimes are identified. The first is a high repetition rate Q-switched mode suitable for the production of high average power. A Q-switched 4.3-μm laser is constructed employing continuous discharge tubes and SF_6 is used to passively Q-switch the sequence oscillator. The average output power at 4.3 μm is 120 mW.

The other operating regime is a high power pulsed mode. This involves scaling the laser to higher operating pressures, which requires the use of high levels of sequence pumping power. To this end, a TEA sequence CO_2 laser having output energies of up to 6 J per pulse was developed, and design criteria for such lasers are presented. The scalability of the 4.3-μm laser, using the TEA sequence laser as the pump source, is discussed. The factors which limit the maximum output power attainable are identified, and guidelines for the construction of high power 4.3-μm lasers are presented.

ACKNOWLEDGEMENTS

I would sincerely like to thank my supervisors, Dr. B.K. Garside and Dr. E.A. Ballik, for their faith in me, and for all that each has given me, throughout the course of this work. To Dr. John Reid, I owe a great deal of appreciation, for the idea that started all of this, and for showing me how much fun it can be. My thanks also to the following three people: Mr. Bob Brimacombe, with whom I shared a most fruitful and enjoyable collaboration on the sequence work; Mrs. Kathy Noon, for her excellent typing, both of this thesis and of the many other writings over the years; and to Mr. Steve Tritchew, for his critical reading of this manuscript, and for other things. And to my parents, a very special thank-you for everything that they have given me, throughout my life.

There are many other people whom I have been fortunate to know and to whom I feel indebted, for their contributions towards the work described in this thesis, for their effort in helping me become a better scientist, and most important, for that which they have done towards helping me become a better person.

And lastly, but for certain, to Raymond and to Sylvia, a hope that I can share a special smile.

TABLE OF CONTENTS

LIST OF FIGURES

LIST OF TABLES

CHAPTER 1

INTRODUCTION

Laser action in CO_2 was first observed by Patel et al. [1,2] in 1964. It soon became apparent that CO_2 lasers possessed high efficiency and excellent output characteristics, in both the cw and pulsed modes of operation. At present, CO_2 lasers are among the most widely used of all laser types, in applications ranging from laser surgery to laser induced fusion research. Prior to 1976, laser oscillation in CO_2 was predominantly confined to two bands, the 10.4-μm band between the $00^0 1$ and $10^0 0$ levels and the 9.4-μm band between the $00^0 1$ and $02^0 0$ levels. (A more comprehensive discussion of CO_2 molecular structure, and an energy level diagram, are given in Sect. 2.2). These two bands contain over 80 laser lines in the 9-11-μm region. Over this range, cw output powers are typically $\geq$10 W and output energies from transversely-excited-atmospheric (TEA) lasers are typically several J per pulse. (These values are representative of commercial CO_2 lasers having 1-m discharge lengths). Because of their excellent output characteristics and relatively low cost, CO_2 lasers have been widely used in applications such as laser isotope separation and laser photochemistry [3], optical pumping of molecular gases to produce mid- and far-infrared lasing [4,5] and non-linear optics [6]. However, in many of these areas, application is limited to those situations where a coincidence exists between a CO_2 laser line and an absorption line

of the molecule under consideration. Consequently the utility of CO_2 lasers in such applications is restricted by the number of laser lines present in the regular CO_2 laser bands*.

In 1976, Reid and Siemsen [7,8] obtained cw laser oscillation on higher lying vibrational bands in CO_2. These transitions, of the type $(00^0n\text{-}10^0n\text{-}1)$, are denoted as sequence band transitions. Lasing on the sequence bands is very similar to lasing on the regular CO_2 laser bands and cw sequence output powers equal to ~50% of the regular output power from the same laser have been observed [8]. However, the sequence band frequencies are different from those of the regular CO_2 laser bands due to the anharmonicity of the CO_2 molecule [9]. Consequently the sequence bands represent a convenient means of improving the line-tunability of CO_2 lasers and thereby increasing the utility of CO_2 lasers in many frequency dependent applications. A more detailed description of sequence lasers is given in Sect. 2.7 and Chapter 6.

The importance of sequence lasers to the topics discussed in this thesis is their use in the production of 4.3-μm lasing in CO_2, which occurs on the $(10^01\text{-}10^00)$ and $(02^01\text{-}02^00)$ transitions. 4.3-μm lasing on the $(10^01\text{-}10^00)$ transitions has previously been observed using a variety of excitation schemes. These include bromine transfer [10,11], optical pumping with HF lasers [12], and pumping from optical parametric oscillators [13]†. Use of the sequence transitions offers an alternate

---

*High pressure ($\gtrsim$10 atm) pulsed CO_2 lasers offer continuous tunability but presently possess poor output characteristics.

†Hocker et al. [14] also observed stimulated emission at 4.3 μm from a Q-switched CO_2 laser, but the transitions involved were not clearly identified.

and much simpler method of producing 4.3-μm lasing. The main advantage is that CO_2 lasers are employed for both the optical pump and the 4.3-μm oscillator. Very briefly, the pumping scheme is as follows. A CO_2 laser discharge is pumped with an intense saturating pulse of 10.4-μm ($00^0 2$-$10^0 1$) sequence radiation. This results in a significant population being transferred to the $10^0 1$ level due to stimulated emission, and, under appropriate operating conditions, an inversion is created in the ($10^0 1$-$10^0 0$) band. In a suitable cavity lasing can then take place at 4.3 μm.

The principal advantage of this type of 4.3-μm laser is that it is based entirely on the readily available and well developed technology of regular CO_2 lasers. In addition, operation is in a wavelength region where few types of lasers are presently available. If sufficient output powers can be attained, then the 4.3-μm laser has great potential for use in many applications currently employing high power mid-infrared lasers.

The primary objective of this thesis is to develop an understanding of the various processes involved in 4.3-μm CO_2 lasing. The experimental results and the theoretical model discussed in the first half of the thesis are intended to elucidate the physics of the 4.3-μm CO_2 laser, and to assess properly the capabilities of the laser under various operating conditions. The latter part of the thesis is devoted to the two principal regimes in which the laser can operate i.e., a high repetition-rate Q-switched mode suitable for the production of high average power and a pulsed mode for producing high peak powers.

A brief outline of the contents of the individual chapters is given below.

Chapter 2 is intended to serve as a general introduction to many of the concepts referred to in the remainder of the thesis. A review is given of the spectroscopy of CO_2 and the important electronic and collisional processes involved in CO_2 lasing are discussed. This is followed by a brief description of the three principal types of CO_2 laser transitions: regular, sequence and 4.3-μm.

Chapter 3 describes the results of a series of preliminary investigations into the 4.3-μm lasing process. The aim of that Chapter is to identify the experimental conditions under which 4.3-μm lasing can be achieved, and to describe the basic mechanisms involved. The two different types of cavity configurations employed in this thesis are introduced: an inter-cavity scheme in which the sequence laser is separate from the 4.3-μm oscillator and an intra-cavity arrangement in which both the sequence and 4.3-μm laser are combined within a single optical cavity. The intra-cavity configuration is attractive in that it possesses a low pump power threshold, and consequently is well suited to the Q-switched operation described in Chapter 5.

A theoretical model of the laser was developed in order to obtain a more thorough understanding of the laser process. The model, described in Chapter 4, is composed of 9 differential rate-equations and is similar in structure to standard CO_2 laser models [15-17]. Good agreement is found between theory and experiment and consequently the model can be used to predict the time dependence of the level populations.

As a result, the specific mechanisms involved in the 4.3-μm lasing process can be clearly identified. It is shown that the rapid collisional de-excitation of the $10^0 1$ level [13] is the controlling factor in 4.3-μm laser gain dynamics. Based on the results of Chapters 3 and 4, three regimes in which the laser can be operated are identified: a low power pulsed mode, a high power pulsed mode and a Q-switched mode. The experiments described in Chapter 3 correspond to operation in the low power pulsed mode and Chapters 5-7 are concerned with the latter two operating regimes.

Q-switched operation of the laser is described in Chapter 5, where it is shown that Q-switching of the sequence pump laser will produce a corresponding train of 4.3-μm pulses. Consequently, high average output powers can be achieved. The Chapter provides a brief description of passive Q-switching of sequence lasers and the 4.3-μm laser output characteristics are presented. Average 4.3-μm output powers of 120 mW are observed, and the laser is scalable to higher power levels. It is demonstrated that 4.3-μm lasing can be achieved using only a single discharge tube, i.e., a cascade-type operation. Section 5.5 describes the use of the Q-switched 4.3-μm laser to probe a CO_2 laser discharge. Information on relaxation rates and level populations is obtained and the significance of these results to CO_2 laser dynamics is discussed.

The scaling of 4.3-μm lasers to higher pressures and correspondingly higher output powers is the subject of Chapters 6 and 7. This scalability requires the use of high power sequence pump lasers.

However, previous attempts to produce high power sequence lasers were unsuccessful [18-20]. The design criteria for high power TEA sequence lasers are given in Chapter 6, where it is shown that sequence output energies (powers) equal to ~50% of the regular output energy (power) can be obtained from the same laser system. Chapter 7 discusses the application of high power sequence lasers to produce high power 4.3-μm lasing. Two important considerations in the scaling of 4.3-μm lasers to higher operating pressure are discussed. These are the rapid collisional de-excitation of the $10^{0}1$ level and the interfering absorptions arising from overlapping absorption bands. Based on these results, guidelines for the construction of high power 4.3-μm lasers are presented. It is shown that 4.3-μm output intensities in the MW range and output energies in excess of 100 mJ per pulse can be obtained from a properly designed system.

Chapter 8 contains a summary of the important results of this thesis. Several potential applications for 4.3-μm lasers are discussed.

CHAPTER 2

THE CO_2 LASER SYSTEM

2.1 Introduction

This chapter gives a brief review of the lasing transitions in the CO_2 molecule which are of especial significance for the present thesis. It is intended to serve as an introduction to the detailed description of the 4.3-μm lasing described in the subsequent chapters and is a convenient place to introduce many of the concepts involved in the CO_2 laser system. A brief description of CO_2 molecular structure is given, with emphasis on the energy levels relevant to regular, sequence and 4.3-μm lasing. The principal processes involved in electronic excitation and collisional relaxation are described. This is followed by a discussion of the origins of gain on the regular and sequence transitions and the means by which sequence oscillation can be achieved. Finally, an introduction to the concept of 4.3-μm lasing in CO_2 is given.

2.2 CO_2 Molecular Structure

The CO_2 molecule is a linear symmetric molecule which has an axis of symmetry, C_∞, and a plane of symmetry perpendicular to the C_∞ axis. There are three normal modes of vibration, i.e., symmetric stretching ν_1, bending ν_2, and asymmetric stretching ν_3, associated with the species $\sum_g^+$, $\sum_u^+$ and π_u, respectively. The species π_u represents a doubly degenerate vibration as the bending vibration can

be considered to occur with equal frequency in two perpendicular planes. Each vibrational energy level is denoted by (n_1, n_2^{ℓ}, n_3), where n_1, n_2 and n_3 are the number of quanta excited in the ν_1, ν_2 and ν_3 modes, respectively, and ℓ denotes the angular momentum associated with the bending vibration. All vibrational levels relevant to CO_2 lasing occur in the ground electronic state. The fundamental frequencies of the three vibrational modes are $\nu_1 = 1337\ cm^{-1}$, $\nu_2 = 667\ cm^{-1}$ and $\nu_3 = 2349\ cm^{-1}$. Anharmonic corrections to the vibrational energy levels become important with increasing quantum number, resulting in frequency shifts between the various overtone bands and their fundamentals. In addition, the $10^0 0$ and $02^0 0$ levels (and similar levels higher in vibrational energy) are almost in resonance, which leads to a perturbation of their energies as first recognized by Fermi [21]. This perturbation leads to a strong mixing of the eigenfunctions. Consequently, the levels are more appropriately represented as $[10^0 0, 02^0 0]_I$ and $[10^0 0, 02^0 0]_{II}$. However, this nomenclature will not be adopted in this thesis. For convenience $10^0 0$ is used to represent the $[10^0 0, 02^0 0]_I$ level, $02^0 0$ for the $[10^0 0, 02^0 0]_{II}$ level, and similar notation for other higher lying Fermi levels. (e.g., $10^0 1$ for the $[10^0 1, 02^0 1]_I$ level.) Figure 2.1 shows the vibrational energy levels of CO_2 relevant to the three principal types of laser transitions considered in this thesis.

2.3 Rotational Structure and Laser Transitions

For every vibrational state there exists a set of rotational levels, with slightly different rotational constants for each vibrational level. The energies E of the rotational levels are given by [22]

Fig. 2.1

Simplified vibrational energy level diagram of CO_2 showing the energy levels relevant to regular, sequence and 4.3-μm lasing.

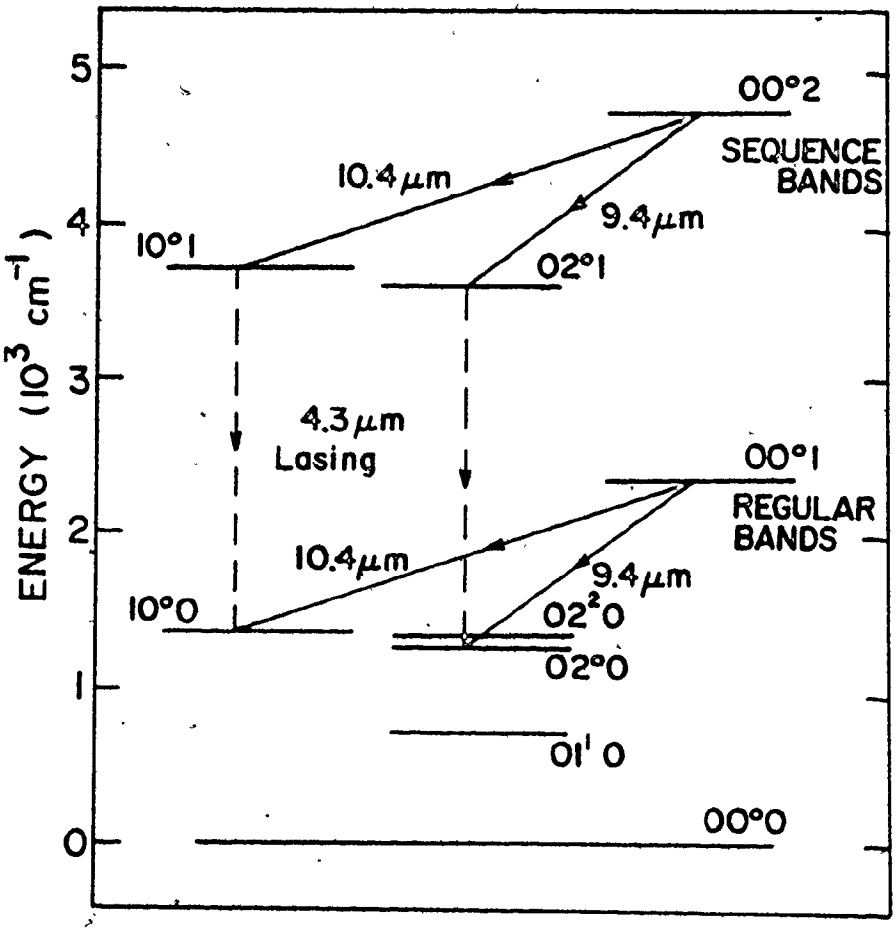
ENERGY (10^3 cm^{-1})
5
4
3
2
1
0
00°2
SEQUENCE BANDS
10.4μm
9.4μm
10°1
02°1
4.3μm Lasing
00°1
REGULAR BANDS
10.4μm
9.4μm
10°0
02²0
02°0
01¹0
00°0

$$E(J) = B_v J(J+1) - D_v J^2(J+1)^2 + \ldots \qquad (2.1)$$

where J is the rotational quantum number and B_v is the rotational constant. The $D_v J^2(J+1)^2$ and higher-order terms are present in Eq. (2.1) because of the non-rigidity of the CO_2 molecule and other effects which are small compared with the first term. The population density n_J of the various rotational levels can be described by a Boltzmann distribution [22]

$$n_J = N\left(\frac{hcB}{kT}\right) g(J) \exp\left(-\frac{E(J)}{kT}\right), \qquad (2.2)$$

where g(J) is the statistical weight, N is the total population density of the vibrational level, and the other constants have their standard meaning. In the case of $C^{12}O_2^{16}$, the spins of the identical oxygen nuclei are zero. As a result, the anti-symmetric rotational levels are missing entirely [22, 23]. Hence, in the $00^0 1$ and $10^0 1$ levels the even rotational levels are absent, whereas for the $00^0 2$ and $10^0 0$ levels the odd rotational levels are absent. For the allowed levels, g(J) = 2J + 1 [22,23].

The selection rules for the vibration-rotation transitions in the IR spectrum are [22]

$$\Delta \ell = 0, \pm 1, \; \Sigma^+ \leftrightarrow \Sigma^-, \; g \not\leftrightarrow g, \; u \not\leftrightarrow u$$

$$\Delta J = 0, \pm 1, \; (J \neq 0) \not\leftrightarrow (J = 0), \; + \not\leftrightarrow -, \; s \not\leftrightarrow a$$

where s and a designate the symmetric and anti-symmetric rotational wavefunction and the symbols $\leftrightarrow$ and $\not\leftrightarrow$ represent "allowed" and "not

allowed" transitions, respectively. Specifically, two of the strongest CO_2 laser bands, the 10.4-μm and 9.4-μm regular bands, arise from the vibrational-rotational transitions of the $\sum_u^+ - \sum_g^+$ vibrational bands, $(00^0 1 \rightarrow 10^0 0)$ and $(00^0 1 \rightarrow 02^0 0)$, respectively. Laser oscillation has been obtained from both the P-branch ($\Delta J = -1$) and R-branch ($\Delta J = +1$) of each band. The Q-branch ($\Delta J = 0$) is not allowed because these transitions cannot occur between two $\sum$ states for which $\ell = 0$. Figure 2.2 is a detailed transition diagram for laser oscillations in both the P and R branches of the 10.4-μm and 9.4-μm regular bands. Note that all the regular transitions are denoted by even quantum numbers. As explained above, the situation reverses for the sequence bands where the transitions are represented by only odd quantum numbers. The 4.3-μm transitions possess the same lower levels as the regular bands and therefore are denoted by even rotational numbers.

In addition to strong transitions such as those in the regular and sequence bands, several weaker transitions with wavelengths in the 9 to 11-μm region have been observed in CO_2 [24,25]. The most important of these is the (01'1-11'0) hot band centered at approximately 11 μm. These transitions are equivalent to the regular 10.4-μm band, except for the addition of a bending mode quantum (ν_2) to each laser level. However, the hot band should not be confused with the sequence bands which, although analogous in nature, are considerably stronger. The additional quanta of the sequence bands are in the ν_3 mode with the result that considerable gain exists on the sequence transitions relative to that present on any of the hot band transitions. The sequence bands are

Fig. 2.2

Detailed transition diagram of laser oscillation in the 10.4-μm and 9.4-μm regular laser bands of CO_2.

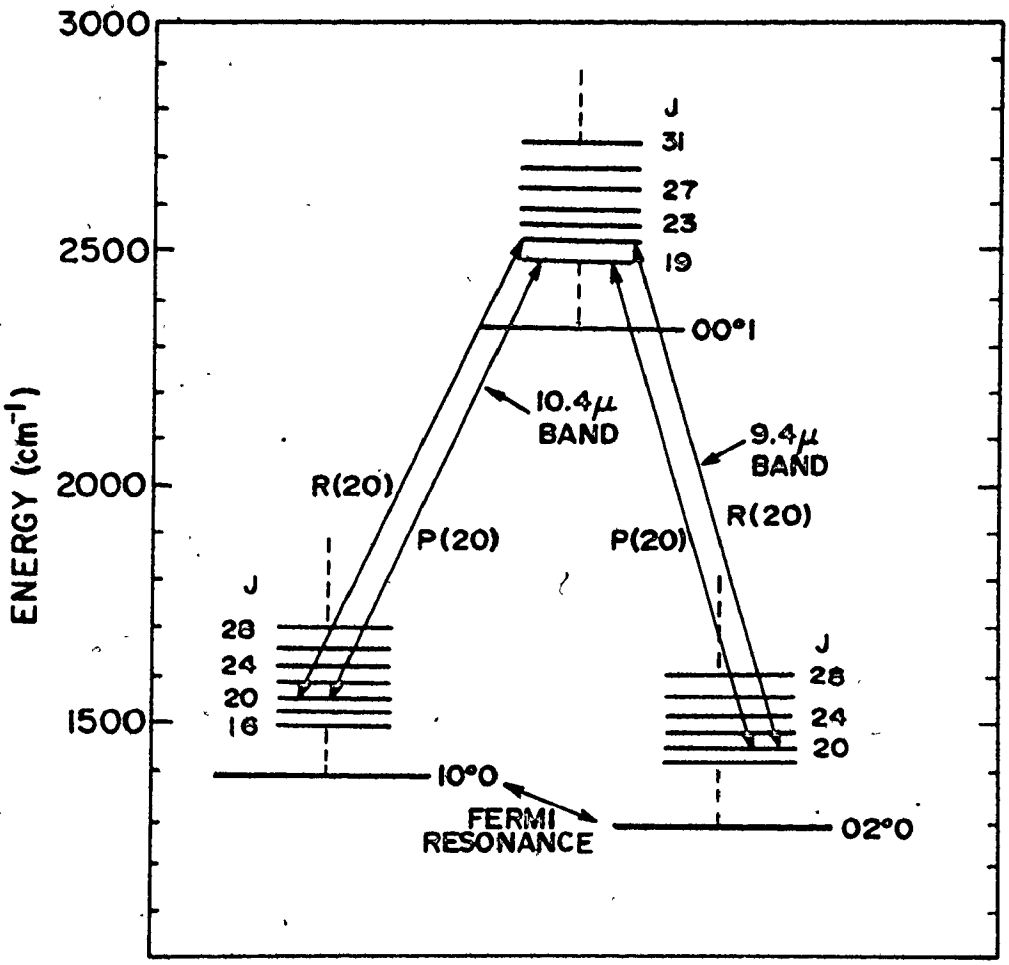
3000
2500
2000
1500
ENERGY (cm⁻¹)
J
31
27
23
19
00°1
10.4μ BAND
9.4μ BAND
R(20)
P(20)
P(20)
R(20)
J
28
24
20
16
J
28
24
20
10°0
FERMI RESONANCE
02°0

described in greater detail in Sect. 2.7. The primary importance of the various hot bands is their contribution to gain and absorption at the regular and sequence frequencies. This topic is discussed in Chapter 6.

2.4 Electronic Excitation Processes

The different types of laser oscillation reported in this thesis are all a result of the excitation of CO_2 molecules in an electrical discharge (either pulsed or continuous) together with the subsequent collisional relaxation processes. This section presents a brief summary of the electronic excitation processes; the collisional relaxation processes are discussed in the next section.

In a discharge, energy is transferred to the vibrational modes of CO_2 by inelastic collisions with electrons, and by resonant energy transfer from vibrationally excited N_2 [26]. To determine the distribution of the input power transferred to the various vibrational modes requires a knowledge of electron density, electron energy distribution (including mean electron energy), and cross-sections for electronic excitation of N_2, CO_2 and He. Because some of these parameters are difficult to measure experimentally, calculated values are heavily relied upon for quantitative predictions of laser performance. Employing numerical solutions of the Boltzmann equation, Nighan [27] and Lowke et al. [28] have calculated the electron distribution function for a variety of discharge conditions. Using the calculated distribution function and measured cross-sections, the fractional

power transferred to electronic excitation, ionization and vibrational excitation of CO_2 and N_2 was determined as a function of E/N, the ratio of the applied electric field to total particle density. Typical values for E/N in pulsed CO_2 lasers are in the range 2-8 x 10^{-16} V-cm^2 [29, 30], resulting in average electron energies ($\bar{u}_e$) of 0.5-3.0 eV. Nigham [27] has calculated the fraction of electrical power transferred to the individual vibrational and electronic processes by employing an equation balancing energy deposition from the electric field against the net rate of vibrational and electronic excitation. These calculations were later extended to a wider range of experimental conditions by Judd [30]. The results are given in terms of effective excitation rates of the various vibrational levels as a function of $\bar{u}_e$, or equivalently, E/N. These excitation rates were used in the laser modeling calculations described in Chapter 6. However, one important feature should be mentioned here. In a CO_2 laser discharge, considerable energy is transferred to the combined bending and symmetric stretching modes and hence to the lower laser levels of the regular, sequence and 4.3-μm transitions. In a pulsed laser, this energy must decay by collisional relaxation in order for peak inversion, and hence peak gain, to be realized.

A second and very efficient mechanism for the excitation of the ν_3 mode in CO_2 involves the transfer of energy from vibrationally excited N_2 to ground state CO_2 molecules by way of the process

$$CO_2(00^0 0) + N_2(v=1) \leftrightarrow CO_2(00^0 1) + N_2(v=0) - 18\ cm^{-1} \qquad (2\text{-}3)$$

The rate for this process is relatively fast (1.9 x 10^4 s^{-1} $Torr^{-1}$ [31])

with respect to the various relaxation processes and N_2 has large cross-sections for vibrational excitation by inelastic collisions with electrons, particularly in the range $\bar{u}_e$ = 2-3 eV [32,33]. Consequently, N_2 is a common constituent of most CO_2 lasers and is especially important in systems such as sequence lasers or 4.3-μm lasers where a high degree of vibrational excitation is desirable.

2.5 Collisional Relaxation Processes

As described above, electrical excitation results in the population of many low-lying vibrational levels in CO_2. The excited molecules must eventually relax to the ground state and it is the relevant relaxation processes which are considered in this section.

In a comprehensive study, Statz et al. [34] have calculated the Einstein A coefficients in CO_2 for all relevant CO_2 transitions. All the spontaneous emission rates are very slow (10^0-10^3 seconds) and hence, in the absence of lasing, collisionally-induced vibrational relaxation dominates the energy relaxation processes in CO_2 lasers*. Due to the great interest in CO_2 lasers over the past decade, a considerable amount of work, both experimental and theoretical, has been carried out to determine these rates accurately. Described below are the collisional processes relevant to the work described in this thesis, and their associated rate constants. The relaxation rates are temperature

---

*At low pressures, diffusion to the walls can also play an important role in the deactivation of the excited CO_2 molecules. However, this effect can be ignored for the range of operating conditions considered in this thesis.

dependent, however, since the temperature rise in TE lasers is generally less than $50^{\circ}C$ the temperature dependence can be ignored.

The fastest vibrational relaxation process which must be considered is the redistribution of energy within the asymmetric stretching mode via processes of the type

$$2CO_2(00^{\circ}1) \leftrightarrow CO_2(00^{\circ}2) + CO_2(00^{\circ}0) + 25\ cm^{-1} \qquad (2.4)$$

Although the rate for this specific process has not been measured directly, measurements of related processes yield a value of 5.3×10^6 s^{-1} $Torr^{-1}$ for the ν_3 mode equilibration rate [35]. In a recent theoretical study, Pack [36] has calculated a rate of 1.8×10^7 s^{-1} $Torr^{-1}$ for the process described by Eq. (2.4). However, the calculations described in the subsequent chapters were found to be only weakly dependent on which of these values was used, a result which is not unexpected considering the very rapid nature of this relaxation process.

Although the equilibration rate within the ν_3 mode is very fast, the relaxation rate of the mode itself is quite slow. This relaxation is generally considered to proceed via the ν_1 and ν_2 modes and the rates are well known for all typical laser gases. CO_2 has a rate constant of 350 s^{-1} $Torr^{-1}$, N_2 a rate constant of 106 s^{-1} $Torr^{-1}$ and He a rate constant of 85 s^{-1} $Torr^{-1}$ [31].

Although it is generally assumed that the bending and symmetric stretching modes in CO_2 are tightly coupled, some controversy persists about the exact mechanism involved. In particular, the rates reported in the literature for the coupling between the $10^{\circ}0$ level (i.e., the

lower level of the 10.4-μm and 4.3-μm laser bands) and the other levels in the bending-stretching mode range over three orders of magnitude, from 10^3-10^6 s^{-1} $Torr^{-1}$ [15, 37-44]. Garside et al. [17] have indicated that the fastest rate reported, 1.3×10^6 s^{-1} $Torr^{-1}$ [15], was in error due to the neglect of rotational relaxation effects and that the slowest rates reported, those of Refs. [37] and [38], appear inappropriate for conditions generally found in a CO_2 laser. The rate constant measured by Garside et al. for the relaxation of the $10^0$0 level was $\sim 3 \times 10^5$ s^{-1} $Torr^{-1}$. This is in good agreement with the values of Stark who determined the rate constants: $k_{CO_2\text{-}CO_2} = 1.42 \times 10^5$ s^{-1} $Torr^{-1}$, $k_{CO_2\text{-}N_2} = 6.5 \times 10^4$ s^{-1} $Torr^{-1}$ and $k_{CO_2\text{-}He} = 7.7 \times 10^3$ s^{-1} $Torr^{-1}$ [41]. Jacobs et al. [42] measured a similar value for the CO_2 rate constant but found that He and N_2 were nearly as effective as CO_2 in relaxing the $10^0$0 level, which is in sharp contrast to the findings of Stark. However, it appears that rotational effects may also have been involved in the measurements of Jacobs et al. Consequently the values of Stark were used for the calculations reported in this thesis.

Due to the strong coupling between the symmetric stretching mode and the bending mode, the relaxation of the lower laser level, $10^0$0, is ultimately controlled by the energy decay in the bending mode, in particular, the vibration-to-translation (V-T) relaxation of the 01'0 level. Numerous measurements of this relaxation rate have been made, as summarized in the review article by Taylor and Bitterman [45]. The rate constants reported for CO_2-CO_2 and CO_2-He collisions are 200 s^{-1} $Torr^{-1}$ and 3.5×10^3 s^{-1} $Torr^{-1}$ respectively. However the rate constants reported there for CO_2-N_2 collisions corresponded to a wide range of

values. Recent measurements [46] are in good agreement with a value of 100 s^{-1} $Torr^{-1}$.

The other V-V process important in the dynamics of both sequence lasers and 4.3-μm lasers is the collisional relaxation rate of the $10^0 1$ level. Finzi and Moore [13] have measured the rate constant for the process

$$CO_2(00^0 0) + CO_2(10^0 1) \leftrightarrow CO_2(10^0 0) + CO_2(00^0 1) - 22\ cm^{-1} \qquad (2.5)$$

and found it to be 4.2×10^6 s^{-1} $Torr^{-1}$. This is in good agreement with the theoretical calculations of Pack [36] which give a value of 4.36×10^6 s^{-1} $Torr^{-1}$. Furthermore, Finzi and Moore conclude that other possible relaxation mechanisms such as

$$CO_2(10^0 1) + CO_2(00^0 0) \leftrightarrow CO_2(02^0 1) + CO_2(00^0 0) + 102\ cm^{-1} \qquad (2.6)$$

proceed slowly relative to the process represented by Eq. (2.5). The $10^0 1$ lifetime is found to be an important factor in the gain dynamics of the 4.3-μm laser, as is discussed in greater detail in Chapter 4.

It should be noted that the rotational sublevels within a vibrational level exchange energy on a very fast time scale, such that almost every collision is effective at maintaining thermal equilibrium amongst the rotational levels. The rate constants are $k_{CO_2\text{-}CO_2} = 1.1 \times 10^7$ s^{-1} $Torr^{-1}$, $k_{CO_2\text{-}N_2} = 1.0 \times 10^7$ s^{-1} $Torr^{-1}$ and $k_{CO_2\text{-}He} = 0.7 \times 10^7$ s^{-1} $Torr^{-1}$ [47]. However, it has been shown [48] that rotational equilibrium can be significantly disturbed by the effect of intense stimulated emission. Consequently, the effects of rotational relaxation were considered in all modelling calculations described in this thesis.

The various collisional relaxation processes are summarized in Fig. 2.3. The times shown there correspond to a 91.5%He:7%N_2:1.5%CO_2 mixture at a total pressure of 30 Torr, which is a typical 4.3-μm CO_2 laser gas mixture.

It is convenient to introduce here another important concept of CO_2 lasers, that of mode temperatures. Due to the rapid intra-mode relaxation rates described above, the population of the various levels in a vibrational mode follows a Boltzmann distribution characterized by a single temperature T_{ν_i} which is appropriate to that particular mode. This concept was first proposed by Gordietz et al. [49] in 1968 and has been recently verified experimentally [50]. Therefore the population of a specific vibrational level can be obtained by applying a simple analytical expression. For example, the population density of the $10^0 1$ level, N_{101}, is given by

$$N_{101} = N_{CO_2} \exp(-E_{100}/kT_1) \exp(-E_{001}/kT_3) Q_v^{-1}, \qquad (2.7)$$

where E_{100} and E_{001} are the energies of the $10^0 0$ and $00^0 1$ levels, respectively, T_1 and T_3 are the temperatures of the ν_1 and ν_3 modes, respectively, Q_V is the vibrational partition function and N_{CO_2} is the number density of CO_2 molecules. The temperatures of the three vibrational modes T_1, T_2 and T_3, the rotational temperature T_R, and the translational temperature T are the necessary parameters for the five temperature model of CO_2 gain dynamics which is used throughout the course of this

Fig. 2.3

Summary of the collisional relaxation rates relevant to 4.3-μm lasing for a 91.5%He:7%N_2:1.5%CO_2 mixture at 30 Torr total pressure. The solid lines indicate collisional processes whereas the dashed lines represent radiative transitions.

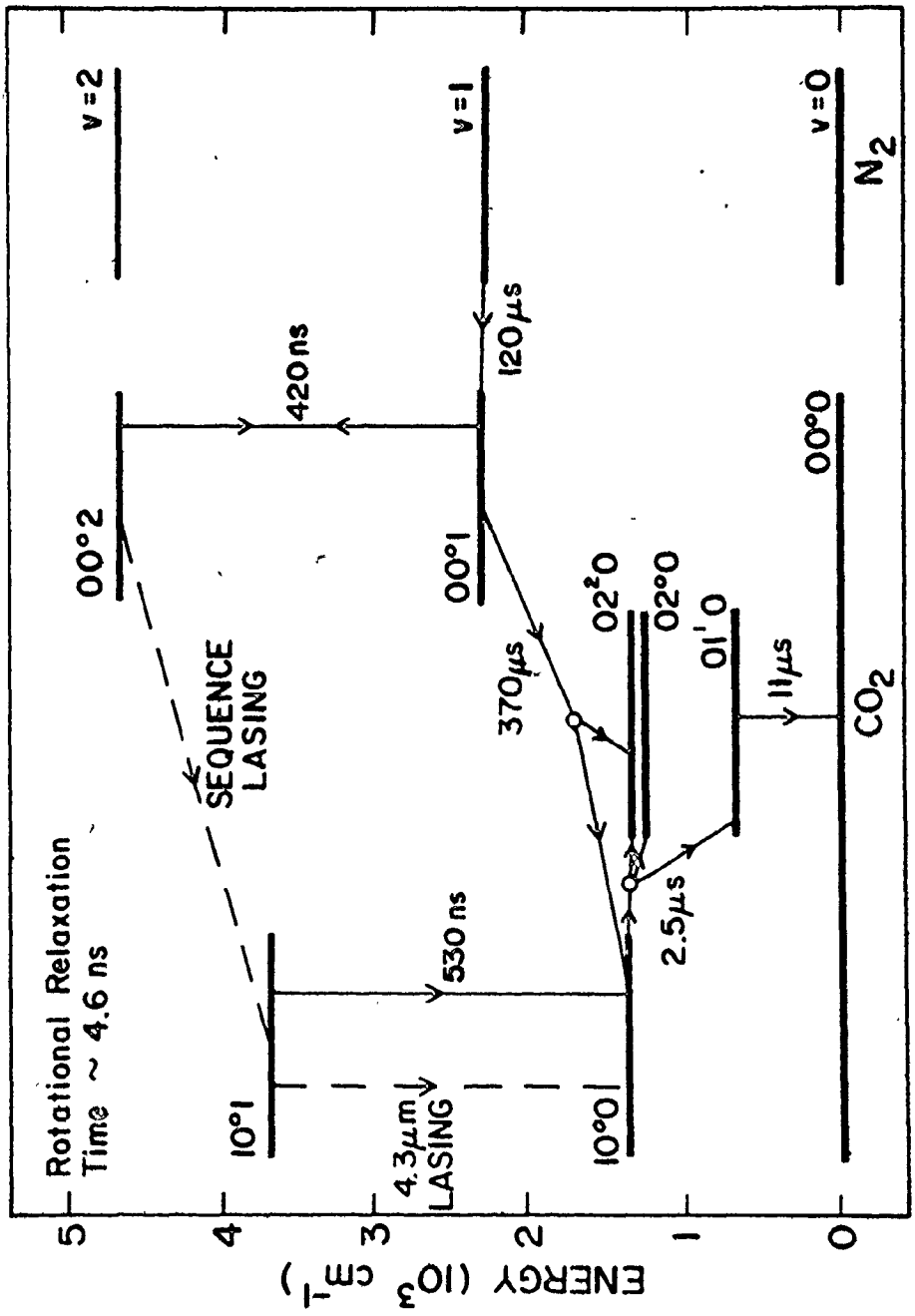
ENERGY (10^3 cm^{-1})
0
1
2
3
4
5
v=2
v=1
v=0
N_2
CO_2
00°2
00°1
00°0
10°1
10°0
02²0
02°0
01¹0
420 ns
120 μs
530 ns
370 μs
11 μs
2.5 μs
SEQUENCE LASING
4.3 μm LASING
Rotational Relaxation
Time ~ 4.6 ns

thesis.*

2.6 Gain in CO_2 Lasers: The Regular Laser Transitions

Gain on the regular laser transitions in CO_2 arises as a result of the combined effects of the electron excitation and collisional relaxation processes detailed above. It is worthwhile at this stage to outline the generally accepted model for regular CO_2 laser dynamics since both sequence and 4.3-μm lasing are dependent on the same processes.

Consider a CO_2 laser gas mixture (CO_2, N_2, He) which is excited in a pulsed electrical discharge. As a result of direct excitation by electrons and collisional transfer from excited N_2 molecules, all the low-lying vibrational levels in CO_2 are populated. The populations in the tightly coupled bending-stretching (BS) mode decay away rapidly relative to the population in the ν_3 asymmetric stretching mode. Consequently, after a period of time (~several V-T relaxation times), the levels in the BS modes are effectively empty, whereas a substantial population still exists in the ν_3 mode. In particular, an inversion has been created between the $00^0 1$ level and the $10^0 0$ and $02^0 0$ levels, which corresponds to gain on the 10.4-μm and 9.4-μm regular laser bands, respectively. The rise and fall-times of the gain reflect the lifetimes of the lower and upper laser levels [51], respectively, while the

---

*Due to the fast rotation-to-translation relaxation rates, it is generally assumed that $T_R = T$. Similarly, $T_1 = T_2$ due to rapid coupling between the ν_1 and ν_2 modes.

peak gain can be obtained from the values of the mode temperatures at that time. For a typical pulsed discharge, $T_1 = T_2 = 400$ K and $T_3 = 2000$ K at the peak of the gain. This corresponds to a fractional population of 12% in the $00^0 1$ level and $\sim 0.5\%$ in the $10^0 0$ level. Substituting these values into the standard expression for small-signal gain in CO_2 (see Appendix A) gives a value of $\sim$3%/cm for the peak small-signal gain.

2.7 Sequence CO_2 Lasers

It is apparent from the previous section that gain will exist on other transitions in addition to the regular laser bands. In particular, there will be appreciable gain on those transitions having upper levels belonging to the ν_3 mode, i.e., transitions of the type $(00^0 n \rightarrow 10^0\ n-1)$.* Although this fact was recognized in earlier studies of CO_2 lasers [52] it was not until 1976 that Reid and Siemsen [7] constructed a laser operating on one of these sequence transitions, specifically the $00^0 2$-$10^0 1$ and $00^0 2$-$02^0 1$ sequence bands. The difficulty in achieving sequence oscillation arises because the population of the $00^0 2$ level, N_{002}, is less than that of the $00^0 1$ level, N_{001}, which lies lower in vibrational energy. (For $T_3 = 2000$ K, $N_{001}/N_{CO_2} \approx 0.12$ while $N_{002}/N_{CO_2} \approx 0.02$, where N_{CO_2} is the total number of CO_2 molecules.) Therefore, the gain on the sequence transitions is also lower ($\sim$40% of the regular gain for T_3=2000 K). Consequently CO_2 lasers usually operate solely on the

*Using tunable diode lasers, gain has been experimentally observed on transitions up to $n = 4$ (i.e., $00^0 4$-$10^0 3$) [53].

regular transitions.

The sequence bands are very similar to the regular laser bands. However, the small anharmonicity of the CO_2 molecule results in sequence band frequencies which are slightly different from those of the regular bands. In general, the differences are too small to permit sequence oscillation from a conventional grating-tuned cavity. Reid and Siemsen originally [7] employed an optical cavity with particularly good wavelength discrimination and optimized discharge conditions to favour sequence gain relative to regular gain and were thereby able to obtain sequence lasing. A more efficient means of achieving sequence oscillation is to use the absorption properties of hot CO_2. This technique is based on the fact that the lower levels of the regular CO_2 laser bands lie only $\sim$1300 cm^{-1} above the ground state, whereas the lower levels of the sequence bands have energies of $\sim$3700 cm^{-1}. Consequently, the regular laser lines experience considerable absorption in hot ($\sim$600 K) CO_2 while the absorption on the sequence lines remains small. Therefore, by placing a hot CO_2 cell inside the optical cavity of a conventional CO_2 laser, the regular lines can be suppressed and lasing will only take place on the sequence lines.

Using an in-cavity hot cell, Reid and Siemsen [8] were able to achieve cw laser oscillation on more than 80 lines in the $00^{\circ}2$ 9.4-μm and 10.4-μm sequence bands, with output powers up to 50% of the power levels available on the regular lines from the same laser. Reference [8] provides a comprehensive discussion of sequence lasing in cw CO_2 lasers. A detailed description of sequence lasing in TEA CO_2 lasers

is given in Chapter 6, where it is shown that the hot cell technique is also an efficient means of achieving high power sequence band oscillation from a conventional TEA CO_2 laser. The use of sequence lasers to produce 4.3-μm lasing in CO_2 is introduced in the next section.

2.8 4.3-μm CO_2 Lasers

As described in the introduction, lasing has previously been reported on 4.3-μm transitions in CO_2 using a variety of excitation schemes. These included bromine-transfer lasers [11], optical pumping with HF lasers [12], and pumping by optical parametric oscillators [13]. However, by employing the sequence laser transitions, 4.3-μm oscillation in CO_2 can be achieved using CO_2 lasers both as the optical pump and the 4.3-μm oscillator. The means by which this can be accomplished is described in this section.

Consider a CO_2 laser gas mixture which is excited in a pulsed electrical discharge. As in regular CO_2 lasers, this results in significant population of the low-lying vibrational levels in the CO_2 molecules. The ν_1 and ν_2 mode populations decay away rapidly producing gain on both the regular and sequence band transitions. At this point the gas mixture is pumped with an intense saturating pulse of sequence radiation. From Fig. 2.1, it can be seen that this results in a significant population being transferred from the 00^02 level to the 10^01 level. The 10^00 level is empty however and, under proper operating conditions, an inversion is created in the $(10^01\text{-}10^00)$ band. In a suitable cavity, lasing can then take place, at a wavelength near 4.3-μm.

The experimental conditions under which 4.3-μm lasing can occur are described in the next Chapter. A more detailed explanation of the gain dynamics is given in Chapter 4 where a theoretical model of the laser is presented. In Chapters 5 and 7 a description is given of how optimum 4.3-μm output can be obtained using both low pressure continuous discharges and high pressure pulsed discharges.

2.9 Summary

This Chapter has presented a review of CO_2 molecular dynamics and specifically how this pertains to three different types of CO_2 lasers: regular, sequence and 4.3-μm. It is intended that the information described here serve as a background for the discussion of the following chapters which are concerned primarily with the 4.3-μm CO_2 laser.

CHAPTER 3

EXPERIMENTAL APPARATUS AND PRELIMINARY RESULTS

3.1 Introduction

In this Chapter, a detailed description is given of a series of initial experiments on the 4.3-μm laser. Important concepts of the laser operation are introduced and the simplicity and efficiency of the sequence bands as a means of producing 4.3-μm lasing in CO_2 is demonstrated. The majority of the experiments are performed using low pressure TE CO_2 lasers and employ a two-cavity arrangement which is described in Section 3.2. This cavity arrangement is conceptually simple and is well suited for comparing experimental results with the theoretical predictions described in the following Chapter. However, it is not the most efficient design available. An intra-cavity configuration whereby the sequence pumping laser and 4.3-μm oscillator are combined in a single optical cavity is described in Sect. 3.4. It is shown that this configuration leads to a substantial improvement in the performance of the laser.

3.2 Experimental Apparatus

The initial experiments involving the 4.3-μm laser were performed using a two-cavity configuration which is commonly employed in many optically pumped lasers. In this arrangement the sequence pump pulses are obtained from a separate cavity and directed into the 4.3-μm

oscillator following the description given in Sect. 2.8. This section outlines the main features of the experimental apparatus employed.

Figure 3.1 is a schematic diagram of the two-cavity configuration. Helical pin CO_2 discharges were used for both the sequence laser and 4.3-μm laser, as these discharges operate reliably over the wide range of gas mixtures and pressures used in these experiments.* Furthermore, the helical array results in a gain medium with cylindrical symmetry which is useful for producing outputs in the fundamental TEM_{00} mode [54]. A schematic diagram of the discharge circuit used is shown in Fig. 3.2. A pulse generator provides a short duration, low voltage pulse to the trigger module. A pulse from the trigger module then causes the spark gap to break down, allowing the capacitor to discharge through the gain medium. The time delay between the firing of the 4.3-μm laser discharge and the sequence laser discharge is varied by adjusting the delay between the low voltage trigger pulses.

The discharge module in the sequence laser had an active length of 1 m and operated on a 80%He:10%N_2:10%CO_2 gas mixture at 100 Torr total pressure. Lasing on the sequence transitions was ensured by using an in-cavity hot CO_2 cell to suppress the regular CO_2 transitions, as described in Sect. 2.7. The hot cell, shown in Fig. 3.3, is of a very simple design, comprising of a 5 cm ID steel tube sealed at both ends with NaCl Brewster-angle windows. A single winding of Nichrome wire (~5 cm pitch) was used to heat the cell. The total length was

---

*The high power TEA sequence laser used in later experiments is described in Chapter 6.

Fig. 3.1

Schematic diagram of the two-cavity configuration used to produce 4.3-μm lasing.

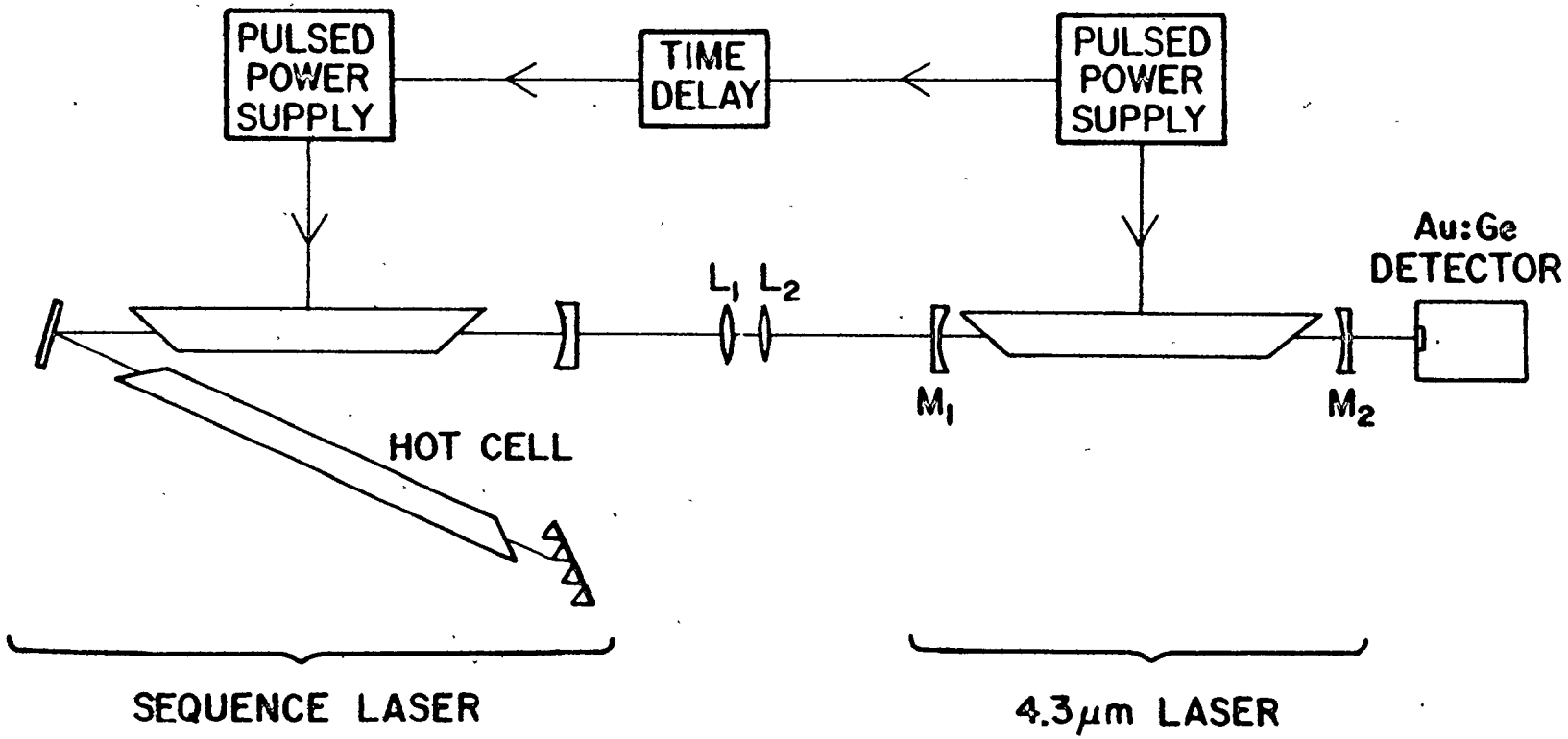
PULSED POWER SUPPLY
TIME DELAY
PULSED POWER SUPPLY
Au:Ge DETECTOR
L1 L2
M1
M2
HOT CELL
SEQUENCE LASER
4.3μm LASER

Fig. 3.2

Schematic diagram of the discharge circuit used for both the sequence laser and the 4.3-μm laser.

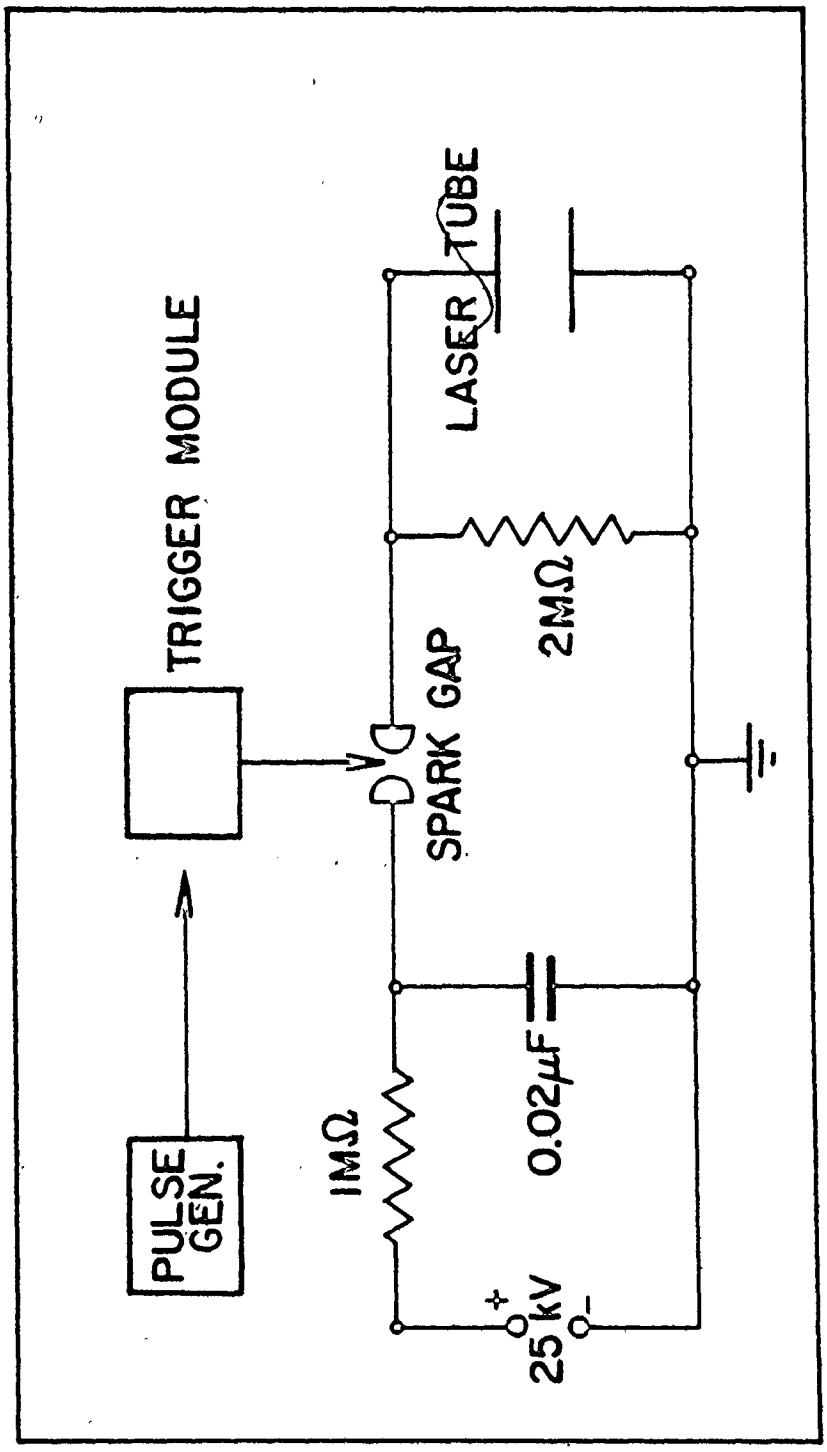
PULSE GEN.
TRIGGER MODULE
SPARK GAP
LASER TUBE
2MΩ
1MΩ
0.02μF
25 kV
+
-

Fig. 3.3

Photograph of the hot CO_2 cell used in the TE sequence laser. Total cell length is 180 cm.

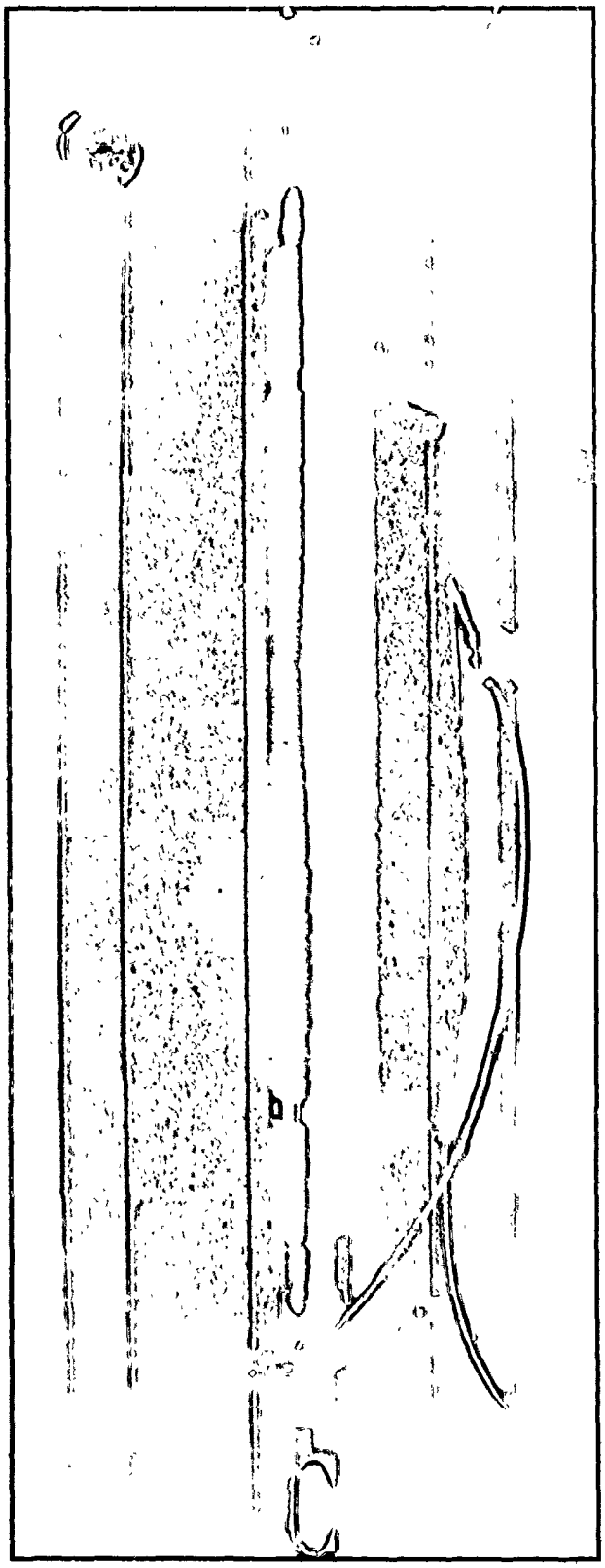

180 cm but the measured temperature profile, obtained using a thermocouple, indicated a central "hot" region of ∿120 cm length surrounded by relatively cool end regions. The cell was filled with 50 Torr of CO_2 at a temperature of 600 K.*

The optical cavity of the sequence laser consisted of a 35% transmitting output coupler and a grating which enabled the laser to be tuned over a range of lines in both the 10.4- and 9.4-μm sequence bands. The cavity-folding mirror had high reflectance and was only used to make the cavity as compact as possible. The sequence output pulses typically consisted of a 600 ns FWHM gain-switched spike followed by a long tail, several μs in duration. Peak output powers ranged from 25 kW on the strong 10.4-μm transitions to 10 kW on the 9.4-μm transitions.

The sequence pulses were directed into the 4.3-μm laser cavity via L_1 and L_2 (see Fig. 3.1) which were 2.5 cm focal length lenses used to match the 10.4-μm output mode to the 4.3-μm cavity mode. Mirror M_1 transmitted ∿70% of the incident 10.4-μm radiation, and had a reflectance of ≳98% at 4.3 μm. Mirror M_2 acted as the output coupler for the 4.3-μm cavity, and had a reflectance of ∿75% at 4.3 μm.† With the sequence laser operating on the P(19) 10.4-μm laser transition, the peak intensity in the 4.3-μm cavity was ∿50 kW/cm^2. The helical

---

*A more efficient design for a hot cell is given in Ref. [55].

†This mirror was originally the output coupler of a CO laser. CO laser mirrors were found to be useful in the present pumping scheme as they generally have high transmission at 10.6 μm and good reflectivity at 4.3 μm.

pin discharge in the 4.3-μm cavity was generally operated with mixtures of low CO_2 content ($\lesssim$2%) at total pressures less than 50 Torr.

3.3 Results and Analysis

To attain lasing at 4.3 μm, the helical discharge in the 4.3-μm cavity was fired first. This excites significant populations in all three vibrational modes of the CO_2 molecules in the gas mixture. However, the ν_1 symmetric stretch mode and the ν_2 bending mode populations decay rapidly relative to the population in the ν_3 asymmetric stretch mode. Hence the sequence band inversion (and gain) builds up quickly, reaching a peak value after 100 to 200 μs in a 30 Torr mixture. Once this peak value is reached, the pump laser is fired, and the sequence band output stimulates molecules inside the 4.3-μm cavity from the $00^0 2$ to the $10^0 1$ level. The Au:Ge detector shown in Fig. 3.1 was used to monitor both the 10.4-μm pump pulse and the 4.3-μm output. Once mirrors M_1 and M_2 were aligned, intense laser pulses at 4.3 μm were observed superimposed on the transmitted 10.4-μm pulses. A LiF flat was then placed in front of the Au:Ge detector to block the 10.4-μm pump, and a systematic study of the 4.3-μm laser output was made. Lasing was quite persistent and appeared over a wide range of discharge pressures and mixtures, indicating that inversion in the 4.3-μm band is relatively easy to attain. The total discharge pressure could be varied from a few Torr at 3% CO_2 concentration, to $\sim$100 Torr at 0.5% CO_2. The N_2 concentration throughout was 7%, the balance of the mixture being He. The low CO_2 content and the relatively low pressures are consistent with the dynamics of this laser being dominated by the very fast collisional de-excitation

of the $10^0 1$ level by CO_2-CO_2 collisions (see Sect. 2.5). The optimum mixture for maximum 4.3-μm stability and power was 91.5%He:7%N_2:1.5%CO_2 at 30 Torr total pressure.

Figure 3.4 illustrates a typical 4.3-μm laser pulse obtained using the above optimum mixture and pressure. The lower trace shows the gain-switched sequence pulse which pumps the 4.3-μm laser. The short time delay observed between the start of the pump pulse and the 4.3-μm laser output is characteristic of a moderately high gain transition. By decreasing the sequence pump power, the time delay could be increased; the longest observed delay being ∿700 ns, corresponding to a five-fold reduction in pumping power, and in good agreement with the calculated $10^0 1$ lifetime of ∿800 ns. The 4.3-μm output power was found to increase linearly with pumping power up to the maximum available power density of ∿50 kW/cm^2. With this maximum input power, a peak 4.3-μm output power density of ∿1 kW/cm^2 was observed, although no attempt was made to optimize the output coupling mirror. The 4.3-μm pulse duration was of the order of 200 ns (FWHM) under all experimental conditions.

Measurements were also made to determine the dependence of the 4.3-μm laser output on the time delay between the triggering of the 4.3-μm laser discharge and the arrival of the pump pulse. Typical results are shown in the lower part of Fig. 3.5. The upper trace in Fig. 3.5 displays the results of a separate experiment in which a cw probe laser operating on the P(19) $00^0 2$ 10.4-μm sequence line was used to determine the temporal profile of the sequence gain in the 4.3-μm helical pin discharge. (Gain measurements were also made on the 10.4-μm regular band and indicated that the ν_3 mode temperature, T_3, was ∿2000 K

Fig. 3.4

Temporal relationship between the P(20) ($10^{0}1$ - $10^{0}0$) 4.3-μm laser output and the P(19) ($00^{0}2$ - $10^{0}1$) 10.6-μm laser pump pulse. The 10.6-μm intensity refers to the peak intensity at the centre of the 4.3-μm laser cavity. The long tail of the 10.6-μm pulse is not shown.

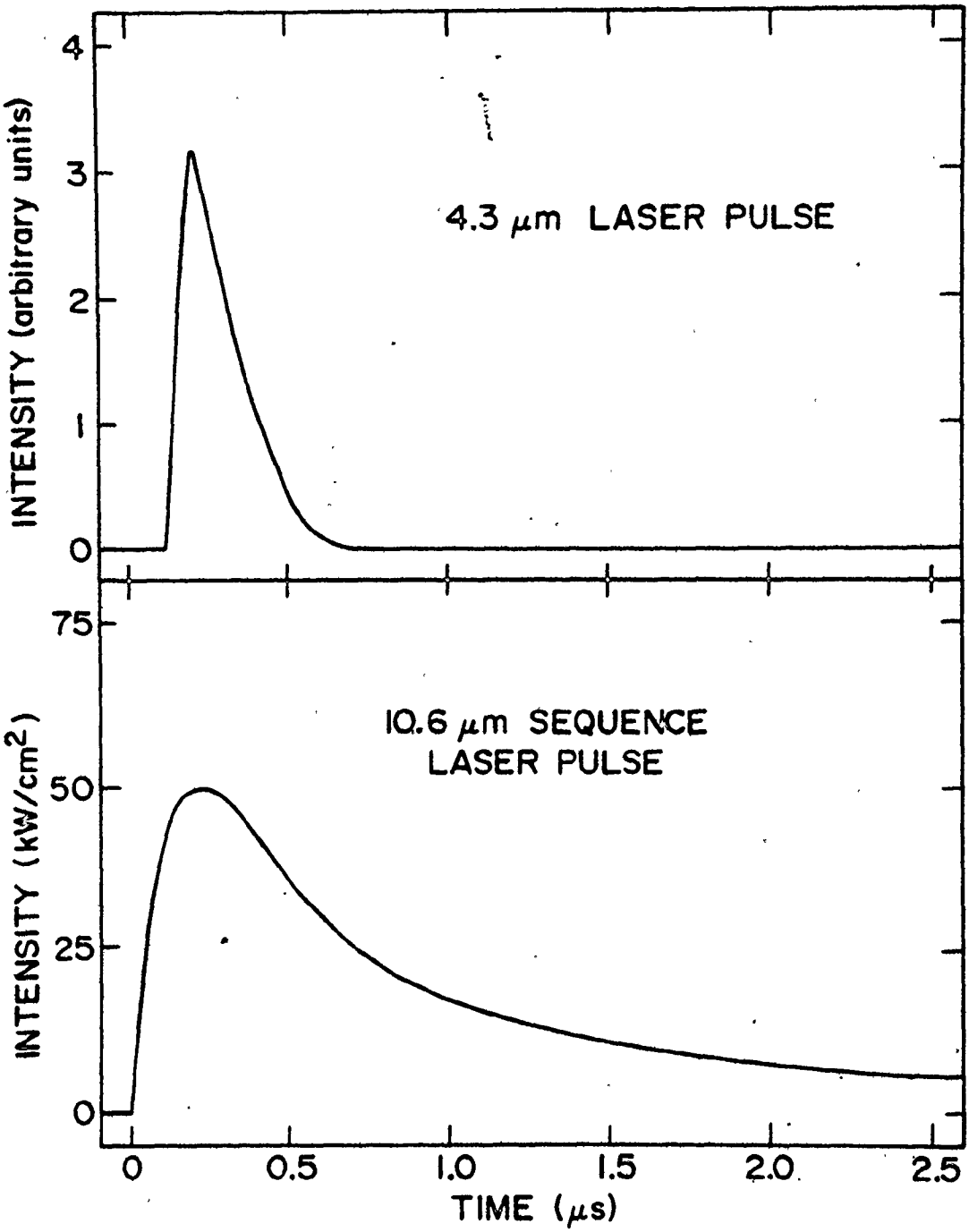
4.3 μm LASER PULSE
INTENSITY (arbitrary units)
4
3
2
1
0
10.6 μm SEQUENCE
LASER PULSE
INTENSITY (kW/cm²)
75
50
25
0
0
0.5
1.0
1.5
2.0
2.5
TIME (μs)

Fig. 3.5

Temporal profile of sequence gain in the 4.3-μm discharge tube, together with the 4.3-μm output intensity as a function of the time delay between the firing of the 4.3-μm discharge and the arrival of the sequence pump pulse. The gas mixture used was 91.5%He:7%N_2:1.5%CO_2 at 30 Torr total pressure.

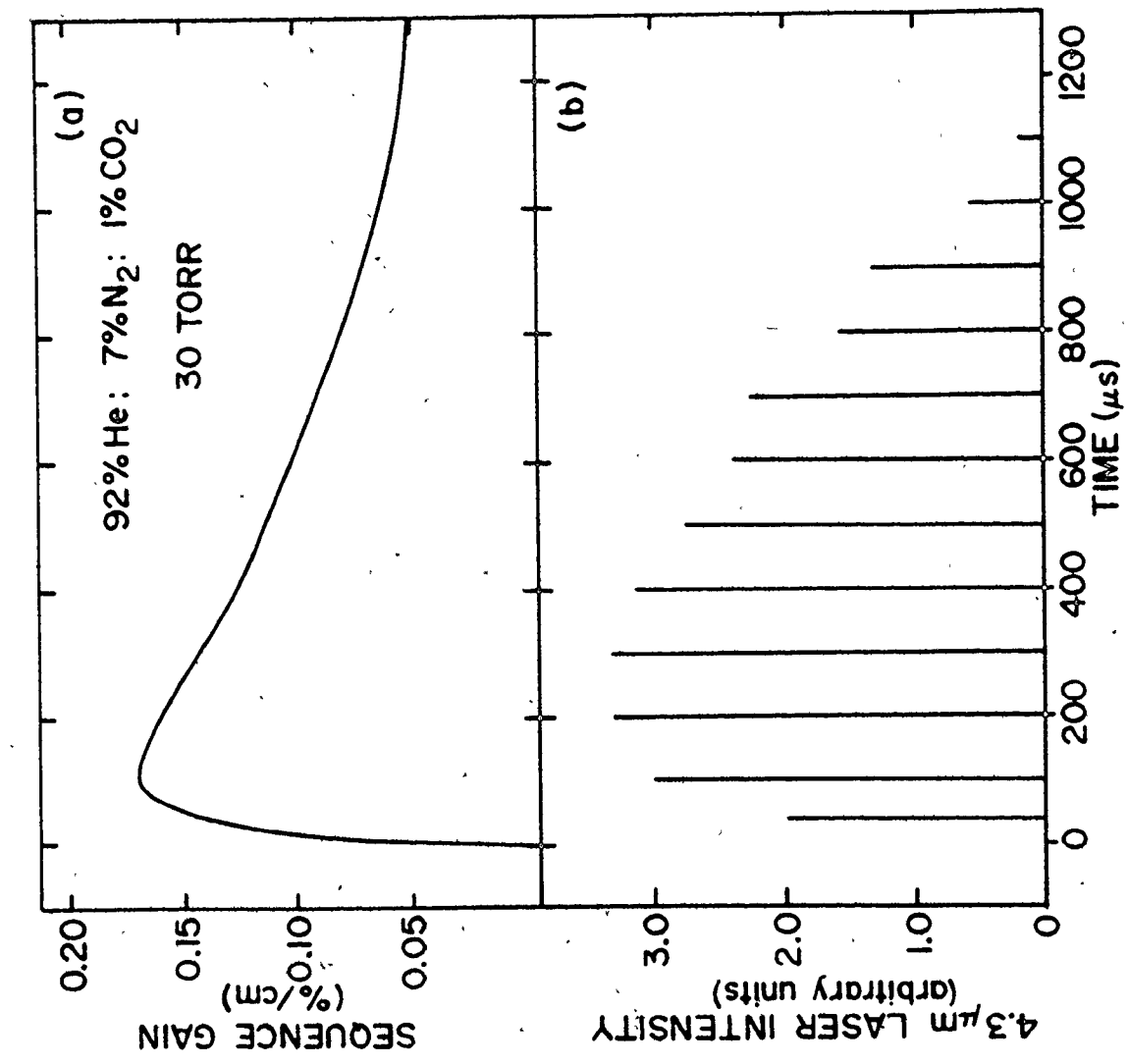
(a)
92% He : 7% N_2 : 1% CO_2
30 TORR
SEQUENCE GAIN
(%/cm)
0.20
0.15
0.10
0.05
(b)
4.3 μm LASER INTENSITY
(arbitrary units)
3.0
2.0
1.0
0
0
200
400
600
800
1000
1200
TIME (μs)

at the time of peak gain [56]). Note that 4.3-μm lasing began abruptly at a time delay of 35 μs and persisted to time delays over 1 ms. Peak 4.3-μm output was obtained somewhat after the peak of the sequence gain. Clearly, it is important that the populations in the ν_2 modes, and particularly the $10^0 0$ level, are given time to decay. The 4.3-μm pulse in Fig. 3.4 corresponds to a time delay of 350 μs.

The output frequencies of the 4.3-μm laser were investigated by using a spectrometer with sufficient resolution to give an unambiguous identification of the lasing transitions, and also to determine if more than one transition lases simultaneously. The initial experiments were made using the P(19) 10.4-μm sequence line as a pump. As expected, the observed 4.3-μm transition was found to be the "connected" P(20) transition of the $(10^0 1 - 10^0 0)$ band. The measured wavenumber of 2309.4 ± 0.5 cm^{-1} is in good agreement with the value of 2309.8025 cm^{-1} calculated from the molecular constants of Ref. [57]. Only one 4.3-μm transition was observed. An identical result was obtained when the pump laser was tuned to the R(19) sequence transition. However, when other sequence lines were used as pumps, several 4.3-μm transitions were observed to lase simultaneously, indicating that some rotational thermalisation is taking place. By varying the pump sequence line from P(9) to P(31) in the 10.4-μm band, 4.3-μm lines from P(10) to P(32) were observed. When the P(19), P(21) or P(25) sequence lines were used as the pumping radiation, only the directly pumped transitions were observed, and these lines gave maximum output power. It is interesting to note that certain 4.3-μm transitions were never observed, e.g., the P(14) and P(30) lines. This behaviour is attributed to chance

coincidences occurring between the laser transitions and absorption lines in other bands, particularly the ν_3 fundamental. Peterson and Wittig [11] observed similar "holes" in the frequency spectrum of their 4.3-μm laser. We also obtained 4.3-μm lasing with the pump laser tuned to the sequence lines in the 9.4-μm band. Stimulated emission now populates the 02^01 level, and 4.3-μm lasing occurs in the (02^01 - 02^00) band. Lasing action was again quite persistent, and was achieved using pump lines from P(13) to P(29). Output powers and spectral properties were very similar to those attained in the (10^01 - 10^00) band.

The line tunability of the 4.3-μm laser was investigated further by replacing M_2 with a grating (PTR ML-402). The insertion of a beam-splitter between L_2 and M_1 permitted M_1 to serve as both the input and output coupler. Numerous 4.3-μm lasing transitions could now be obtained from any single sequence pump transition. Figure 3.6 shows the 4.3-μm output powers obtained from the grating-tuned cavity when pumped with the P(17) sequence line. Notice that maximum output does not correspond to the directly pumped transition which indicates the likelihood of an interferring absorption on the P(18) 4.3-μm transition. Similar distributions were obtained using other sequence pump transitions. However, when the sequence pumping transition employed was away from band center (i.e. away from P(19)) lasing from far-removed rotational levels was not observed. For instance, 4.3-μm lines such as P(10) and P(12) did not lase when pumping was on the P(27) sequence line. These results indicate that although rotational relaxation is plainly evident,

Fig. 3.6

4.3-μm output power versus wavenumber for the ($10^{0}1$-$10^{0}0$) band. The sequence pump transition was P(17) and the in-cavity pumping power was ∿60 kW/cm^2. The 4.3-μm cavity consisted of a grating and a 75% reflectance mirror which was used as the output coupler. The dashed lines represent those transitions on which the pulse-to-pulse stability was poor.

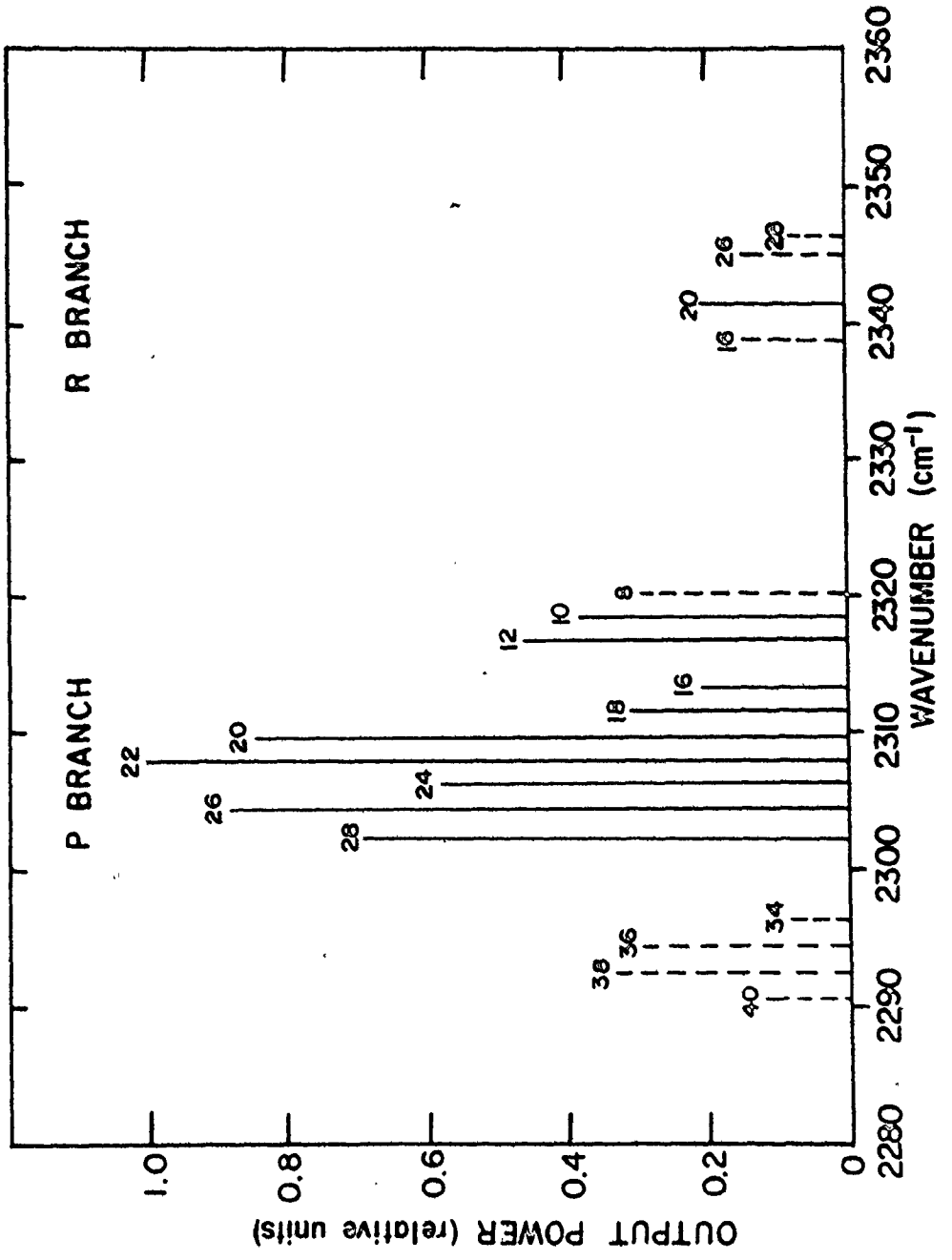
OUTPUT POWER (relative units)
0
0.2
0.4
0.6
0.8
1.0
2280
2290
2300
2310
2320
2330
2340
2350
2360
WAVENUMBER (cm⁻¹)
P BRANCH
R BRANCH
8
10
12
16
18
20
22
24
26
28
34
36
38
40
16
20
26
28

total rotational thermalization does not take place within a few hundred ns of the arrival of the sequence pulse. Higher sequence pump powers and higher pressures in the 4.3-μm discharge should result in an increase in the number of 4.3-μm laser lines observed when pumping with a particular sequence line. The frequencies of transitions in both 4.3-μm bands were calculated using the molecular constants of Ref. [57] and are given in Tables 3.1 and 3.2.

The experimental results described thus far suggest that the use of sequence lasers to optically pump TE CO_2 lasers can lead to the development of high power sources of line-tunable 4.3-μm radiation. It is therefore pertinent at this stage to estimate the efficiency of the present low pressure laser system, and consider its scalability to higher pressures. Preliminary calculations were performed to determine how many of the CO_2 molecules were excited to the $00^0 2$ level in the 30 Torr 91.5%He:7%N_2:1.5%CO_2 mixture, and what fraction of these $00^0 2$ molecules are transferred to the $10^0 1$ level and subsequently emit 4.3-μm radiation. Based on measurements of small-signal gain on the regular and sequence 10.4-μm bands, it was determined that, at the optimum time for pumping, the $00^0 2$ level population is ∿2.5% of the total CO_2 molecules. Hence, in the absence of coherent processes, the maximum possible inversion in the ($10^0 1$ - $10^0 0$) 4.3-μm band corresponds to ∿1.2 of the available CO_2 molecules. In a 1.5% CO_2 mixture, this inversion will give a gain of ∿5%/cm, based on the transition strengths in Ref. [34]. The actual 4.3-μm gain present was estimated by reducing the active length and the cavity Q until the laser was close to threshold. These measurements indicate a gain of at least 3%/cm which is close to the estimated maximum. These calculations also show that stimulated

TABLE 3.1

Calculated wavenumbers of transitions in the ($10^{o}1$-$10^{o}0$) 4.3-μm band. Strongest lines observed are indicated with an asterisk.

J	P(J)	R(J)
2	2325.0270	2328.8976
4	2323.4350	2330.4021
6	2321.8181	2331.8814
8	2320.1762	2333.3358
10	2318.5094	2334.7650
12	2316.8177	2336.1690
14	2315.1011	2337.5480
16	2313.3597	2338.9018
18	2311.5935	2340.2304
20	2309.8025*	2341.5338
22	2307.9867*	2342.8120
24	2306.1462	2344.0650
26	2304.2810*	2345.2928
28	2302.3911	2346.4953
30	2300.4766	2347.6725
32	2298.5374	2348.8244
34	2296.5737	2349.9510
36	2294.5854	2351.0523
38	2292.5725	2352.1283
40	2290.5352	2353.1790

TABLE 3.2

Calculated wavenumbers of transitions in the ($02^{o}1$-$02^{o}0$) 4.3-μm band. Strongest lines observed are indicated with an asterisk.

J	P(J)	R(J)
2	2325.8641	2329.7391
4	2324.2724	2331.2474
6	2322.6570	2332.7318
8	2321.0178	2334.1922
10	2319.3550	2335.6287
12	2317.6684	2337.0412
14	2315.9582	2338.4296
16	2314.2244	2339.7940
18	2312.4670	2341.1343
20	2310.6860*	2342.4505
22	2308.8815*	2343.7425
24	2307.0535	2345.0103
26	2305.2020	2346.2539
28	2303.3270	2347.4733
30	2301.4287	2348.6683
32	2299.5069	2349.8390
34	2297.5617	2350.9854
36	2295.5932	2352.1073
38	2293.6013	2353.2048
40	2291.5862	2354.2779

emission competes very effectively with the collisional losses from the $10^0 1$ level. Thus, at 30 Torr pressure, and 1.5% CO_2 content, the present technique is efficient at extracting 4.3-μm photons from molecules originally excited to the $00^0 2$ level. In order to scale the laser to higher pressures and CO_2 content, and thereby to greater output powers, a more intense sequence pump pulse is required to compete with the increased collisional de-excitation of the $10^0 1$ level. Alternatively, the 4.3-μm laser discharge can be placed inside the sequence cavity with the appropriate use of a dispersive element such as a grating. The first option is discussed in Chapter 7; the latter option is described in the next section.

3.4 Intra-cavity Configuration

A unique feature of the optical pumping scheme described in this thesis is that the pumping (sequence) photons experience gain in the pumped medium rather than absorption. Consequently, the 4.3-μm laser was incorporated inside the same optical cavity as the sequence laser. The resulting intra-cavity configuration is shown in Fig. 3.7. As before, the high pressure discharge and the hot CO_2 cell ensure sufficient sequence pumping power, whereas the optical pumping and subsequent 4.3-μm gain occur in the low pressure discharge, which was formerly part of the separate 4.3-μm oscillator. The cavity is folded using a standard 10-μm CO_2 laser grating (PTR ML-303) positioned so that the sequence radiation is reflected in first order while the 4.3-μm radiation is reflected in second order. In this manner, both the sequence and 4.3-μm radiation are present in the low pressure discharge, but the 4.3-μm photons are isolated from the hot cell where they would

Fig. 3.7

Intra-cavity configuration used to produce 4.3-μm lasing. The 10.6-μm radiation is reflected from the grating in first order while the 4.3-μm radiation is reflected in second order.

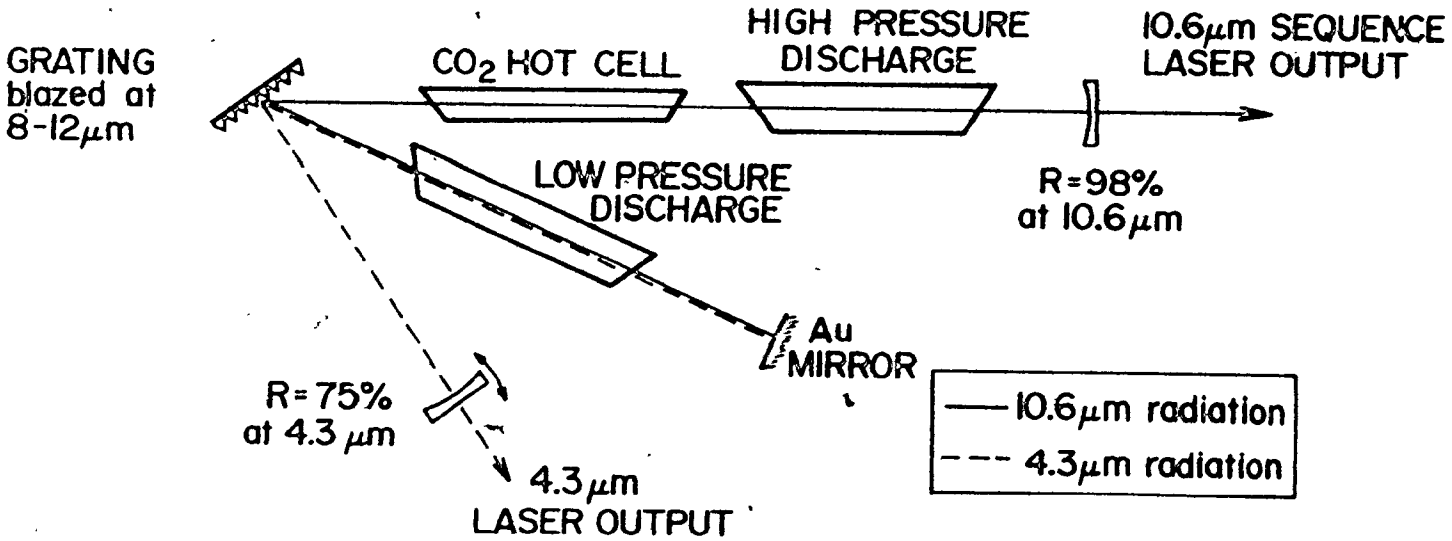
GRATING
blazed at
8-12μm
CO2 HOT CELL
HIGH PRESSURE
DISCHARGE
10.6μm SEQUENCE
LASER OUTPUT
LOW PRESSURE
DISCHARGE
R=98%
at 10.6μm
Au
MIRROR
R=75%
at 4.3 μm
4.3μm
LASER OUTPUT
10.6μm radiation
4.3μm radiation

otherwise experience considerable absorption. The sequence cavity has a high-Q and the optics are chosen to provide the maximum possible sequence pumping intensity in the low pressure discharge. The choice of the 4.3-μm output coupler is much less critical and a relatively high transmission optic (50%) is used to achieve large 4.3-μm output power. The 4.3-μm laser could be line-tuned either by rotating the 4.3-μm output coupler, or alternatively by rotating the grating, thereby changing the sequence pumping line, and then adjusting the 4.3-μm output coupler.

When using the same experimental conditions as described in Section 3.2 for both the high pressure (80%He:10%N_2:10%CO_2 at 100 Torr) discharge and the low pressure (91.5%He:7%N_2:1.5%CO_2 at 30 Torr) discharge, considerable improvement in the 4.3-μm output parameters is observed. Small-signal 4.3-μm gains greater than 4%/cm were achieved and output power on the strong 4.3-μm transitions was in excess of 1 kW. It should be noted that although the output intensity, which was $\sim$1 kW/cm^2, was identical to that obtained from the two-cavity configuration, the output power was a factor of 20 greater due to a substantial increase in the mode size of the 4.3-μm radiation. These improvements are a direct result of the more efficient utilization of sequence pumping photons in the new configuration. This can be attributed to two factors. Firstly, by employing a single optical cavity, all inter-cavity coupling losses have been eliminated. Secondly, by pulsing the low pressure discharge first, the sequence oscillation will be restricted to a relatively narrow linewidth,

which is in fact that linewidth over which the optical pumping that produces the 4.3-μm gain will occur. The mechanism involved in the matching of linewidths is the same as that used to achieve lasing on a single longitudinal mode in a hybrid TEA CO_2 laser [58].

Another improvement realized in the new configuration is the reduction of the threshold pumping power. This was investigated in the following manner. First, the low pressure pulsed discharge was replaced with a continuous longitudinal discharge and only a small decrease in 4.3-μm output was observed. The high pressure discharge was then replaced with another longitudinal discharge, identical to the first. By pulsing this discharge, long sequence pulses (10-1000 μs FWHM) of relatively high power could be obtained. A typical sequence pulse is shown in Fig. 3.8, along with the corresponding 4.3-μm pulse. By decreasing the Q of the sequence cavity the pumping power could be reduced until 4.3-μm lasing ceased. The lowest value of threshold pumping power obtained was $\sim$100 W/cm^2. This value is particularly significant since it now represents an in-cavity intensity rather than an intensity which must be achieved inside another, separate optical cavity. Through the use of the intra-cavity configuration, efficient 4.3-μm lasing can be achieved using low power sequence pulses, and in particular, Q-switched sequence laser pulses. The use of Q-switched sequence laser pulses to produce 4.3-μm lasing is described in detail in Chapter 5.

It should also be noted at this point that the large disparity in pulse durations shown in Fig. 3.8 was observed for a wide range of

Fig. 3.8

Output pulses obtained from the intra-cavity configuration using a continuous discharge in the low pressure (92%He:7%N_2:1%CO_2 mixture at 5 Torr total pressure) tube and a longitudinally pulsed discharge in the high pressure (80%He:10%N_2:10%CO_2 mixture at 20 Torr total pressure) tube. The sequence pulse duration could be varied from 10 μs to 1000 μs by decreasing the discharge voltage.

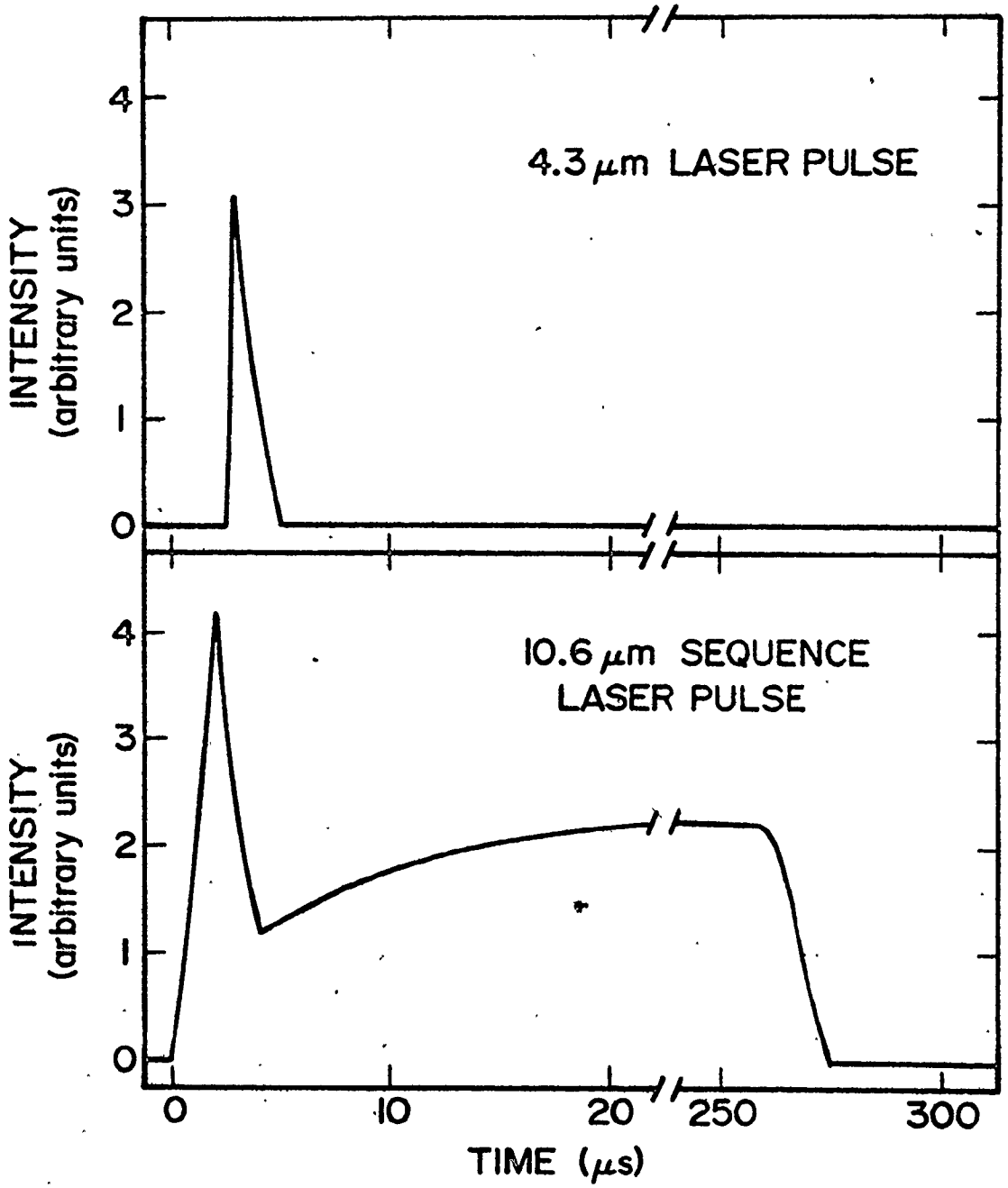
4.3 μm LASER PULSE
10.6 μm SEQUENCE
LASER PULSE
INTENSITY
(arbitrary units)
INTENSITY
(arbitrary units)
0
1
2
3
4
0
10
20
250
300
TIME (μs)

experimental conditions. It was further determined that this was not the result of insufficient pumping power. Rather, the relatively short 4.3-μm pulse durations appear to be a direct consequence of the gain dynamics of the laser, and in particular, the short $10^0$1 lifetime (4.8 μs for the conditions given in Fig. 3.8 [13]). This is verified in the next Chapter where a theoretical model of the 4.3-μm laser is presented.

3.5 Summary

This Chapter contains a detailed description of the experimental apparatus employed to achieve 4.3-μm lasing. Two important cavity configurations were introduced and the results of a series of preliminary experiments were described. These results serve to delineate the basic mechanisms involved in 4.3-μm lasing which are described in greater detail in the following Chapter.

CHAPTER 4

COMPUTER MODELING OF 4.3-μm LASERS

4.1 Introduction

The experimental results and subsequent analysis reported in the previous Chapter serve as an introduction to the basic mechanisms involved in 4.3-μm lasing. It was shown i) that the optical pumping of discharge excited CO_2 by a CO_2 sequence laser can result in an inversion on the ($10^0 1$-$10^0 0$) (or ($02^0 1$-$02^0 0$)) transitions and ii) that stimulated emission at 4.3 μm can compete effectively with the collisional de-excitation of the $10^0 1$ level. However, a comprehensive model of the 4.3-μm laser gain dynamics is needed so that a more thorough understanding of the lasing process can be achieved. In particular, it is important to identify the mechanisms responsible for the relatively short duration of the 4.3-μm output pulses (relative to the sequence pump pulse) and the fact that, at low pumping powers, 4.3-μm lasing is restricted to low CO_2 concentration and low total gas pressure. This Chapter describes a rate-equation model for the laser, and the use of this model in assessing the capabilities of the laser system.

The rate equations comprising the model are described in Sect. 4.2 and comparisons between the model predictions and experimental results are presented in Sect. 4.3. Section 4.4 discusses the importance of the two principal collisional processes: the relaxation of the $10^0 1$ and $10^0 0$ levels. Good agreement is shown to exist between the model

predictions and the experimental results. Therefore, the model can be used to predict the time evolution of the level populations. In this manner, three regimes of operation are identified and these are explained in Sect. 4.5.

4.2 The 4.3-μm Laser Rate-Equation Model

The 4.3-μm laser rate-equation model described below is similar to standard CO_2 laser models [15-17] except that additional equations are used to describe explicitly the populations of the $00^0 2$, $10^0 1$ and $10^0 0$ levels. The resulting set of differential equations are as follows:

$$\frac{dN_{002}}{dt} = - fg_{seq} c\delta_{seq} \rho_{seq} - \frac{2(N_{002} - N^e_{002}(T_3))}{\tau_{\nu_3}} \tag{4.1}$$

$$\frac{dN_{101}}{dt} = fg_{seq} c\delta_{seq} \rho_{seq} - fg_{4.3} c\delta_{4.3} \rho_{4.3} - \frac{N_{101} - N^e_{101}(T_1, T_3)}{\tau_{101}} \tag{4.2}$$

$$\frac{dN_{100}}{dt} = fg_{4.3} c\delta_{4.3} \rho_{4.3} + \frac{N_{101} - N^e_{101}(T_1, T_3)}{\tau_{101}} - \frac{N_{100} - N^e_{100}(T_1)}{\tau_{100}} \tag{4.3}$$

$$\frac{dE_{BS}}{dt} = \frac{E_3}{\tau_3} + \frac{E_{100} - E^e_{100}(T_1)}{\tau_{100}} - \frac{E_{BS} - E^e_{BS}(T)}{\tau_{VT}} \tag{4.4}$$

$$\frac{dE_3}{dt} = \frac{E_4 - E^e_4(T_3)}{\tau_{N_2}} + \left(\frac{\nu_3}{\nu_1 + \nu_3}\right) \frac{E_{101} - E^e_{101}(T_1, T_3)}{\tau_{101}}$$

$$+ \frac{2(E_{002} - E^e_{002}(T_3))}{\tau_{\nu_3}} - \frac{E_3}{\tau_3} \tag{4.5}$$

$$\frac{dE_4}{dt} = - \frac{E_4 - E^e_4(T_3)}{\tau_{N_2}} \tag{4.6}$$

$$\frac{d\delta_{seq}}{dt} = -2fg_{seq}c\delta_{seq}\rho_{seq} + fg_{4.3}c\delta_{4.3}\rho_{4.3} - \frac{\delta_{seq} - K(J)(N_{002}-N_{101})}{\tau_R} \quad (4.7)$$

$$\frac{d\delta_{4.3}}{dt} = fg_{seq}c\delta_{seq}\rho_{seq} - 2fg_{4.3}c\delta_{4.3}\rho_{4.3} - \frac{\delta_{4.3} - K(J+1)(N_{101}-N_{100})}{\tau_R} \quad (4.8)$$

$$\frac{d\rho_{4.3}}{dt} = fg_{4.3}c\delta_{4.3}\rho_{4.3} - \frac{\rho_{4.3}}{\tau_c} + \beta K(J+1)N_{101} \quad (4.9)$$

Here, N_{002} (E_{002}), N_{101} (E_{101}) and N_{100} (E_{100}) are the populations (stored energies) of the respective levels, E_{BS} is the energy stored in the combined bending-symmetric stretching mode, excluding the $10^0 1$ and $10^0 0$ levels [17], E_3 is the stored energy of the ν_3 mode, excluding the $00^0 2$ level, E_4 corresponds to the vibrational energy stored in the nitrogen molecules and δ_{seq} and $\delta_{4.3}$ are the rotational inversions for the sequence transition and 4.3-μm transition, respectively (e.g., $\delta_{seq} = n_{J-1}^{002} - n_J^{101}$, where n_{J-1}^{002} and n_J^{101} are the populations of the particular rotational levels on which lasing occurs. For simplicity, the degeneracy factors have been neglected.). $\rho_{4.3}$ and ρ_{seq} are the in-cavity 4.3-μm and sequence photon densities, respectively. T_1 is the temperature of the combined bending-stretching (BS) mode, T_3 is the temperature of the ν_3 mode, and T represents the translational temperature. Variables denoted with the superscript e represent the equilibrium value of that variable at the temperature indicated in brackets. $K(J)(N_{002}-N_{101})$ and $K(J+1)(N_{101}-N_{100})$ are the equilibrium

values of the sequence and 4.3-μm rotational inversions, respectively ($K(J) \approx K(J+1) \sim \frac{1}{15}$ for P(19)), and $\beta K(J+1)N_{101}$ is the term representing the spontaneous emission, as discussed in Ref. [16]. The parameters g_{seq} and $g_{4.3}$ are constants which relate the rotational inversion to the small-signal gain such that the products $g_{seq}\delta_{seq}$ and $g_{4.3}\delta_{4.3}$ are the familiar small-signal gain coefficients in units of cm^{-1}. f is the cavity filling factor (i.e., ratio of discharge length to total cavity length).

The various molecular relaxation times are given below. The values in parentheses correspond to a 91.5%He:7%N_2:1.5%CO_2 mixture at a total pressure of 32 Torr, which is the mixture used in the experiments reported in the next section. τ_{ν_3} is the ν_3 intra-mode coupling time (390 ns [35]), τ_{10^01} is the relaxation time of the 10^01 level (500 ns [13]), τ_{100} is the coupling time between the 10^00 level and the rest of the BS mode (2.3 μs [41]), τ_{VT} is the vibration-to-translation relaxation time (10 μs [45]), τ_{N_2} is the coupling time between the ν_3 mode and the excited vibrational levels in the N_2 molecules (110 μs [31]), τ_3 is the collisional relaxation time of the ν_3 mode (350 μs [31]) and τ_R is the rotational relaxation time (4.3 ns [47]). The cavity decay time τ_c is given by $-2L/c\ \ell nR$ where L is the cavity length, R is the cavity reflectance and c is the speed of light.

The model is implemented in the following manner. The initial values of the mode temperatures (i.e., the values at the time of peak sequence gain in the pulsed discharge) are used to calculate initial values for the populations and energies in Eqs. (4.1)-(4.9). The

measured sequence pump pulse profile is used to determine the successive values of ρ_{seq} and the differential equations are solved simultaneously beginning with a time corresponding to the start of the sequence pump pulse. The numerical technique used is the Hamming predictor-corrector method [59] and the solutions are obtained using a CDC CYBER 170/730 computer.

4.3 Comparison with Experiment

In order to test the validity of the model, a series of experiments were performed and the results compared with the model predictions. The experiments employed the two-cavity configuration described in Sect. 3.2, using a helical pin discharge in the 4.3-μm laser cavity and the high power TEA sequence laser described in Chapter 6 as the pump source. A low pressure pulsed discharge was included in the pump laser cavity to ensure good matching of linewidths between the sequence pumping radiation and the 4.3-μm laser discharge [58]. The various input parameters required for the model were measured experimentally. Gas concentrations were obtained using calibrated flow-meters and total pressures were measured using barometrically compensated dial gauges calibrated against a Hg manometer. Time delays between firing of the discharge and introduction of the pump pulse were adjusted to give maximum 4.3-μm output power. The value of T_3 at this point was determined from gain measurements on the sequence and regular transitions using a cw CO_2 laser [56]. It is shown in Sect. 5.5 that $T_1 \sim T$ at the gain peak and T was estimated to be 350 K. The sequence pump pulse

intensity was measured using a calibrated photon drag detector* (response time < 1 ns) and the pump pulse shape was obtained from oscilloscope photographs. 4.3-μm output pulses were monitored with a Au:Ge detector (response time < 2 ns), which had been calibrated using the Q-switched 4.3-μm laser described in Chapter 5*. Fig. 4.1 shows the observed 4.3-μm output, together with the model predictions, for two different gas mixtures in the 4.3-μm discharge tube. It can be seen that the model accurately predicts the pulse rise-time, FWHM, and fall-time under these conditions. In order to provide a more rigorous test of the accuracy of the model, 4.3-μm output was monitored as a function of sequence pumping power over a wide range of pumping powers and for different gas mixtures. Measurements were made on three output parameters: 4.3-μm output intensity, FWHM and the time delay between the start of the sequence pulse and the start of the 4.3-μm pulse. Experimental results are shown in Figs. 4.2, 4.3 and 4.4, together with the model predictions.† The overall agreement between theory and experiment is quite good and any discrepancies are attributed to uncertainties in the numerous experimental input parameters required by the model. It should be stressed that no variable parameters were used in the model. All input parameters were either measured experimentally or taken from the literature. The significance of these results is discussed in the next two sections.

---

*A Scientech Inc. Laser Power Meter Model 360001 was used in the calibration of both the photon drag and Au:Ge detectors.

†The output intensities predicted by the model have been scaled down by a factor of 5.

Fig. 4.1

Comparison of computed (solid lines) and observed (data points) 4.3-μm laser pulses for two different sets of experimental conditions. The gas mixture was 91.5%He:7%N_2:1.5%CO_2.

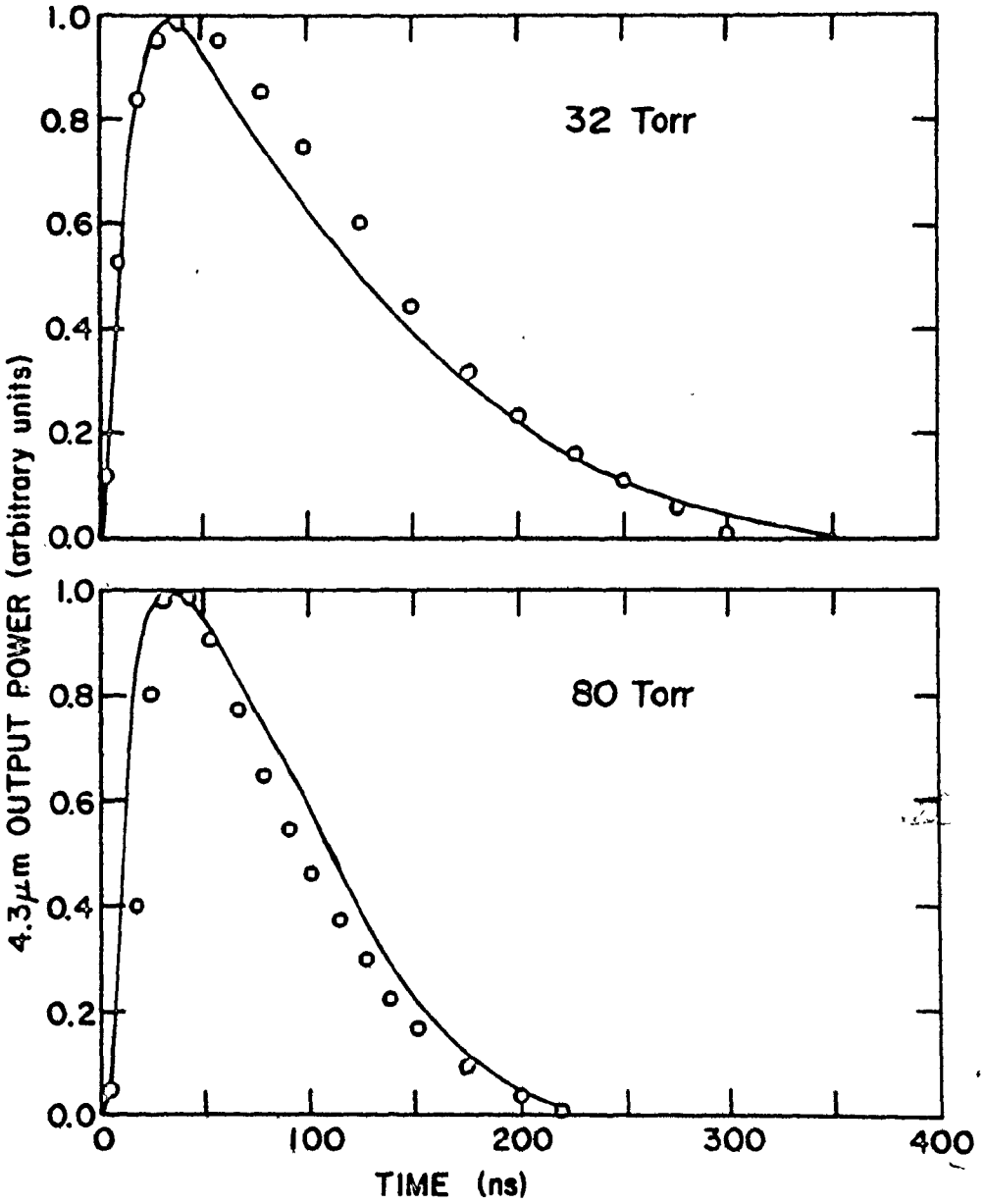
32 Torr
80 Torr
4.3μm OUTPUT POWER (arbitrary units)
TIME (ns)
0.0
0.2
0.4
0.6
0.8
1.0
0
100
200
300
400

Fig. 4.2

Comparison of the computed (solid lines) and observed (data points) 4.3-μm pulse durations (FWHM), for three different sets of experimental conditions, as a function of sequence pumping power. A 91.5%He:7%N_2:1.5%CO_2 mixture was used for the 32 Torr data; a 91.9%He:7%N_2:1.1%CO_2 mixture was used for both the 52 and 80 Torr data. The initial value of T_3 was 3150 K and the cavity reflectance was 0.36.

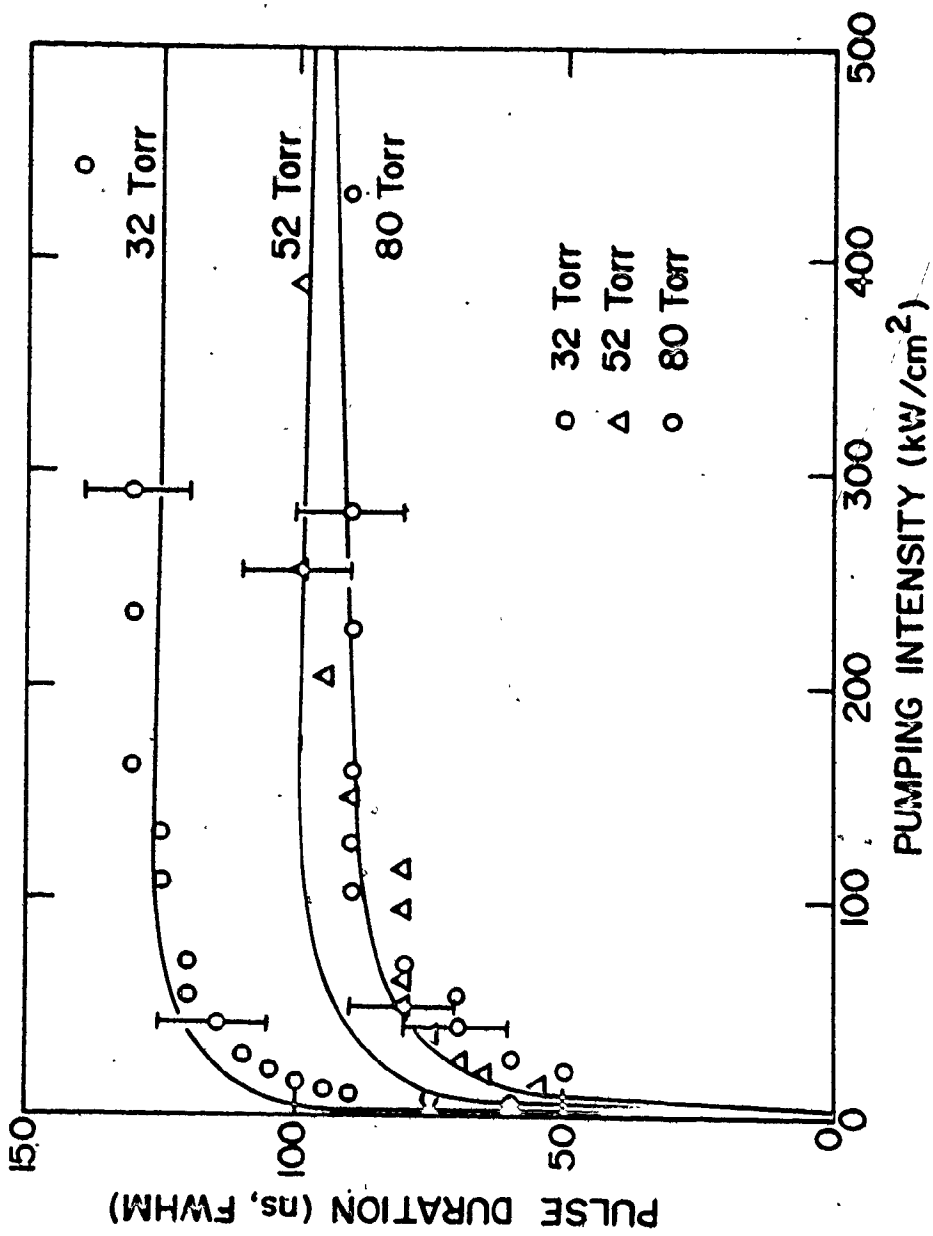
PULSE DURATION (ns, FWHM)
150
100
50
0
0
100
200
300
400
500
PUMPING INTENSITY (kW/cm²)
32 Torr
52 Torr
80 Torr
32 Torr
52 Torr
80 Torr

Fig. 4.3

Comparison of the computed (solid lines) and observed (data points) values of the time delays between the start of the sequence pump pulse and the start of the 4.3-μm laser pulse, as a function of sequence pumping power. Experimental conditions are identical to those of Fig. 4.2.

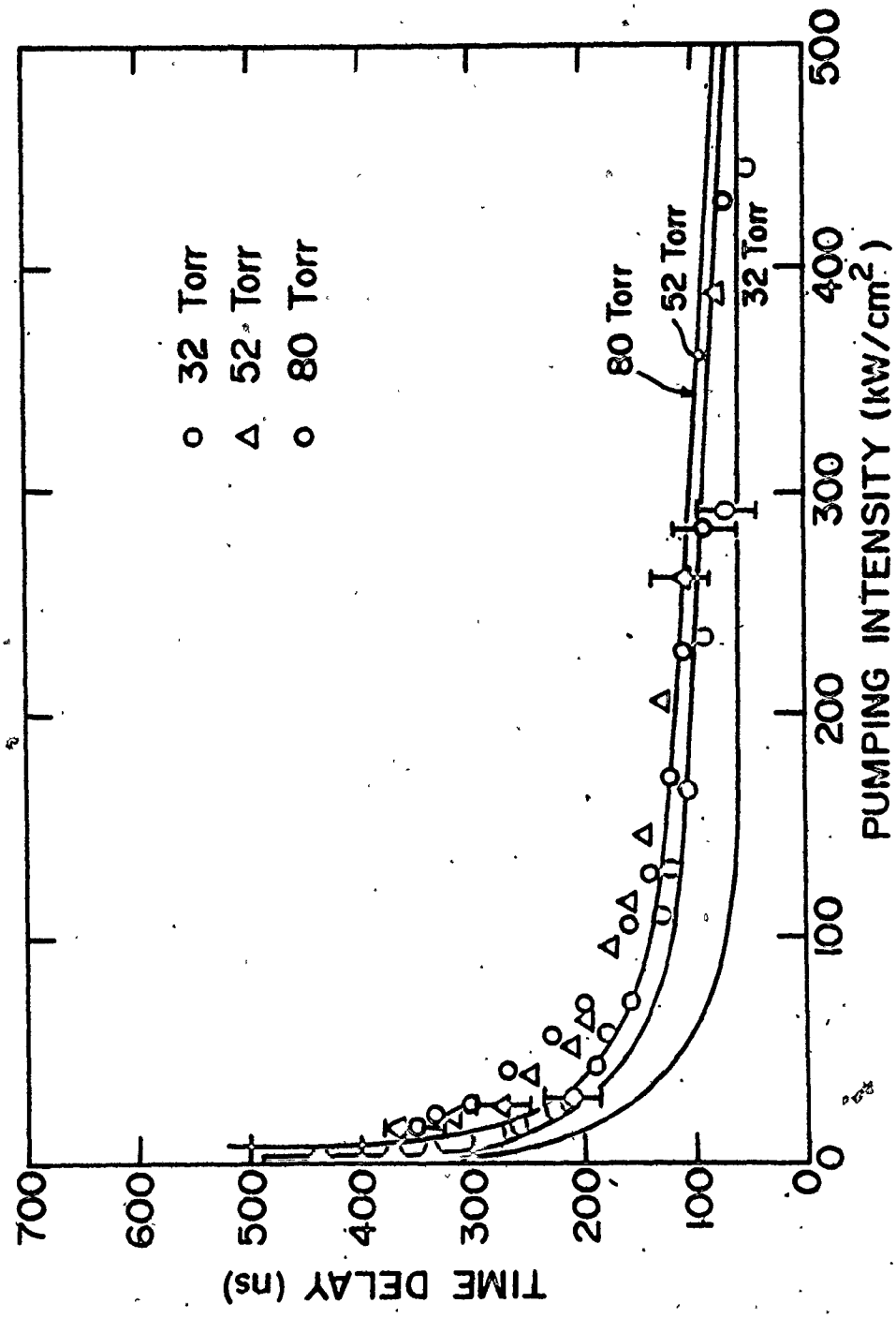
TIME DELAY (ns)
PUMPING INTENSITY (kW/cm²)
32 Torr
52 Torr
80 Torr
80 Torr
52 Torr
32 Torr
0
100
200
300
400
500
600
700

Fig. 4.4

Comparison of the computed (solid lines) and observed (data points) values of 4.3-μm output intensity, as a function of sequence pumping power. Experimental conditions are identical to those of Fig. 4.2. (80 Torr is lacking due to detector malfunction).

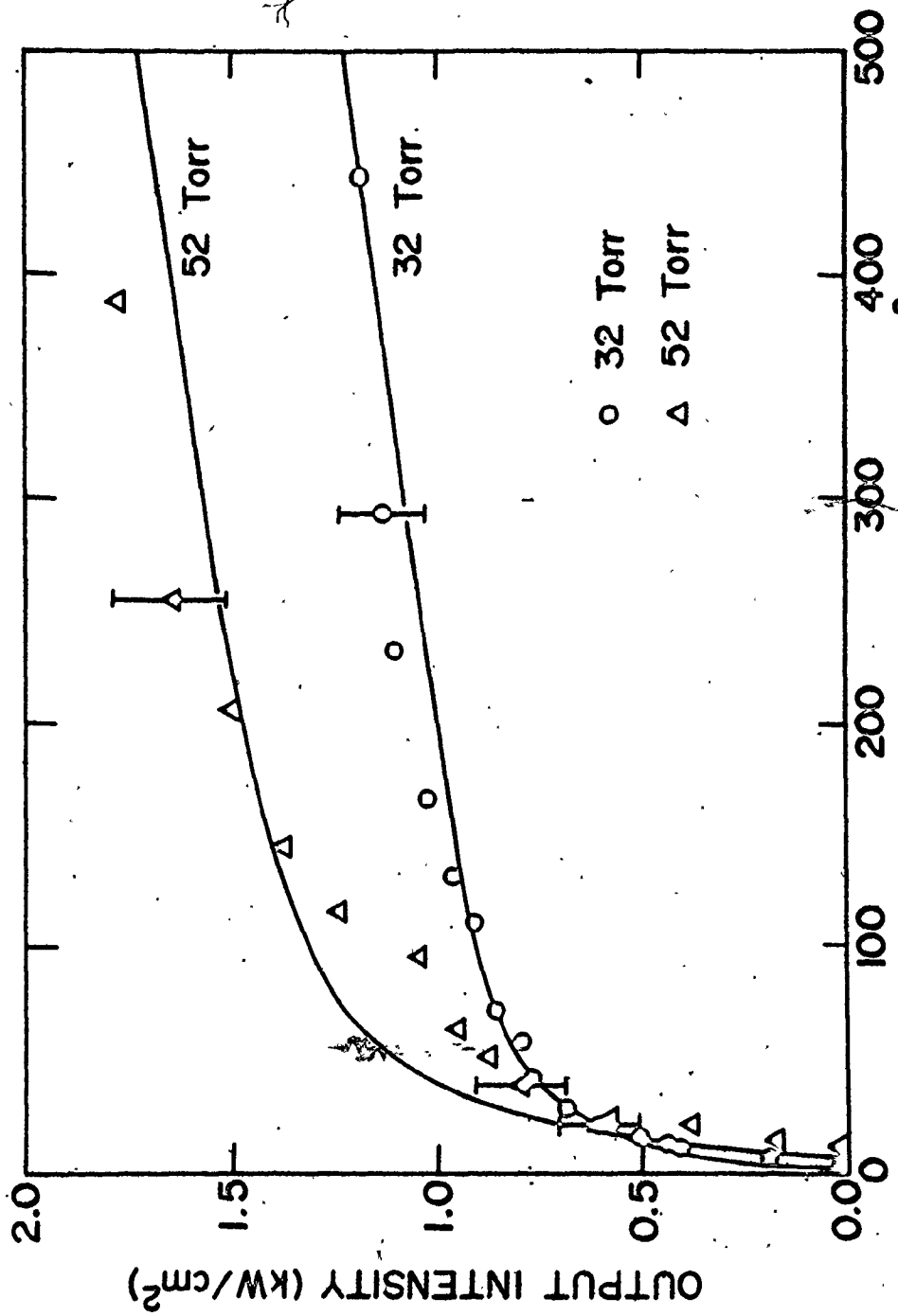
52 Torr
32 Torr
32 Torr
52 Torr
0
100
200
300
400
500
PUMPING INTENSITY (kW/cm²)
0.0
0.5
1.0
1.5
2.0
OUTPUT INTENSITY (kW/cm²)

4.4 Vibrational Relaxation Rates

The values for all the collisional relaxation rates present in the model were obtained from the literature. However, in some cases, there is considerable uncertainty in the actual value of the rate constants. This is especially true of the two most important processes i.e., the collisional relaxation of the $10^0 1$ and $10^0 0$ levels. It is therefore important to determine the specific values of these rates so that their effect on 4.3-μm laser gain dynamics can be correctly ascertained. One approach is to use the comparison of predicted and observed 4.3-μm output to extract rate constants for these processes. These considerations are the topic of this section.

As discussed in Sect. 2.4, the collisional relaxation rate of the $10^0 0$ level has been studied extensively and the reported rate constants range over three orders of magnitude [15,17,37-44]. At present, the values of Stark [41] and those of Jacobs et al. [42] are widely used in the literature. The principal difference between these two sets of values is that Jacobs et al. find that He, N_2 and CO_2 are all very efficient at relaxing the $10^0 0$ level, whereas Stark concludes that the He-CO_2 rate is very slow. Since He is the major constituent in many CO_2 laser gas mixtures, the resulting rates for $10^0 0$ relaxation are quite different. For example, for the 91.5%He:7%N_2:1.5% CO_2 mixture at 32 Torr total pressure, used in Sect. 4.3, the Jacobs value for τ_{100} is ∿320 ns whereas the Stark value is ∿2.5 μs. A faster rate for $10^0 0$ relaxation would lead to longer 4.3-μm pulses as can be seen from Fig. 4.5 which is a plot of observed pulse duration, as a

S&A

Fig. 4.5

Comparison of the computed and observed (data points) values for 4.3-μm pulse duration (FWHM) as a function of sequence pumping power. The experimental data corresponds to a 91.5%He:7%N_2:1.5%CO_2 mixture at a total pressure of 30 Torr, and an initial T_3 of 2000 K. The cavity reflectance was 0.95. The solid curve is the model prediction using a value of τ_{100} taken from the rate constants given by Stark [41]. The dashed curves show the effect of a factor of 5 change in τ_{100}.

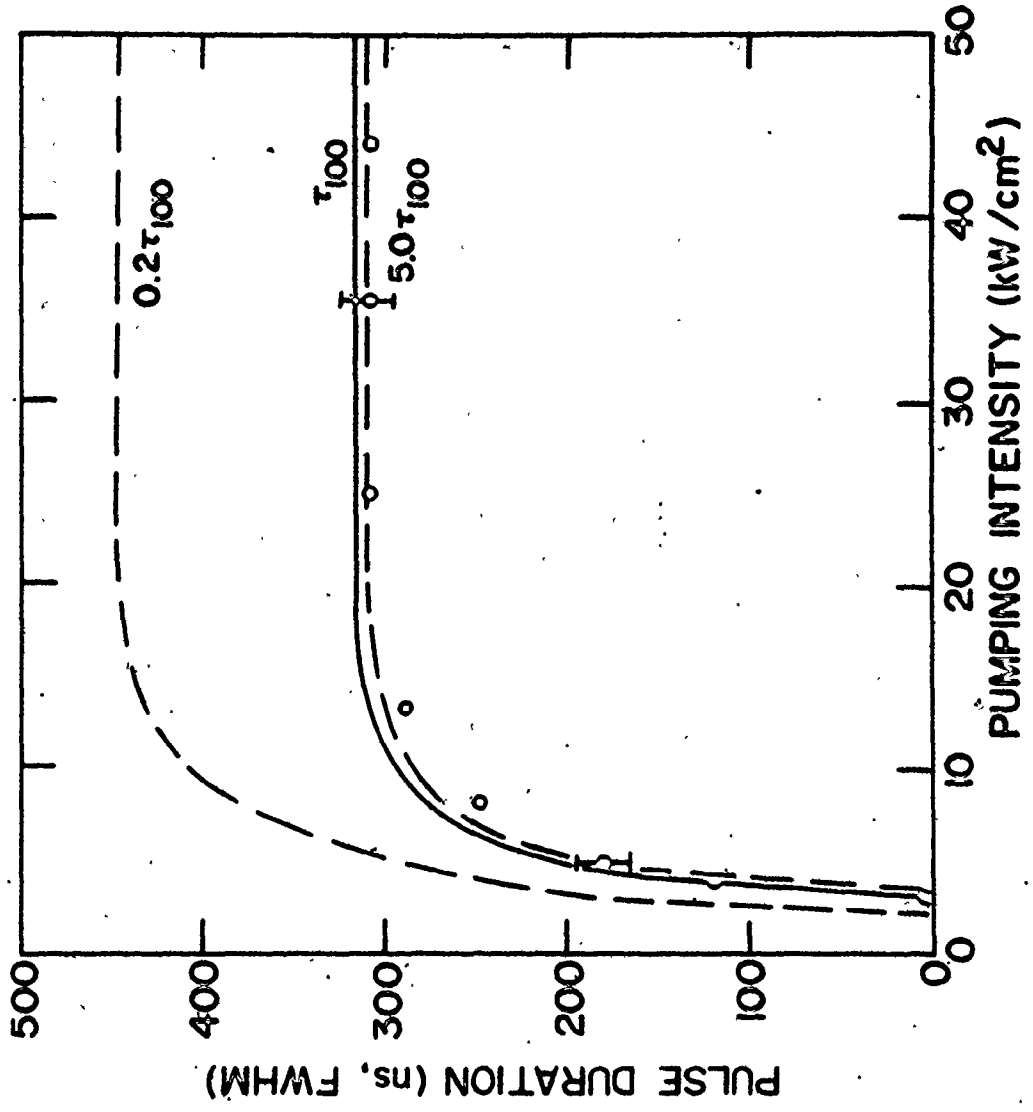
PULSE DURATION (ns, FWHM)
500
400
300
200
100
0
0
10
20
30
40
50
PUMPING INTENSITY (kW/cm²)
0.2τ100
τ100
5.0τ100

function of pumping intensity, for the above mixture.* Included are the model predictions using the value of τ_{100} taken from Stark as well as predictions for a factor of 5 change in τ_{100}.† The results suggest that a value for the $10^{0}0$ relaxation rate equal to or slower than the value reported by Stark is consistent with the observed 4.3-μm output. The faster rates reported by Jacobs would give pulse durations much greater than those actually observed and consequently there is some doubt as to the accuracy of Jacobs' values. Additional experimental data is required before more quantitative conclusions can be drawn.

The most important rate in 4.3-μm laser gain dynamics is the collisional de-excitation of the $10^{0}1$ level. These collisional losses determine the threshold pumping power required to produce 4.3-μm gain and these losses compete with the subsequent stimulated emission. Figure 4.6 shows the dependence of 4.3-μm pulse duration on the value of the above rate. As was the case previously, the FWHM shows the most marked dependence on the value of the $10^{0}1$ collisional relaxation rate, although the 4.3-μm output power also increased somewhat if a slower value for the rate was used. The solid curve in Fig. 4.6 corresponds to a value for the $10^{0}1$ collisional relaxation rate of 4.2×10^{6} s^{-1} $Torr^{-1}$, as measured by Finzi and Moore [13].

---

*The output intensity and time delay are found to be relatively insensitive to changes in τ_{100}.

†These experiments were performed with lower excitation in the discharge ($T_3 \sim 2000$ K initially, see Chapter 3) because the 4.3-μm pulse durations were more sensitive to changes in the vibrational relaxation rates under these conditions.

Fig. 4.6

Comparison of the computed and observed values for 4.3-μm pulse duration (FWHM) as a function of sequence pumping power. The experimental conditions are identical to those of Fig. 4.5. The solid curve is the model prediction using a value of τ_{101} calculated from the rate constant of Finzi and Moore [13]. The dashed curves show the effect of a factor of 2 change in τ_{101}.

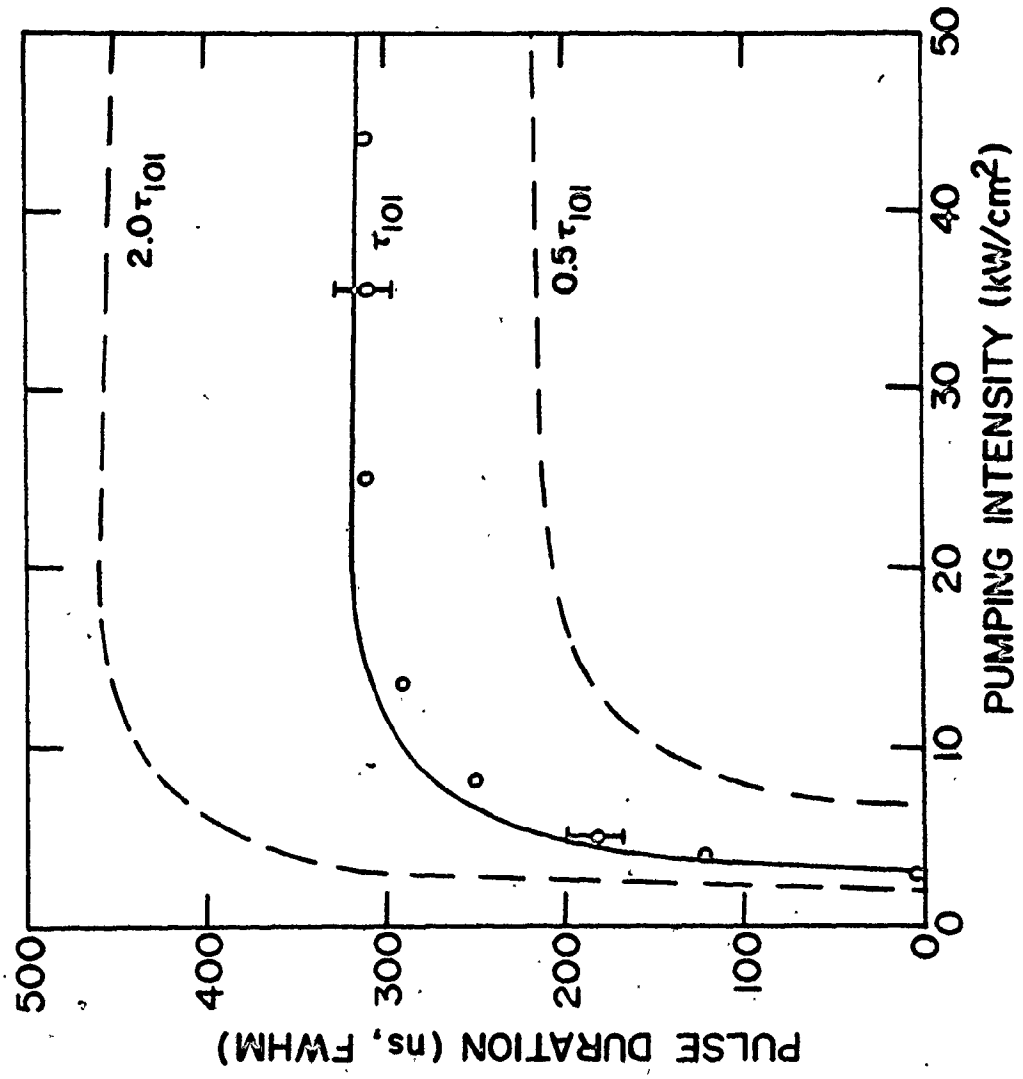
PULSE DURATION (ns, FWHM)
PUMPING INTENSITY (kW/cm²)
2.0τ101
τ101
0.5τ101
0
100
200
300
400
500
10
20
30
40
50

The fact that a factor of two change in this rate constant results in nearly a 50% change in FWHM attests to the importance of this rate in the gain dynamics of the system. Furthermore, this strong dependence, together with the good agreement between the experimental and theoretical values of FWHM in Fig. 4.2 and 4.6, strongly supports the value for the $10^0 1$ rate as determined by Finzi and Moore. Presently, their value is the only experimental measurement of this rate, though Pack [36] has calculated a value of 4.36×10^6 s^{-1} $Torr^{-1}$. The results of this section show that a systematic study of 4.3-μm laser output under different experimental conditions serves as an excellent means of determining this rate constant. Such investigations are beyond the scope of this thesis, however, this section was intended to introduce the technique by which these measurements could be made. The importance of this rate to both 4.3-μm and sequence (see Chapter 6) laser gain dynamics suggests that this possibility merits further investigation.

4.5 Discussion

The previous two sections compare the predictions of the rate-equation model to the experimentally observed output parameters. The good agreement between theory and experiment supports the validity of the model in describing the various processes involved in the 4.3-μm gain dynamics. Therefore, the model can serve as an excellent means of predicting the time dependence of the level populations as the optical pumping and 4.3-μm lasing is taking place. A set of typical results is shown in Fig. 4.7. The experimental conditions correspond to the 32 Torr data of Figs. 4.2-4.4, at a pumping power of 500 kW/cm^2.

Fig. 4.7

Calculated values of the $00^{0}2$, $10^{0}1$ and $10^{0}0$ level populations as a function of time. The experimental conditions correspond to the 32 Torr data of Fig. 4.2, and the sequence pumping power was 500 kW/cm^2.

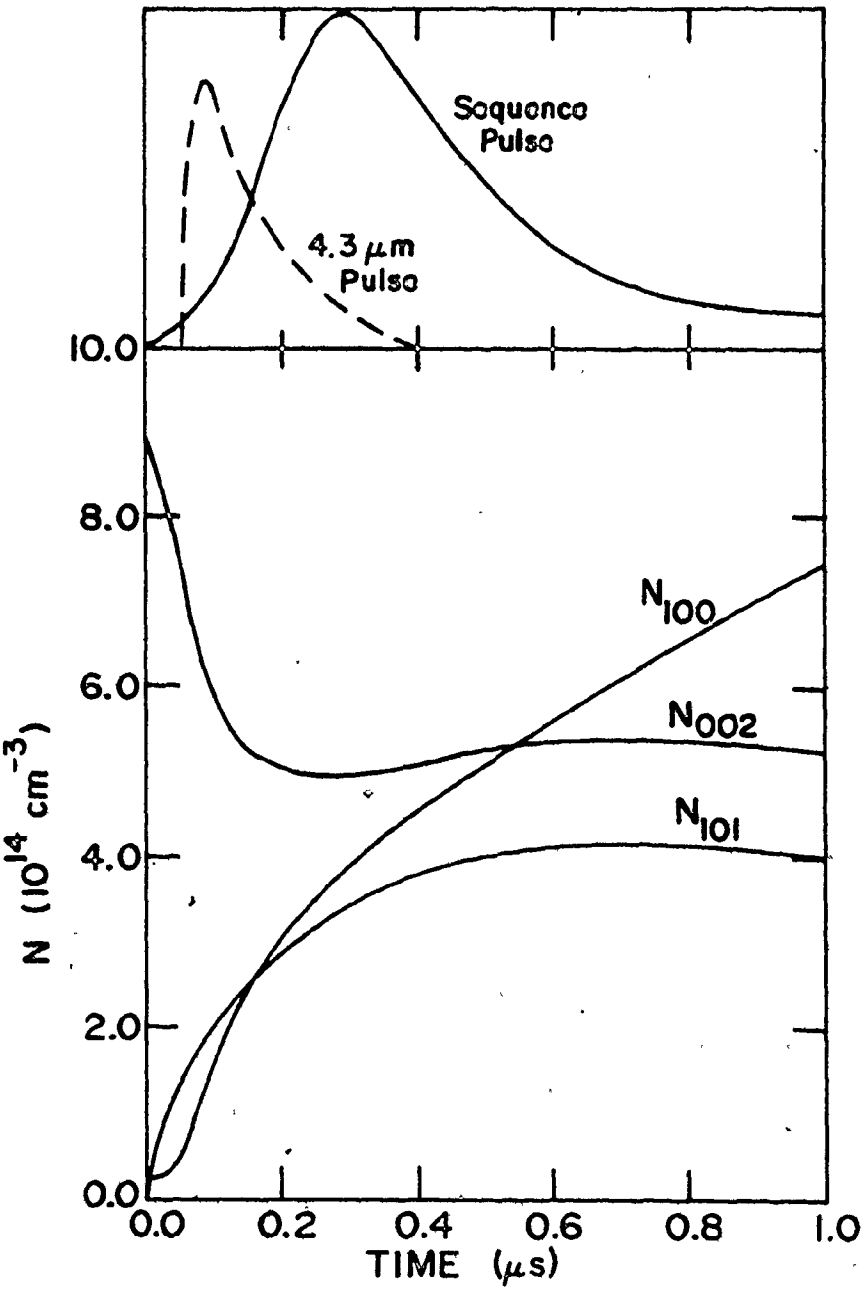
Sequence Pulse
4.3 μm Pulse
10.0
8.0
6.0
4.0
2.0
0.0
N (10^14 cm^-3)
N100
N002
N101
0.0
0.2
0.4
0.6
0.8
1.0
TIME (μs)

From Fig. 4.7, it is apparent that the sequence pumping radiation is able to maintain the $10^0 1$ population well above its equilibrium value despite the rapid collisional de-activation of this level. Unfortunately, the collisional relaxation of the $10^0 0$ level proceeds much more slowly and it is the build-up of population in the $10^0 0$ level that ultimately reduces the 4.3-μm gain below threshold. By using the rate equation model, it was determined that this behavior is common to a large range of experimental conditions, from low pressure continuous discharges to TEA pulsed laser discharges. These results identify three possible regimes in which the 4.3-μm CO_2 laser can operate. The regimes, which can be characterized by considering the $10^0 1$ lifetime, τ_{101}, relative to the duration of the sequence pumping pulse, τ_p (typically, several hundred ns), are as follows: i) $\tau_{101} << \tau_p$: This corresponds to the situation in which high pressure (>100 Torr) laser mixtures are pumped by high power ($\sim$ MW/cm^2) sequence pulses. The short $10^0 1$ lifetime (typically 10's of ns) implies that only the initial portion of the sequence pump pulse would provide useful optical pumping, thereby limiting the energy extraction via 4.3-μm lasing. However, 4.3-μm output powers in excess of 1 MW (from large aperture discharges) and pulse durations less than 10 ns can be expected in this regime. This possibility is examined more fully in Chapter 7. ii) $\tau_{101} \sim \tau_p$: At intermediate pressures (20-100 Torr) and low CO_2 content (< 2%) the $10^0 1$ lifetime is comparable to the sequence pulse duration. Consequently, most of the sequence pulse will provide effective optical pumping, producing 4.3-μm pulses of a few hundred ns duration with output powers in the kW range. The preliminary experiments reported

in Chapter 3 correspond to operation in this regime. iii) $\tau_{10^01} > \tau_p$: In low pressure continuous discharges the lifetimes of the 10^01 and 10^00 levels become relatively long (typically, 5 μs and 50 μs, respectively). Under such conditions the laser is well suited to operation in a high repetition rate ($\gtrsim$ 1 kHz) Q-switched mode, resulting in moderately high 4.3-μm average output powers (> 0.1 W). This mode of operation is described in the next Chapter.

4.6 Summary

A rate-equation model of the 4.3-μm laser is presented in this Chapter. The model is an expanded version of standard CO_2 laser models and good agreement is found between the model predictions and experimental results. This allows the model to be used as a means of predicting the populations of the relevant vibrational levels as a function of time. In this manner, an accurate description of 4.3-μm laser dynamics can be given. The importance of the collisional relaxation rates of the 10^01 and 10^00 levels is discussed. The short lifetime of the 10^01 level is shown to be a crucial factor in 4.3-μm gain dynamics. The results of this Chapter are used to identify the three different regimes in which the laser can operate. The low power pulsed regime was described in Chapter 3 and the remainder of this thesis is devoted to the other two modes of operation. Q-switched 4.3-μm lasing is discussed in the next Chapter, while high power pulsed operation is covered in Chapters 6 and 7.

CHAPTER 5

Q-SWITCHED 4.3-μm LASING

5.1 Introduction

The description of the 4.3-μm laser gain dynamics given in the previous Chapter indicates that the laser is well suited for operation in a rapidly Q-switched mode. In particular, the train of sequence pump pulses produced by Q-switching the sequence laser should, under proper operating conditions, produce a corresponding train of 4.3-μm laser pulses. Potentially, this will result in high 4.3-μm average output powers. This Chapter describes the techniques employed in the production of Q-switched 4.3-μm lasing and discusses one possible application of such a laser.

The experimental apparatus is described in Sect. 5.2. Particular emphasis is given to Q-switching of sequence lasers since this has not been previously reported in the literature. The operating conditions under which Q-switched 4.3-μm lasing can be achieved are given in Sect. 5.3. Section 5.4 describes how a conventional CO_2 laser, containing a single discharge tube, can be converted to operation at 4.3 μm. The use of 4.3-μm lasers to probe CO_2 laser discharges is discussed in Sect. 5.5.

5.2 Experimental Apparatus

The experimental apparatus is shown schematically in Fig. 5.1 and photographically in Fig. 5.2. The single-cavity configuration

Fig. 5.1

Schematic diagram of the Q-switched 4.3-μm laser.

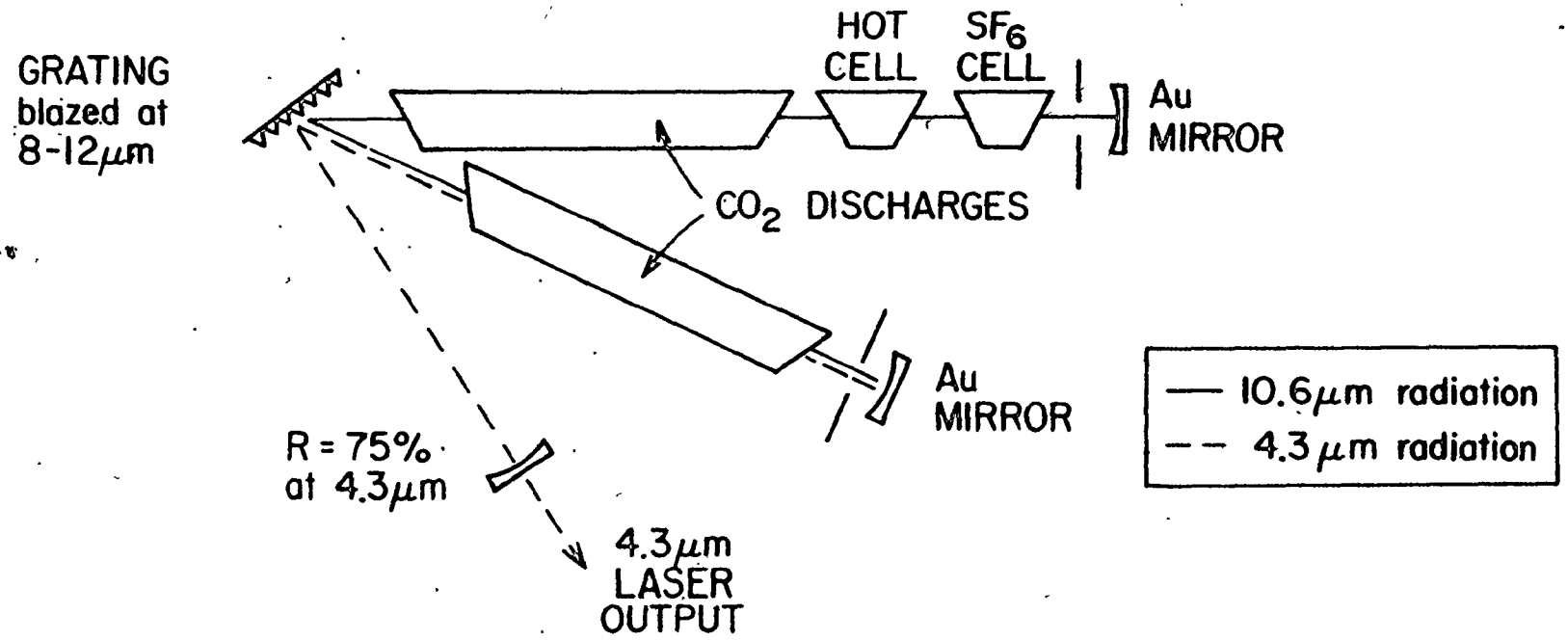
GRATING
blazed at
8-12μm
HOT
CELL
SF6
CELL
Au
MIRROR
CO2 DISCHARGES
Au
MIRROR
R = 75%
at 4.3μm
4.3μm
LASER
OUTPUT
10.6μm radiation
4.3μm radiation

Fig. 5.2

Photograph of the Q-switched 4.3-μm laser. The solid line indicates the path of the 10.6-μm sequence radiation whereas the dashed line represents the 4.3-μm radiation.

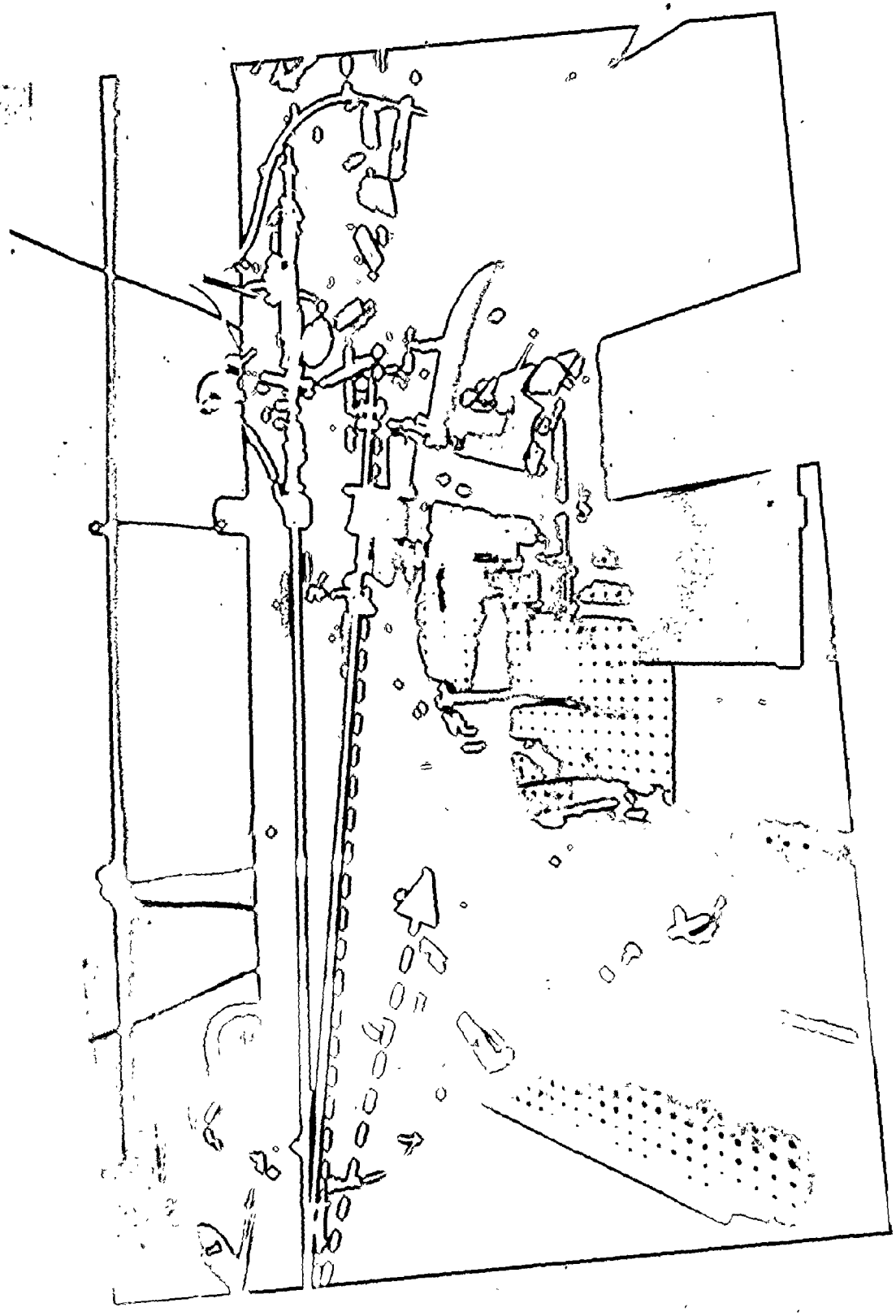

employed is well suited to the use of Q-switched sequence pump pulses since it possesses a low threshold pumping power, as discussed in Sect. 3.4. For Q-switched operation, both discharges are operated continuously. The two discharge tubes are identical, having an active length of 1.0 m and a bore diameter of 1.5 cm. Both tubes are methanol cooled in order to maintain the wall temperatures at ∿260 K. Since the gain per pass in a continuous discharge is lower than that in a pulsed discharge, the long hot cell (Sect. 3.2) necessary for the pulsed work can be replaced by a shorter cell. This allows the use of shorter cavities and a corresponding reduction in diffraction losses [60]. The short hot cell is shown in Fig. 5.3. This cell has a quartz body, is 25 cm long and is sealed with NaCl Brewster windows. It contains an internal heater coil wound from Nichrome wire as shown in Fig. 5.3. Complete details of hot cell construction can be found in Ref. [55]. Sequence oscillation can be attained with ∿50 Torr of CO_2 in the cell at a temperature of 600 K. However, the substantial difference in gain and absorption lengths (2 m and 25 cm, respectively) restricts operation to sequence lines well removed from nearby regular lines (i.e. the strongest sequence lines such as P(19) and P(21) cannot be used). Consequently, the P(25) 10.6-μm sequence transition was used for most of the work reported in this Chapter.

Although any technique for Q-switching the sequence laser would be suitable for the production of 4.3-μm lasing, a passive technique was used because of its simplicity and high-repetition rate capabilities. Passive Q-switching of regular CO_2 lasers has been studied extensively

Fig. 5.3

Photograph of the hot cell used in the Q-switched 4.3-μm laser. Also shown is the Nichrome wire heater coil.

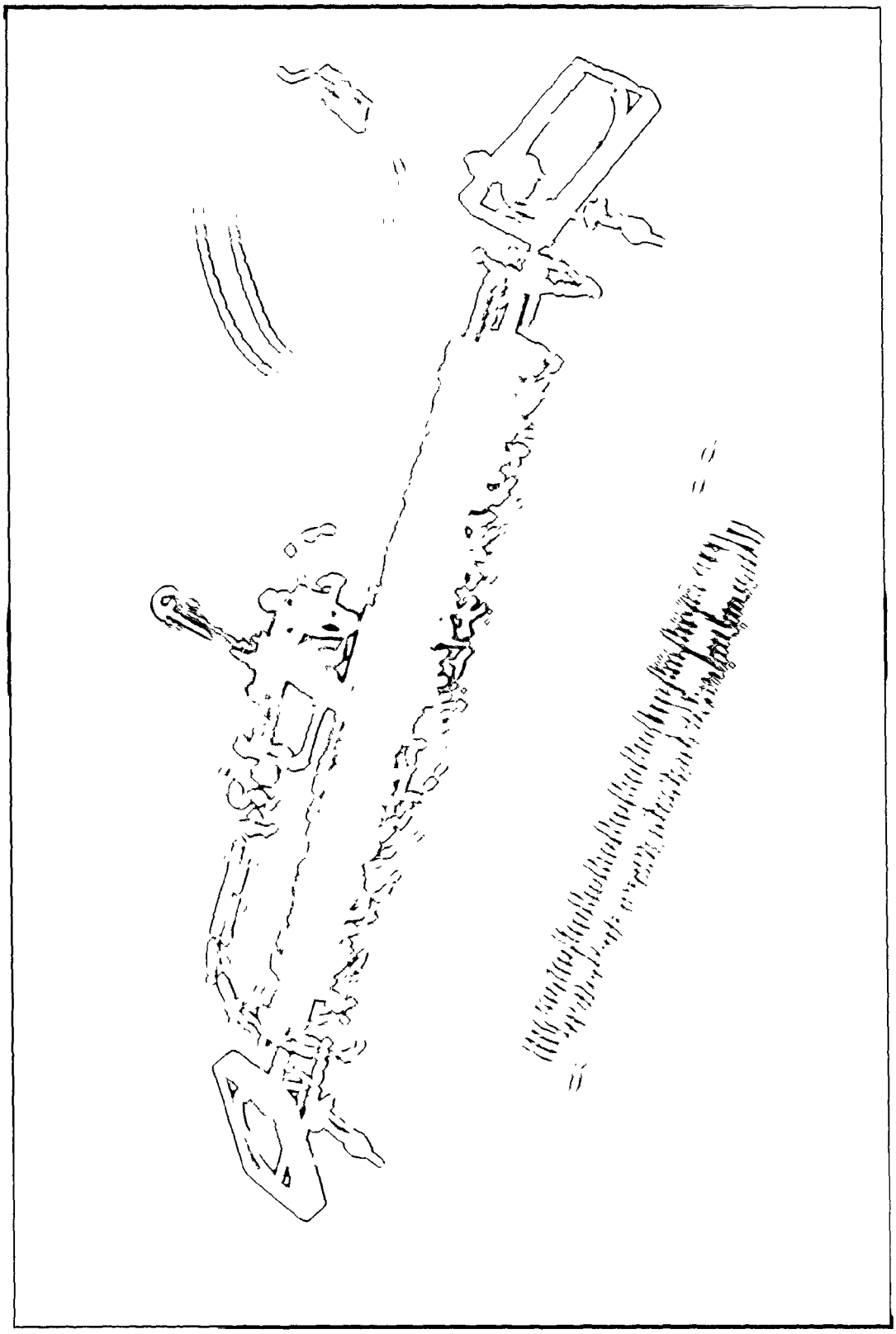

[61-63], whereas Q-switching of sequence CO_2 lasers has not been reported previously. However, the results obtained with regular CO_2 lasers were found to be readily applicable to the case of sequence CO_2 lasers, due to the similarities in the gain dynamics of the two systems (Ref. [8] and Chpt. 6). Q-switching of the sequence laser was achieved by placing a short (10 cm) cell containing SF_6 inside the optical cavity, as shown in Fig. 5.1. The range of SF_6 pressures for which Q-switching was observed depended on the laser transition. For example, the P(25) 10.6-μm line could be Q-switched with 0.5-1.0 Torr of SF_6 in the cell, whereas more weakly absorbing lines such as P(29) required SF_6 pressures of ∿2 Torr. This behavior is consistent with the known absorption coefficients of SF_6 in the 10.6-μm region [64]. When sufficient SF_6 has been added to just Q-switch the laser, the temporal pulse shapes comprise of an ∿500 ns (FWHM) Q-switched spike followed by a long tail lasting over 100 μs. The long pulse tails have also been observed when SF_6 is used to Q-switch regular CO_2 lasers [62]. The tails could be eliminated and the repetition rate increased by the addition of several Torr of He buffer gas. The sequence pulses were now ∿500 ns (FWHM). For the P(25) sequence line, repetition rates ranged from 1 kHz for 0.5 Torr of pure SF_6 in the absorber cell to 40 kHz for 0.5 Torr of SF_6 and ∿15 Torr of He. The average 10.6-μm output power (monitored using the zeroeth order reflection off the grating) increased from ∿1/10 to ∿1/3 of the cw output power (∿1 W) as the repetition rate was increased. Furthermore, both the repetition rate and peak powers were found to be extremely sensitive to cavity length tuning and hence a piezo-electric transducer was used to achieve

maximum output. In general, the observed behavior for the Q-switched sequence laser was very similar to that observed in Ref. [62] for regular CO_2 lasers. The only significant difference is the need for a lower small-signal absorption loss (i.e., shorter absorption cell length or lower SF_6 pressure) in the case of sequence Q-switching, due to the reduced gain present.

5.3 Results and Analysis

Each discharge tube was operated with a flowing gas mixture containing 70%He:24%N_2:6%CO_2 at a total pressure of 8 Torr and a current of 15 mA. The cavity was initially aligned to operate on the P(25) sequence line and sufficient SF_6 and He added to the absorber cell to produce stable Q-switched sequence pulses without pulse tails*. The Q-switched sequence pulses saturate the (00^02 - 10^01) transition, increasing the $[10^01]_1$ population and causing the 4.3-μm cascade to occur. Each sequence pulse produced a 4.3-μm pulse, the start of which was delayed ∿400 ns from the start of the sequence pulse. The average output power on the directly coupled P(26) (10^01 - 10^00) transition was 25 mW at a repetition rate of 6 kHz.†

Typical pulse shapes are shown in Fig. 5.4. The peak output powers of the sequence and 4.3-μm pulses were 20 W and 25 W respectively. The pulse-to-pulse stability of the 4.3-μm output was excellent, as shown in Fig. 5.4(c). The repetition rate of the 4.3-μm pulses could be

---

*Tails on the sequence pump pulses are detrimental to 4.3-μm lasing since they effectively slow the rate at which the 10^00 level empties.

†Average output powers were measured using a Scientech Inc. Laser Power Meter Model 360001.

Fig. 5.4

Temporal dependence of the laser output: a) P(25) 10.6-μm sequence pulse, b) P(26) 4.3-μm pulse, c) train of 4.3-μm pulses. The risetime of the detection system is 10 ns. The arrow in a) indicates the position of the peak of the 4.3-μm pulse relative to the sequence pulse.

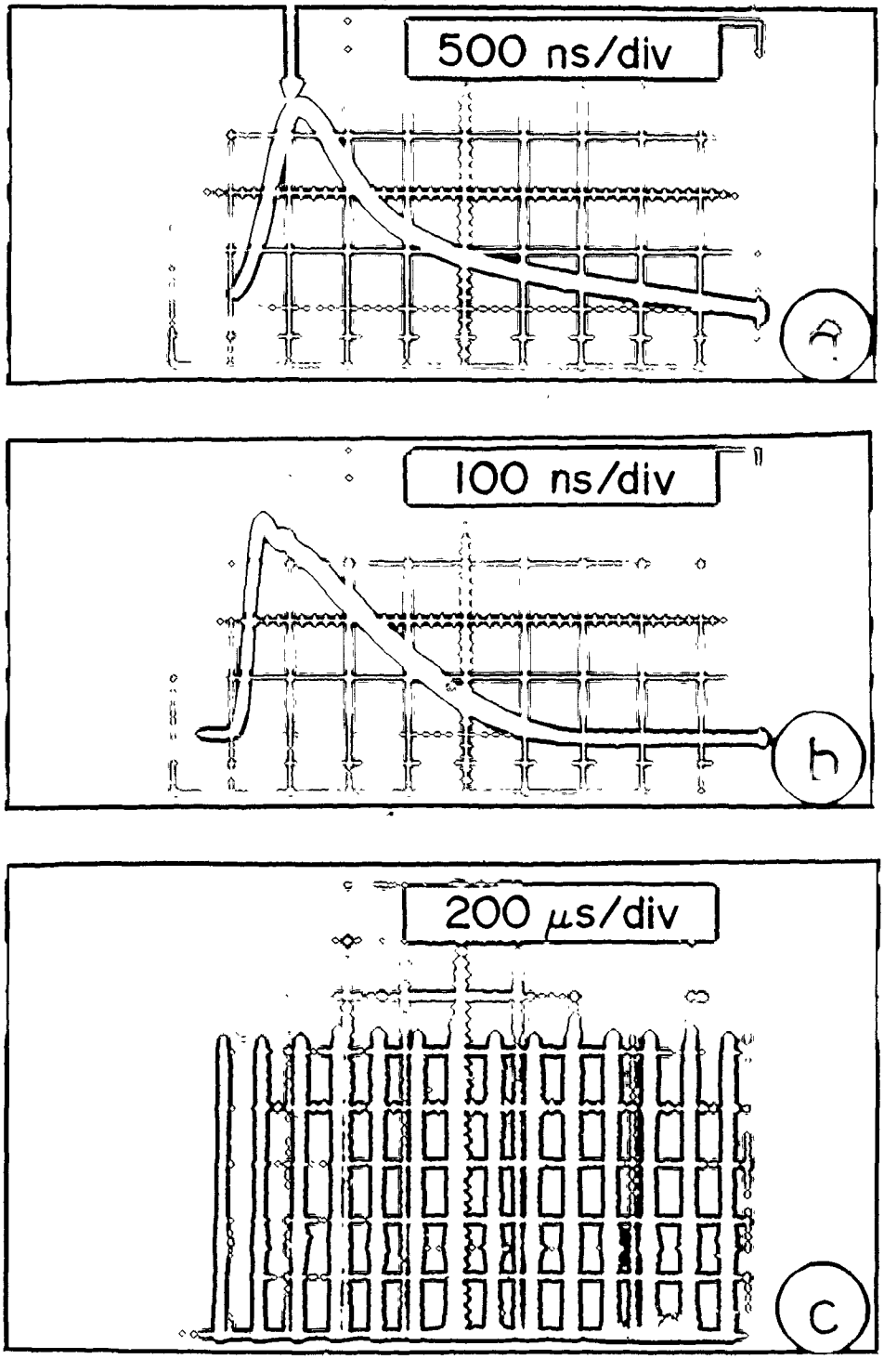
500 ns/div
a
100 ns/div
b
200 μs/div
c

increased to >10 kHz, but with reduced average output power, as shown in Fig. 5.5. This reduction is attributed to the inability of the $10^0 0$ level to empty completely between pulses once the pulse separation approached a V-T relaxation time (50 μs [45] for the present mixture).

The 4.3-μm output could be tuned over several rotational lines in the $(10^0 1 - 10^0 0)$ band by rotating the 4.3-μm output coupler. Alternatively, the grating could be rotated to select another sequence pump line and the 4.3-μm output coupler adjusted accordingly. In general, the tunability was similar to that reported in Chapter 3 for the TE 4.3-μm CO_2 laser with maximum 4.3-μm output occurring on the P(20), P(22) and P(26) transitions.

Also shown in Fig. 5.5 is the effect of adding 2% Xe to the discharge tube in the common (i.e., both 10.6-μm and 4.3-μm radiation present) branch of the cavity. The energy per pulse was increased and the laser could be operated at higher repetition rates, resulting in a substantial increase in the average output power. The maximum output power observed under these conditions was 120 mW. The principal effect of adding Xe to a CO_2 laser discharge is a decrease in the rate of dissociation, particularly at higher discharge currents [65]. This has been attributed to the large Xe cross-section for high energy electrons [65]. The net result is a higher value of T_3 in the discharge, and consequently a larger number of molecules taking part in 4.3-μm lasing.

5.4 4.3-μm Cascade Laser

The use of two discharge tubes in the Q-switched 4.3-μm laser shown in Fig. 5.2 followed from the work on pulsed 4.3-μm lasing

Fig. 5.5

Dependence of average 4.3-μm output power on repetition rate. The crosses correspond to a 84%He:11%N_2:5%CO_2 mixture at 7 Torr total pressure and a discharge current of 15 mA in the discharge tube in the common branch (see text) of the cavity. The dots represent a 82%He:11%N_2:5%CO_2: 2%Xe mixture at 7 Torr total pressure and a current of 20 mA. In both cases the discharge in the 10.6-μm branch of the cavity was operated using a 74%He:17%N_2:9%CO_2 mixture at 11 Torr total pressure and a discharge current of 16 mA. A 50% transmitting 4.3-μm output coupler was used.

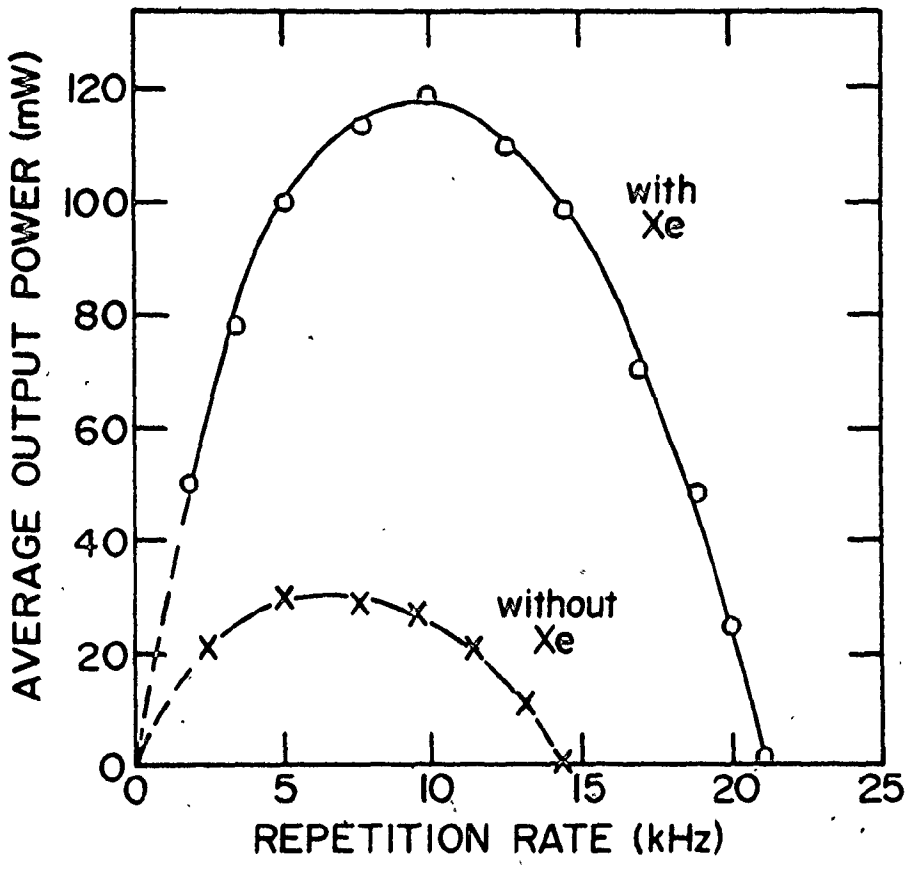
AVERAGE OUTPUT POWER (mW)
120
100
80
60
40
20
0
0
5
10
15
20
25
REPETITION RATE (kHz)
with Xe
without Xe

reported in Chapter 3. However, in the case of the Q-switched laser the two tubes can be operated under identical conditions. Thus the function of the discharge tube in the 10-μm branch of the cavity is solely to increase the sequence pumping power. Under certain operating conditions this tube could be switched off and the 4.3-μm laser would operate using only the remaining discharge tube.

Figure 5.6 is a schematic diagram of the 4.3-μm cascade laser. The discharge was operated with a flowing gas mixture containing 82%He:11%N_2:5%CO_2:2%Xe at a total pressure of 7 Torr and a current of 20 mA. The conditions in the hot cell and the SF_6 cell were similar to those reported in Section 5.2. The average 4.3-μm output power was 40 mW at a repetition rate of 10 kHz. The output characteristics of the cascade laser were very similar to those observed when the laser was operated using two discharge tubes. However, use of the single discharge tube greatly simplifies the cavity design. The only significant difference between the 4.3-μm cascade laser and a conventional CO_2 laser is the presence of the in-cavity hot CO_2 cell. Furthermore, proper scaling of the discharge tube and hot cell length, together with the use of careful cavity design to reduce diffraction losses will result in a substantial increase in 4.3-μm output. The development of high power cw sequence lasers [8] suggests that average 4.3-μm output powers in excess of 1 W should be attainable. Another possible improvement is the use of a sealed-off discharge tube and isotopic forms of CO_2. In this manner the tuning range of the laser could be greatly extended, resulting in the generation of numerous laser lines having reasonable output powers in the 2220-2320 cm^{-1} range.

Fig. 5.6

Schematic diagram of the 4.3-μm cascade laser.

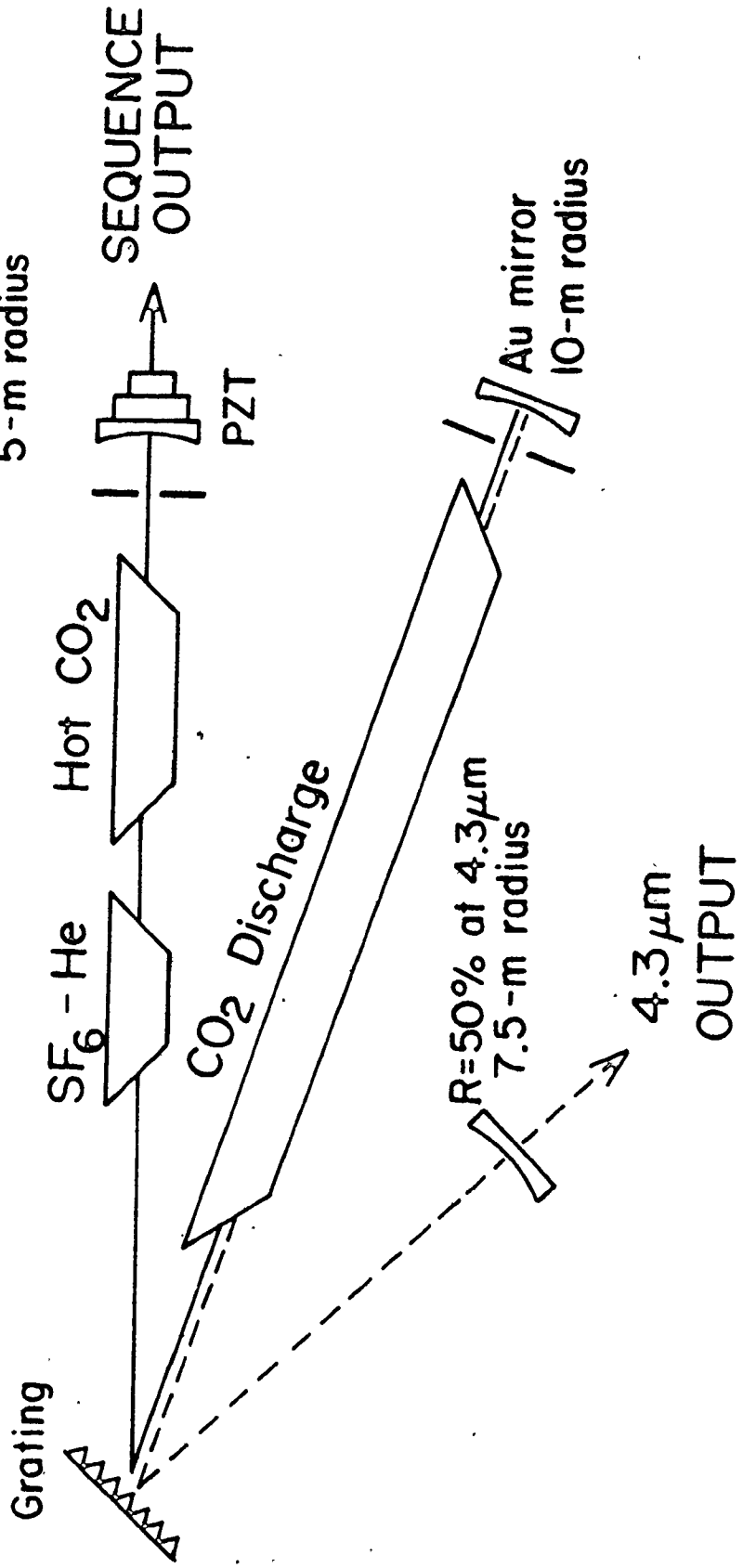
R=95% at 10.6μm
5-m radius
SEQUENCE
OUTPUT
PZT
Au mirror
10-m radius
Hot CO_2
SF_6 - He
CO_2 Discharge
R=50% at 4.3μm
7.5-m radius
4.3μm
OUTPUT
Grating

5.5 Application to the Study of CO_2 Laser Dynamics

The previous sections were concerned with the development of a simple Q-switched 4.3-μm laser. One particularly interesting application of such a laser is in the study of CO_2 laser dynamics. This section describes a series of experiments which demonstrate the usefulness of the 4.3-μm laser in such studies.

Since the lower level of the 4.3-μm laser transitions is the same as that of the regular 10.4-μm laser band, the 4.3-μm laser can be used as a probe to monitor the population of the 10^00 level in a pulsed CO_2 laser.* Although attempts have been made in the past to use 10-μm CO_2 lasers for this purpose [41,42], these lasers are only capable of providing information on the population difference between the 10^00 level and the heavily populated 00^01 level. In contrast, the 4.3-μm upper level, 10^01, is essentially empty during a CO_2 laser discharge. Therefore, monitoring the absorption on one of the 4.3-μm laser transitions provides a direct measurement of the 10^00 population.

In the following experiment a Q-switched 4.3-μm laser is used to monitor the absorption on the (10^00-10^01) transition in a pulsed CO_2 discharge. In this manner, the population of the 10^00 level can be monitored as a function of time, and the rate at which the level population relaxes can be ascertained. The 4.3-μm laser is identical to the one described in Sect. 5.2, except that the Q-switching is

*Tunable diode lasers can be used in a similar manner for continuous discharges. However, they are unsuitable for operation in the high electrical noise environment of pulsed CO_2 lasers.

achieved using a rotating mirror (at ∿100 Hz) rather than an in-cavity SF_6 cell. This provides for a simple means of synchronizing the probe pulses and the pulsed discharge. Specifically, a 6328 Å HeNe laser "trigger" beam is also reflected from the rotating mirror, before it comes into alignment with the sequence branch of the 4.3-μm laser cavity. The reflected trigger beam is then directed onto a photodiode and the resulting train of pulses fed to a repetition rate control unit [66]. In this manner, the time delay between the discharge and the probe pulse could be varied from 2 μs to 100 μs. The 4.3-μm probe beam is gently focussed into a 30-cm long helical pin discharge containing a 97%He:3%CO_2 mixture. The pressure in the discharge is monitored using two vacuum gauges placed at the inlet and outlet of the discharge tube. For each pressure, absorption measurements were made as a function of time delay from where the discharge is fired.

A set of typical results is shown in Fig. 5.7. The straight lines indicate the presence of a single exponential decay in the absorption and hence in the population of the $10^0$0 level. (Generally this decay is followed by a much slower decay in the absorption, not shown in Fig. 5.7, which is attributed to diffusion). The slopes of the lines in Fig. 5.7 correspond to the decay rate and Fig. 5.8 shows a plot of these decay rates as a function of pressure. The measured rate constant is $3.1\pm0.4 \times 10^4$ s^{-1} $Torr^{-1}$. This is in good agreement with the accepted value of the vibration-to-translation (V-T) relaxation rate for He-CO_2 collisions (3.27×10^4 s^{-1} $Torr^{-1}$ [45]). As noted in Sect. 2.4, N_2 and CO_2 have much slower rate constants for this process. It was verified experimentally that large increases in either the N_2

Fig. 5.7

Measured absorptions on the P(26) ($10^{0}0$-$10^{0}1$) transition as a function of time delay from the start of the discharge (t = 0). The gas mixture used was 97%He:3%CO_2. αL = 0 represents the transmission through the unexcited gas mixture and the curves have been scaled to give the same value of αL at t = 4 μs.

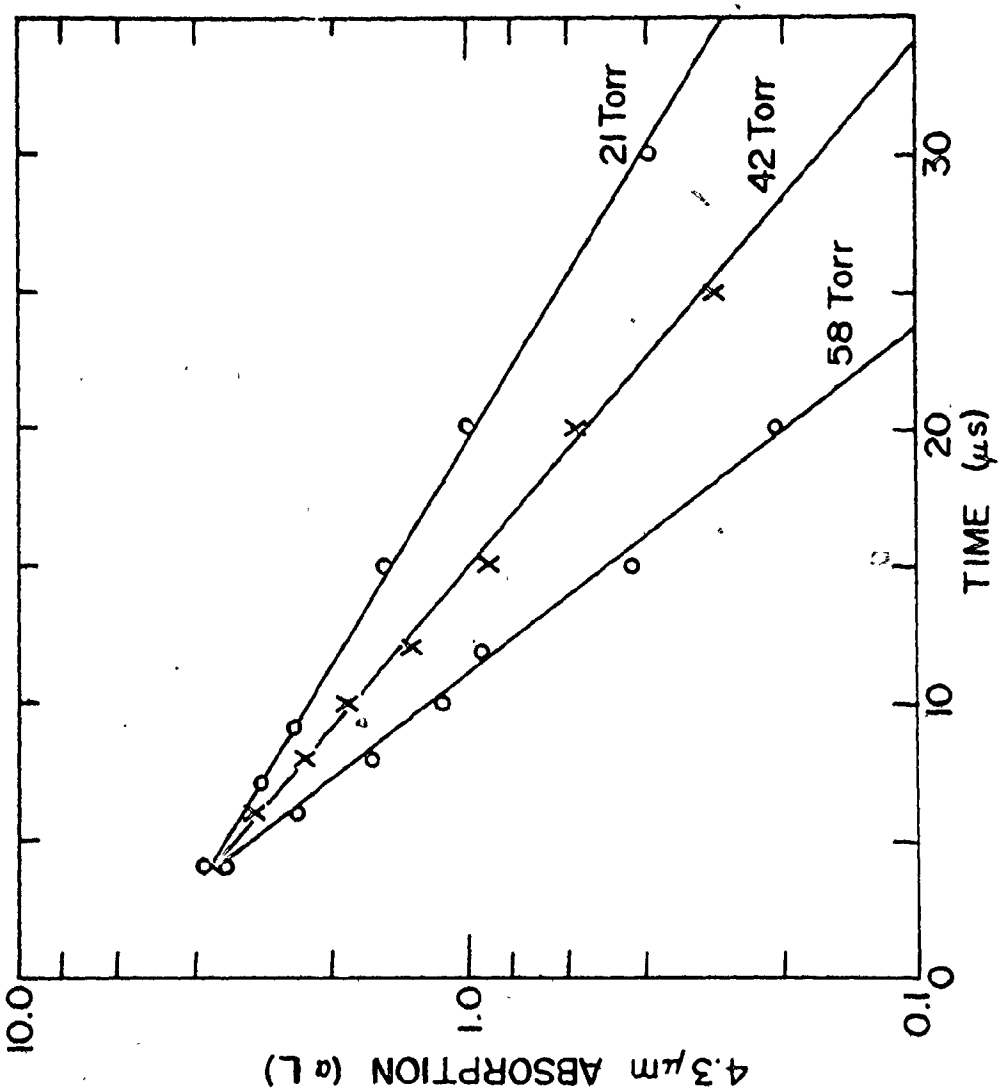
21 Torr
42 Torr
58 Torr
10.0
1.0
0.1
0
10
20
30
TIME (μs)
4.3μm ABSORPTION (α L)

Fig. 5.8

Plot of observed relaxation rate (see Fig. 5.7) as a function of total pressure using a 97%He:3%CO_2 mixture. The associated rate constant is $3.1 \pm 0.4 \times 10^4$ s^{-1} $Torr^{-1}$.

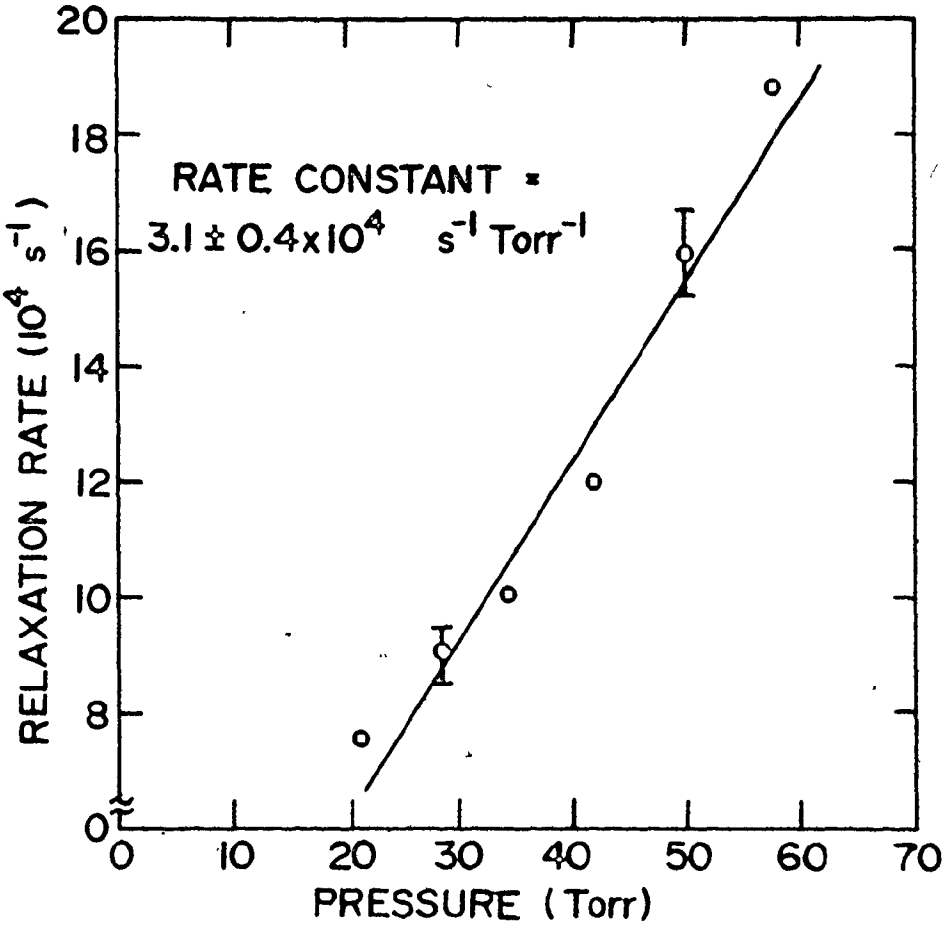
RATE CONSTANT =
3.1 ± 0.4x10^4 s^-1 Torr^-1
RELAXATION RATE (10^4 s^-1)
PRESSURE (Torr)
0
8
10
12
14
16
18
20
0
10
20
30
40
50
60
70

or CO_2 content of the gas mixture had little effect on the measured rates. The results reported here confirm that energy deposited by the discharge into the combined bending-stretching modes of CO_2 decays away at a V-T relaxation rate. This decay also corresponds to the risetime of the gain on the regular CO_2 laser transitions as shown in Ref. [51]. What is particularly significant about the above results is that the small absorptions present after several V-T relaxation times (i.e. at the time of peak gain) correspond to $10^0 0$ level populations which are <0.15% of the total number of CO_2 molecules. This corresponds to a T_1 of ~310 K. Some earlier studies of CO_2 lasers concluded that a substantial population existed in the $10^0 0$ level at the peak of the gain, a conclusion which was disproved in Ref. [17]. The measurements reported here provide direct experimental evidence that the $10^0 0$ level is effectively empty at the gain peak, thereby supporting the results of Ref. [17].

The present experiment demonstrates the utility of the 4.3-μm laser for monitoring the $10^0 0$ level population in a CO_2 laser discharge. Since the measurements were made in the absence of 10-μm lasing however, no information can be obtained on the faster rates by which the various levels within the BS mode couple. Rather, it is only the relaxation rate of the entire mode which is observed. It would be of considerable interest to probe the $10^0 0$ level population after passage of a high power 10.6-μm laser pulse, and thereby measure the rate at which the $10^0 0$ level couples to the remainder of the BS mode. As was discussed in Sect. 2.5, a large range of values have been reported

for this rate and discrepancies persist between "accepted" values [41,42]. A serious limitation in the techniques previously used to monitor the $10^{0}0$ level population has been that 9 or 10-μm probe beams can actually only determine population differences, as mentioned earlier. Use of the 4.3-μm laser would eliminate this problem. The experiment would proceed in a manner similar to the one described above, except that absorption measurements would be made after passage of a laser pulse (generated externally or in the discharge itself). The present apparatus is incapable of maintaining accurate time synchronization over the short time intervals (0.1-2.0 μs) involved in such an experiment. However, the use of a more sophisticated means of Q-switching (e.g., electro-optic or acousto-optic techniques), together with a stable source of 10-μm pulses would overcome this restriction. The importance of the $10^{0}0$ level coupling rate to the dynamics of CO_2 lasers suggests that this type of experiment merits further investigation.

5.6 Summary

This Chapter has dealt with Q-switched operation of the 4.3-μm laser. Passive Q-switching of a sequence CO_2 laser was reported for the first time, and this was incorporated into the intra-cavity configuration described in Chapter 3. The Q-switched sequence pulses were used to produce 4.3-μm lasing resulting in 4.3-μm average output powers of 120 mW. The laser is scalable and output powers in excess of 1 W appear feasible. Under a restricted range of operating conditions the Q-switched laser can be operated using only a single discharge tube, resulting in what may appropriately be termed a 4.3-μm cascade laser.

This cascade laser is very similar to a conventional CO_2 laser, except that a hot cell has been placed inside the optical cavity. Applications of the Q-switched 4.3-μm laser will be discussed in Chapter 8 although one important application, that of probing a regular CO_2 laser discharge, was presented here. The V-T relaxation rate of He on CO_2 was measured and it was shown that the $10^{\circ}0$ level is empty at the time of peak regular gain. In Chapter 7 the Q-switched 4.3-μm laser is used in a similar manner to measure 4.3-μm absorption to higher discharge pressures, which, as will be shown, is an important consideration in the scalability of the 4.3-μm laser.

CHAPTER 6

DESIGN OF EFFICIENT TEA SEQUENCE LASERS

6.1 Introduction

It was established in Sect. 4.4 that the present technique for producing 4.3-μm lasing was well suited to two modes of operation: a low pressure Q-switched mode and a high pressure pulsed mode. Q-switched operation of the laser, as described in the previous chapter, was based on previously reported techniques for producing high power cw sequence lasing [8]. The production of high 4.3-μm output powers from pulsed discharges requires the use of high power pulsed sequence lasers, which had not been developed at the time this research was undertaken. The design of efficient TEA sequence lasers is the subject of this Chapter. In Chapter 7 the application of these lasers to the production of 4.3-μm lasing is considered.

Laser emission in the $(00^{o}2\text{-}10^{o}1)$ and $(00^{o}2\text{-}02^{o}1)$ sequence bands of CO_2 was first reported by Reid and Siemsen in 1976 [7,8]. They employed an in-cavity hot CO_2 cell to convert a conventional cw CO_2 laser to operation on the sequence lines, and were able to obtain cw output powers equivalent to ~50% of the regular output power from the same laser. In general, the sequence bands are very similar to the regular laser bands but the small anharmonicity of the CO_2 molecule causes the frequencies of the sequence laser lines to lie between those of the regular lines. Consequently, cw sequence

lasers found immediate use in applications such as optical pumping of molecular gases to produce FIR lasers [67]. In principle, the sequence bands also provide a simple means of translating the inherent advantages of regular TE CO_2 lasers to a new set of frequencies, with corresponding applications to optical pumping, laser isotope separation, laser photochemistry and non-linear optics. Recently, several groups have produced sequence laser pulses from TE CO_2 oscillators [18-20]. However, none of these experiments with pulsed lasers were very successful, and maximum output energies ranged from 50 to 185 mJ per pulse.

The use of sequence lasers to produce 4.3-μm lasing led to a re-examination of the possibility of obtaining efficient sequence operation from a conventional TEA CO_2 laser. Through the use of an in-cavity hot cell and a commercial TEA discharge, sequence pulses with energies as high as 6J have been obtained, as reported in Ref. [68]. More than 30 sequence lines having output energies greater than 2 J were observed from a grating-tuned cavity. Since the sequence lines differ in frequency from the regular CO_2 laser lines this result represents a significant improvement in the line-tunability obtainable from a TEA CO_2 laser. Furthermore, any conventional TEA CO_2 laser can be converted to operation on the sequence lines simply by incorporating a hot CO_2 cell inside the optical cavity.

The purpose of this Chapter is to outline the design criteria for construction of high energy TEA sequence CO_2 lasers. Although use of the in-cavity hot cell is a simple technique to implement, certain considerations must be taken into account if efficient

sequence operation is to be achieved. Otherwise output energies are low as can be seen from the values reported in Refs. [18-20]. In the following section, a theoretical model is presented which is suitable for both regular and sequence operation of TEA CO_2 lasers. Sections 6.3 and 6.4 discuss the importance of the various gain and loss mechanisms. Factors such as hot cell length, temperature and operating pressure, discharge length, and degree of excitation in the discharge are shown to be important considerations. It is demonstrated that in-cavity hot CO_2 cells are an effective means of achieving efficient TEA sequence lasing, contrary to the conclusions of Ref. [18]. Several applications of high power sequence lasers are described in Sect. 6.5.

6.2 Theory

To obtain a better understanding of the gain dynamics of a TEA CO_2 laser operating on either the regular or sequence bands, a rate equation model of the system was developed. The model is similar to other CO_2 laser models [15-17] except that separate equations are used to describe the populations of the upper and lower laser levels, as was done in the 4.3-μm laser model presented in Chapter 4. The sequence laser model is described in detail below. The model describing operation on the regular bands is similar except that the equations (see Appendix B) are adjusted to account for the different levels involved.

The eight differential equations governing sequence operation of a TEA CO_2 laser are as follows:

$$\frac{dN_{002}}{dt} = -fgc\delta\rho - \frac{2(N_{002}-N^e_{002}(T_3))}{\tau_{\nu_3}} \tag{6.1}$$

$$\frac{dN_{101}}{dt} = fgc\delta\rho - \frac{N_{101}-N^e_{101}(T_1,T_3)}{\tau_{101}} \tag{6.2}$$

$$\frac{dN_{100}}{dt} = \frac{N_{101}-N^e_{101}(T_1,T_3)}{\tau_{101}} - \frac{N_{100}-N^e_{100}(T_1)}{\tau_{100}} \tag{6.3}$$

$$\frac{dE_{BS}}{dt} = N_e(t)N_{CO_2}h\nu_{BS}X_{BS} + \frac{E_3}{\tau_3} + \frac{E_{100}-E^e_{100}(T_1)}{\tau_{100}} - \frac{E_{BS}-E^e_{BS}(T)}{\tau_{VT}} \tag{6.4}$$

$$\frac{dE_3}{dt} = N_e(t)N_{CO_2}h\nu_3X_3 + \frac{E_4-E^e_4(T_3)}{\tau_{N_2}} + \left(\frac{\nu_3}{\nu_1+\nu_3}\right)\frac{E_{101}-E^e_{101}(T_1,T_3)}{\tau_{101}} + \frac{2(E_{002}-E^e_{002}(T_3))}{\tau_{\nu_3}} - \frac{E_3}{\tau_3} \tag{6.5}$$

$$\frac{dE_4}{dt} = N_e(t)N_{N_2}h\nu_3X_4 - \frac{E_4-E^e_4(T_3)}{\tau_{N_2}} \tag{6.6}$$

$$\frac{d\delta}{dt} = -2fgc\delta\rho - \frac{\delta-K(J)(N_{002}-N_{101})}{\tau_R} \tag{6.7}$$

$$\frac{d\rho}{dt} = fgc\delta\rho - \alpha c\rho - \frac{\rho}{\tau_c} + \gamma K(J)N_{002} \tag{6.8}$$

where N_{002} (E_{002}), N_{101} (E_{101}) and N_{100} (E_{100}) are the populations (stored energies) of the respective levels, E_{BS} is the energy stored in the combined bending-symmetric stretching ($\nu_1+\nu_2$) modes, excluding the $10^0 1$ and $10^0 0$ levels [17], E_3 is the stored energy of the ν_3 mode,

excluding the $00^{0}2$ level, E_4 corresponds to the vibrational energy stored in the nitrogen molecules, δ is the rotational inversion (i.e., $\delta = n_{J-1}^{002} - n_{J}^{101}$, where n_{J-1}^{002} and n_{J}^{101} are the populations of the particular rotational levels on which lasing occurs), and ρ is the in-cavity photon density. T_1 and T_3 are the vibrational temperatures of the combined $\nu_1+\nu_2$ mode and the ν_3 mode, respectively, while T represents the translational temperature. Variables denoted with the superscript e represent the equilibrium value of that variable at the temperature indicated in brackets. $K(J)(N_{002}-N_{101})$ is the equilibrium value of the rotational inversion ($K(J) \sim \frac{1}{15}$ for P(20)), and $\gamma K(J) N_{002}$ is the term representing the spontaneous emission, as discussed in Ref. [16]. The parameter g is a constant which relates the rotational inversion to the small signal gain such that the product $g\delta$ is the familiar small-signal gain coefficient in units of cm^{-1}, and f is the cavity filling factor (i.e., ratio of discharge length to total cavity length).

The instantaneous value of the electron density $N_e(t)$ is obtained from the relation [16]

$$N_e(t) = \frac{i(t)}{ev_dA} \tag{6.9}$$

where $i(t)$ is the value of the discharge current at time t, e is the electronic charge, v_d is the electron drift velocity and A is the area of cross-section of the discharge. The X_i's are the effective electron-vibration excitation rates for the vibrational modes (see Sect. 2.4), and $h\nu_3$ and $h\nu_{BS}$ are the energies of one ν_3 quantum and one average BS quantum ($h\nu_{BS} = h(\nu_1+\nu_2)/2$), respectively. Values for the X_i's

and v_d are taken from Ref. [30] and are based on the E/N values obtained from the measured current and voltage pulses.

The various molecular relaxation times are as follows (with the values in the parentheses corresponding to a 73%He:16%N_2:11%CO_2 mixture at a pressure of 1 atm): τ_{v_3} is the v_3 intra-mode coupling time (2.3 ns [35]), τ_{10^01} is the relaxation time of the 10^01 level (2.8 ns [13]), τ_{10^00} is the coupling time between the 10^00 level and the rest of the BS mode (42 ns [41]), τ_{VT} is the vibration-to-translation relaxation time (0.52 μs [45]), τ_{N_2} is the coupling time between the v_3 mode and the excited vibrational levels in the N_2 molecules (0.63 μs [31]), τ_3 is the collisional relaxation time of the v_3 mode (11 μs [31]), and τ_R is the rotational relaxation time (0.17 ns [47]). The cavity decay time τ_c is given by $-2L/c\ \ell nR$ where L is the cavity length, R is the cavity reflectance (see Fig. 6.1) and c is the speed of light.

Notice the presence of the term $\alpha c\rho$ in Eq. (6.8). This represents all losses which are present in the cavity other than the output mirror coupling, and is an important term in the modeling of sequence lasers. Consider Fig. 6.1 which is a schematic diagram of the sequence laser used in Ref. [68]. The optical cavity was formed by a copper mirror and a partially transmitting Ge mirror, and contained a TEA discharge and hot CO_2 cell. The cavity loss per pass $\bar{L}$ is defined as the sum of the internal optical losses $\bar{L}_{opt}$, due to Brewster windows and diffraction losses, etc., and the loss introduced by the hot CO_2 cell, $\alpha_{hot}L_{hot}$. The parameter α appearing in Eq. (6.8) is then

Fig. 6.1

Schematic diagram of a TEA CO_2 sequence laser. Generally M_1 is a total reflector while the reflectance R of M_2 is optimized to give maximum output energy for either regular or sequence operation.

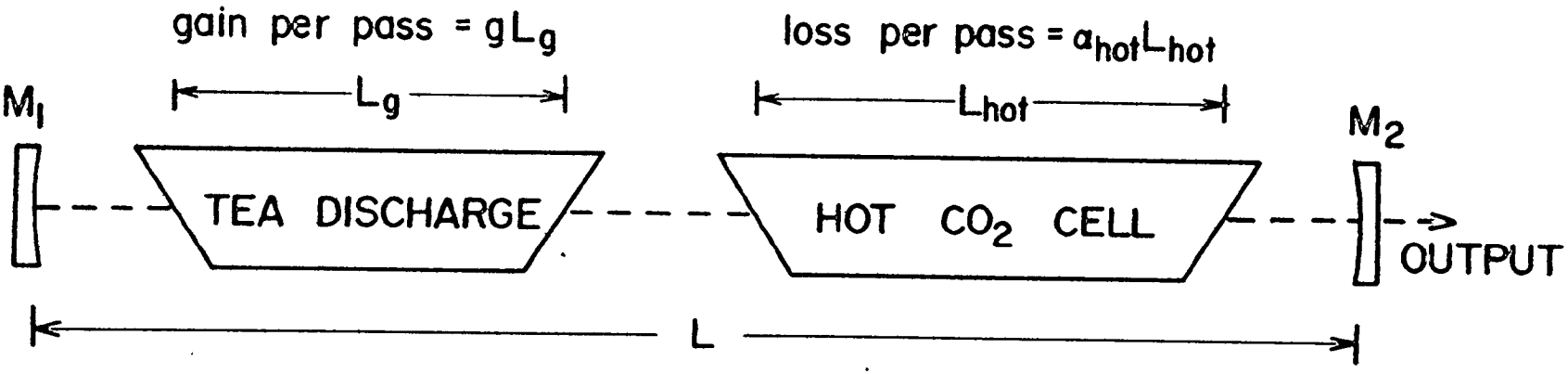
gain per pass = gL_g
loss per pass = $\alpha_{hot}L_{hot}$
M_1
L_g
L_{hot}
M_2
TEA DISCHARGE
HOT CO_2 CELL
OUTPUT
L

given by $\bar{L}$ divided by the total cavity length L. Preliminary applications of the model indicate that the gain dynamics of sequence lasers and regular lasers are similar, and that the differences in laser output are primarily due to the relative magnitudes of the gain and loss terms, in particular of the terms gL_g and $\alpha_{hot}L_{hot}$. Consequently, we decided to investigate these terms in detail and the results are presented in the next section.

6.3 Gain and Loss Considerations

Although in-cavity hot CO_2 cells are a simple and effective means of producing efficient sequence lasers, care must be taken when determining the operating parameters. The most critical parameter is that of hot cell pressure. While the sequence transitions themselves are too high in vibrational energy to produce any absorption at a temperature of ~600 K, absorption at the sequence frequencies can arise due to Lorentz broadening of nearby absorption lines, and this becomes appreciable at pressures in excess of a few hundred Torr. The result is a substantial decrease in sequence output energy, as was noted in Ref. [18].

To determine the absorption at the sequence frequencies in our hot cell, measurements were made of absorption as a function of CO_2 pressure using a cw CO_2 probe laser capable of operation on both the sequence and regular transitions. Results are plotted in Figs. 6.2 and 6.3 for two pairs of lines. As expected the regular transitions experience an order of magnitude more absorption in hot CO_2, but absorption on the sequence transitions becomes appreciable at

Fig. 6.2

Hot cell absorption as a function of CO_2 pressure for the P(18) regular and P(15) sequence lines. $\alpha_{hot} L_{hot} = \ell n\ (I/I_o)$ where I is the transmitted power with CO_2 in the hot cell and I_o is the transmitted power for the hot cell evacuated. The average temperature of the 120-cm "active" region is 600 K.

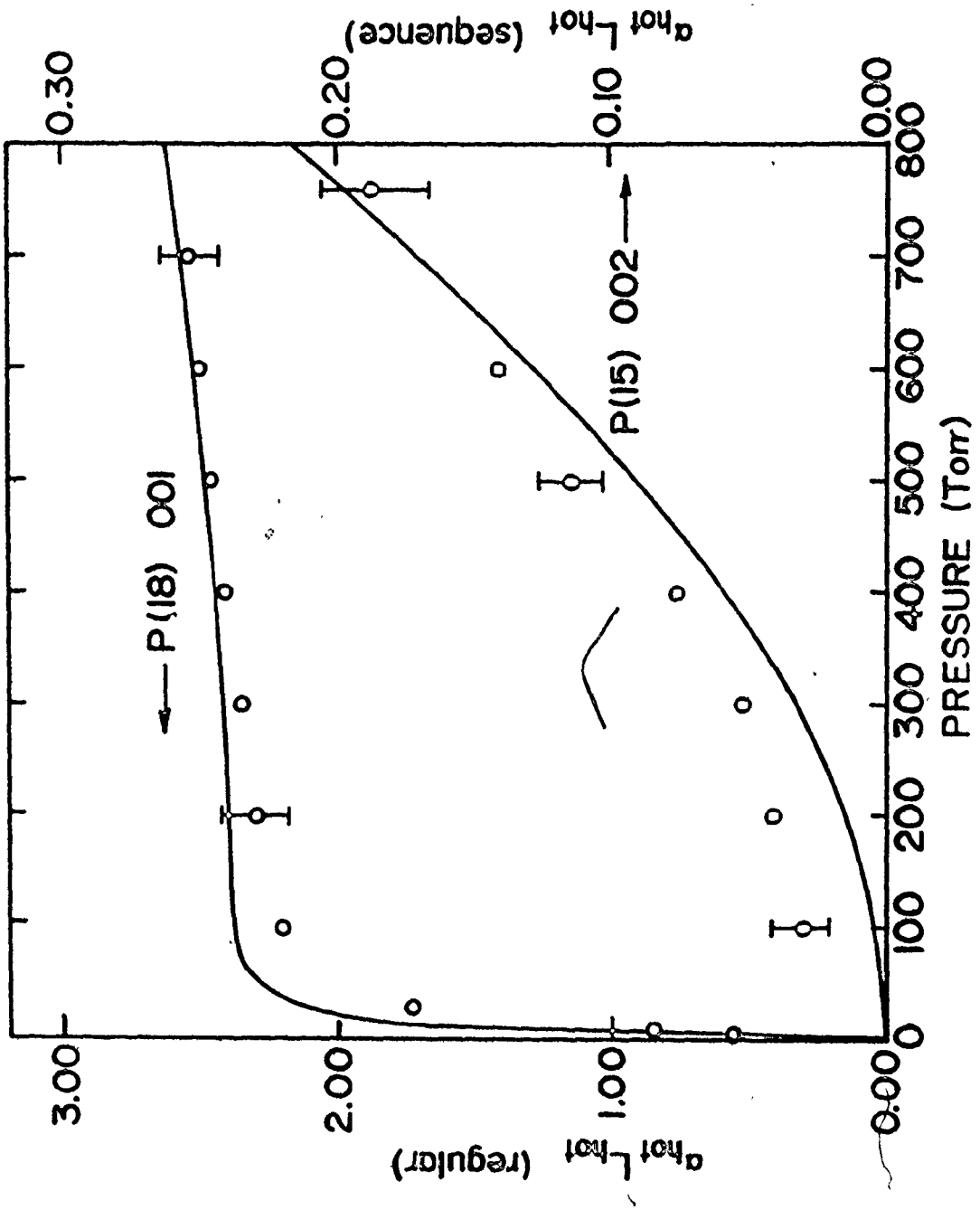
$\alpha_{hot} L_{hot}$ (regular)
$\alpha_{hot} L_{hot}$ (sequence)
PRESSURE (Torr)
P(18) 001
P(15) 002
0.00
1.00
2.00
3.00
0.00
0.10
0.20
0.30
0
100
200
300
400
500
600
700
800

Fig. 6.3

Hot cell absorption as a function of CO_2 pressure for the P(20) regular and P(17) sequence lines. $\alpha_{hot} L_{hot} = \ln (I/I_o)$ where I is the transmitted power with CO_2 in the hot cell and I_o is the transmitted power for the hot cell evacuated. The average temperature of the 120-cm "active" region is 600 K.

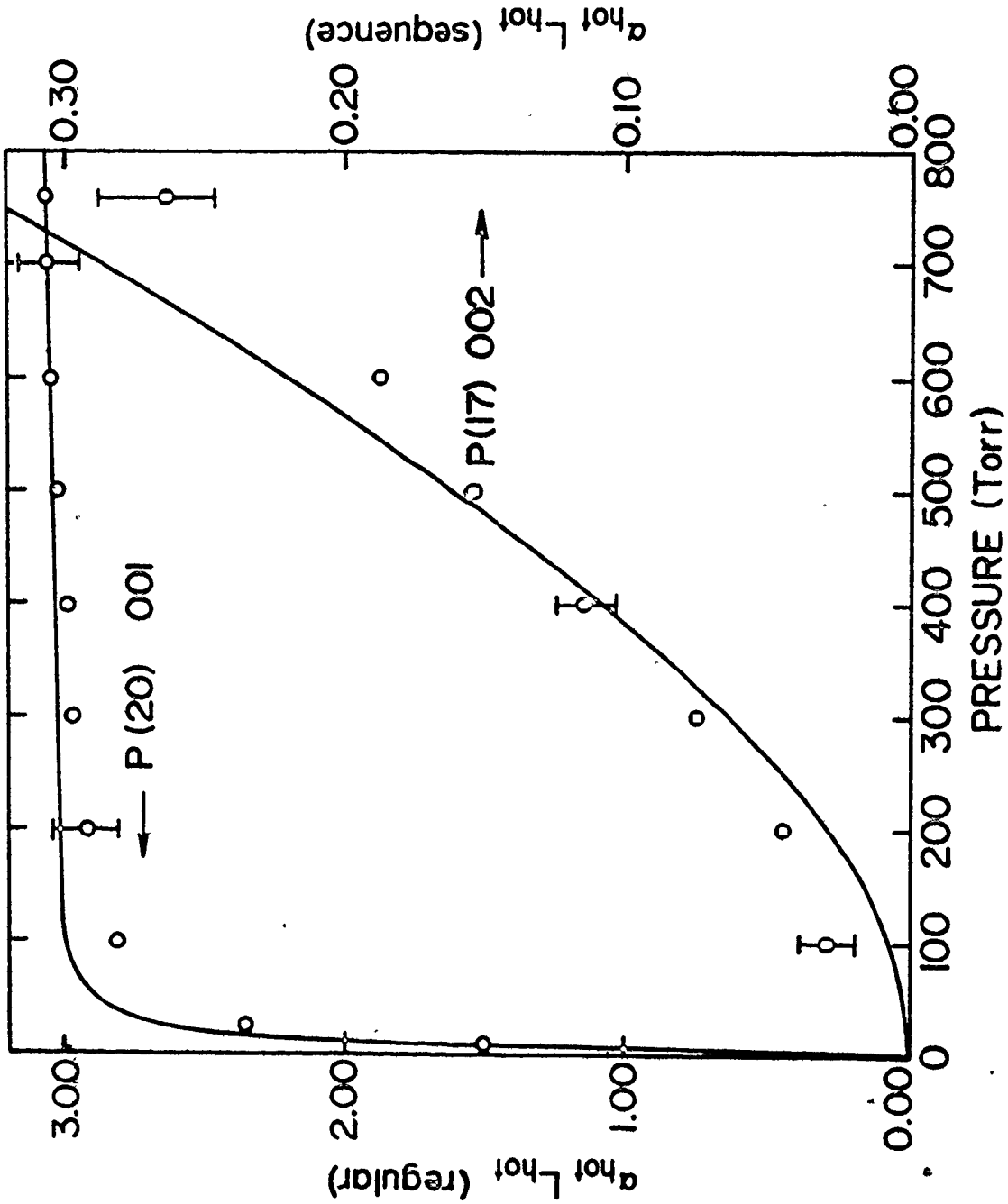
$\alpha_{hot} L_{hot}$ (regular)
$\alpha_{hot} L_{hot}$ (sequence)
PRESSURE (Torr)
P (20) 001
P(17) 002
0.00
1.00
2.00
3.00
0.00
0.10
0.20
0.30
0
100
200
300
400
500
600
700
800

atmospheric pressure. The hot cell temperature was 600 K which represents the average temperature over an active length of 120 cm (see Sect. 3.2). Also shown in Figs. 6.2 and 6.3 are calculated curves based on the data of Ref. [69]. Included are contributions from the regular laser bands ($10^{\circ}0$-$00^{\circ}1$), the hot bands ($11'0$-$01'1$), and various "hot-hot" bands such as ($12^{\circ}0$-$02^{\circ}1$). Although the absorption coefficients of this final group are relatively small, their contributions were found to be significant when calculating absorptions at the sequence frequencies. The overall agreement between calculation and experiment shown in Figs. 6.2 and 6.3 is very good, and we attribute the small discrepancies observable on the sequence transitions to uncertainties in the exact positions of the hot-hot bands.

The most important conclusion that can be drawn from the results shown in Figs. 6.2 and 6.3 is that the hot cell pressure should be kept as low as possible. However, if one is to convert an atmospheric pressure TE CO_2 laser to operation on the sequence lines, the hot cell pressure cannot be reduced below a certain minimum value. Although 100 Torr of CO_2 in the hot cell produces optimum absorption at line center of the regular transitions, the large gain bandwidth of an atmospheric pressure discharge enables regular lasing to continue off line center [70]. The hot cell pressure must be increased until regular lasing is suppressed over a major portion of the gain profile, and all calculations of net gain must consider the effects of line overlap and pressure broadening in both the discharge and the hot cell.

To a good approximation, the ratio of sequence gain to regular gain, g_{002}/g_{001} is given by [71]

$$g_{002}/g_{001} = 2 \exp(-h\nu_3/kT_3) \qquad (6.10)$$

If T_3 = 1800 K, this ratio is ∿30%. However, to determine the true gain ratio at line center in an atmospheric pressure discharge one must include the significant gain contributions which arise from overlapping bands [71]. A detailed calculation following the formalism given in Ref. [71] was performed to determine all the significant gain contributions present, for both the sequence and regular lines. The calculation included contributions from neighbouring regular or sequence lines, and also from hot bands ($01^{1}1$-$11^{1}0$), higher sequence transitions ($00^{0}3$-$10^{0}2$), and hot sequence bands ($01^{1}2$-$11^{1}1$). A typical gain profile is shown in Fig. 6.4a, and the gain contributions at line center for several transitions are summarized in Table 6.1. The temperatures used in the calculations, as given in Table 6.1, are typical of conventional TEA CO_2 discharges. It can be clearly seen from Table 6.1 that the sequence transitions possess large gain contributions from overlapping bands. For example, the gain coefficient of the P(15) $00^{0}2$ transition is only 66% of the actual gain present at line center of that transition. The presence of substantial additional gain permits increased output coupling and a corresponding increase in the output energies available on the sequence transitions. It should also be noted that due to the presence of overlapping bands, use of experimental gain ratios as a means of determining T_3 should be

Fig. 6.4

Net gain per pass ($gL_g - \alpha_{hot} L_{hot}$) on the P(18) regular and P(15) sequence lines. Traces (a), (b) and (c) are plotted for pressures of 0, 450 and 760 Torr of CO_2, respectively, in the hot cell.

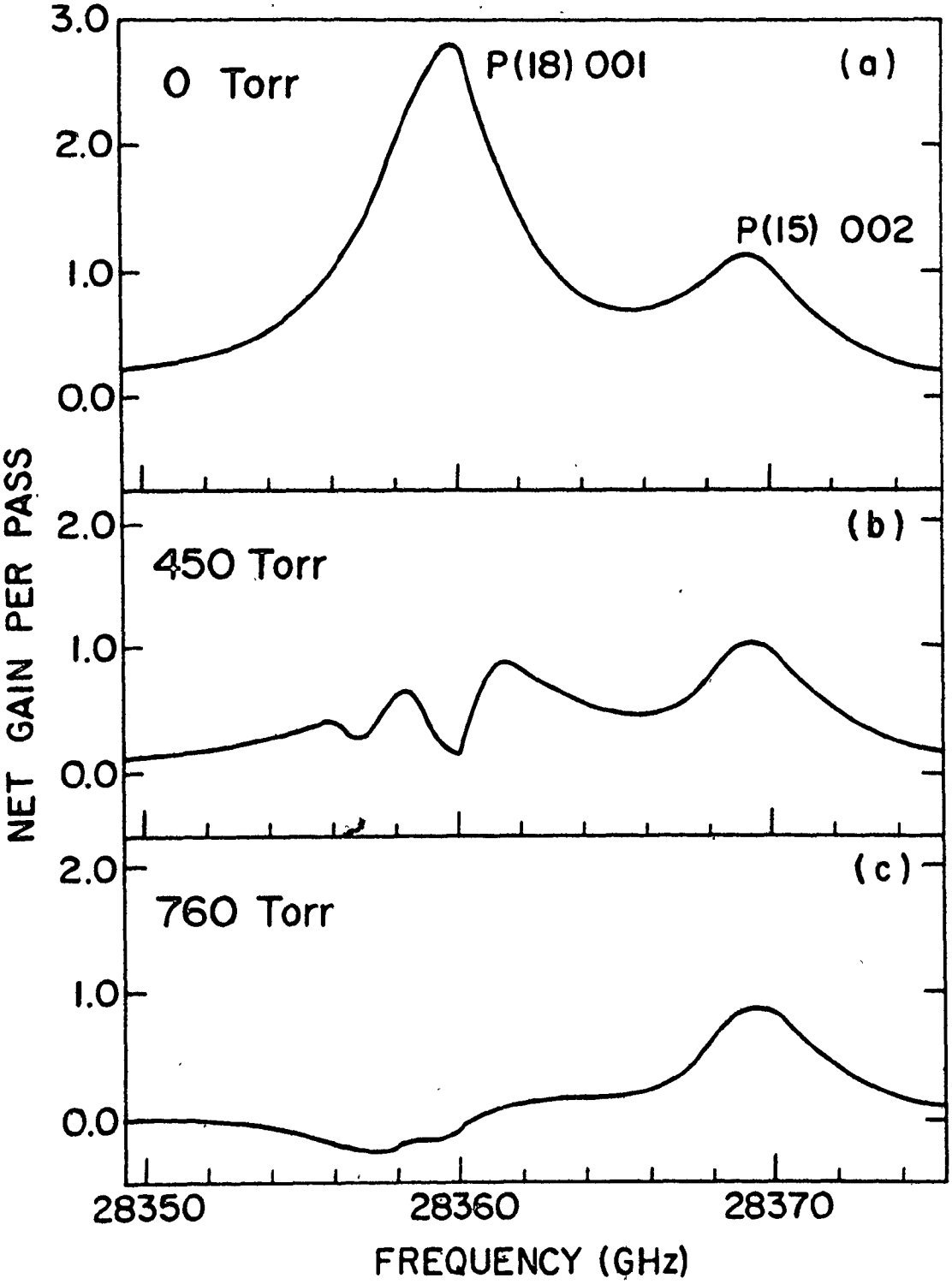
3.0
2.0
1.0
0.0
0 Torr
P(18) 001
(a)
P(15) 002
2.0
1.0
0.0
450 Torr
(b)
2.0
1.0
0.0
760 Torr
(c)
NET GAIN PER PASS
28350
28360
28370
FREQUENCY (GHz)

limited to low pressure discharges.*

Using the gain profiles as shown in Fig. 6.4a and the absorption calculations described above, one can determine the net gain which would exist inside the cavity of Fig. 6.1 as the hot cell pressure is increased. Typical curves are shown in Figs. 6.4b and 6.4c for hot cell pressures of 450 and 760 Torr, respectively. The effect of different linewidths in the hot cell and the discharge is evident, and sufficient CO_2 must be added to reduce the net gain in the wings of the regular gain profile to less than the net sequence gain. At this point the laser will switch from oscillation on the regular transition to oscillation on the sequence transition. In fact the situation is somewhat more complex due to the J-dependence of gain and absorption. What is actually observed in a non-selective cavity as the hot cell pressure is increased from 350 to 450 Torr is that the laser switches from oscillation on the P(18) 10-μm transition to simultaneous lasing on the P(12), P(14) and P(16) 10-μm lines plus the R(10) 9-μm line and then finally to oscillation on the P(15) 10-μm sequence line with some contribution from P(17). This behavior is in good agreement with the calculations shown in Table 6.1. Further increase of the CO_2 pressure in the hot cell simply introduces additional loss on the sequence transition with a corresponding reduction in output power. This point is discussed in greater detail in the next section.

---

*The measurements made by Feldman et al. [19] for a 1800 Torr discharge will clearly lead to an overestimate of T_3. This accounts for the surprisingly high values of T_3 given in their Fig. 2.

Table 6.1

Summary of significant gain and absorption contributions at various frequencies in the 10.4-μm regular and sequence bands. The listings for the sequence lines correspond to the values at line center whereas the values for the regular transitions are given for both line center and for the offset frequency $\Delta\nu$ at which the maximum net gain occurs. Discharge conditions are T_3 = 1750 K, $T_1 = T_2$ = 450 K, T = 350 K and L_g = 1.0 m. The measured hot cell temperature profile (see Sect. 3.2) was used and the CO_2 pressure in the hot cell was 450 Torr. Net gain refers to the difference $gL_g - \alpha_{hot}L_{hot}$ (see Fig. 6.1)

		SEQUENCE		REGULAR			
		P(17)	P(15)	P(20)		P(18)	
				$\Delta\nu = 0$	$\Delta\nu$ = 1.8 GHz	$\Delta\nu = 0$	$\Delta\nu$ = 1.7 GHz
GAIN	001-100	0.11	0.15	2.67	1.67	2.60	1.76
	002-101	0.79	0.74	0.04	0.05	0.05	0.07
	003-102	0.13	0.13	-	-	-	-
	011-110	0.12	0.02	0.29	0.19	0.12	0.06
	012-111	-	0.07	0.03	0.06	-	-
	gL_g (total)	1.16	1.12	3.03	1.97	2.78	1.91
ABSORPTION	001-100	0.033	0.045	2.48	0.83	2.36	0.91
	011-110	0.091	0.013	0.54	0.18	0.10	0.05
	021-120	0.007	0.016	-	-	-	-
	$\alpha_{hot}L_{hot}$	0.137	0.075	3.03	1.01	2.46	0.96
	Net gain	1.03	1.05	0.0	0.95	0.32	0.95

6.4 Optimization

The results of the previous section can now be incorporated into the rate equation model described in Sec. 6.2. A hot cell loss of 6%/pass (corresponding to a hot cell pressure of ~450 Torr, see Fig. 6.2) is included in the sequence modeling, in addition to an optical loss of 4%/pass present in both the sequence and the regular models. The additional gain due to overlapping bands is accounted for by increasing the magnitude of the gain coefficient g in the stimulated emission terms. This assumption is based on the rapid ν_3 intra-mode relaxation time [35] and eliminates the need for additional rate equations. Figure 6.5 shows experimental and theoretical pulse shapes for the P(15) sequence and P(20) regular lines. The output coupling is optimized in each case and the time delays are measured from the start of the current pulse. The cavity configuration is the same as that shown in Fig. 6.1. The experimental P(20) pulse was observed with the hot cell evacuated, while the P(15) pulse was obtained with ~450 Torr of CO_2 in the hot cell. The discharge module (Lumonics Inc. K-902-2) was operated with a 73%He:16%N_2:11%CO_2 mixture* at a total pressure of 1 atm and an input energy of 90 J/ℓ·atm. The measured sequence output energy was 3 J per pulse, and the longer time delay associated with the sequence pulse is due to the reduced gain present when the laser is operating on one of the sequence transitions. The agreement between theory and experiment is good,

---

*The sequence energies reported in this work and in Ref. [68] were not found to be strongly dependent on mixture, which agrees with the sequence gain measurements of Lavigne et al. reported in Ref. [72]. In general, the optimum mixtures were ~10% CO_2, 10-20% N_2 and the balance He.

Fig. 6.5

Comparison of theoretical and experimental pulse shapes for both the P(15) sequence and P(20) regular lines. Time delays are measured from the start of the current pulse, which has a peak value of 8 kA. The output coupler has a reflectivity of 65% for sequence operation and 34% for regular operation. The gas mixture is 73%He:16%N_2:11%CO_2 and the excitation energy is 90 J/ℓ·atm.

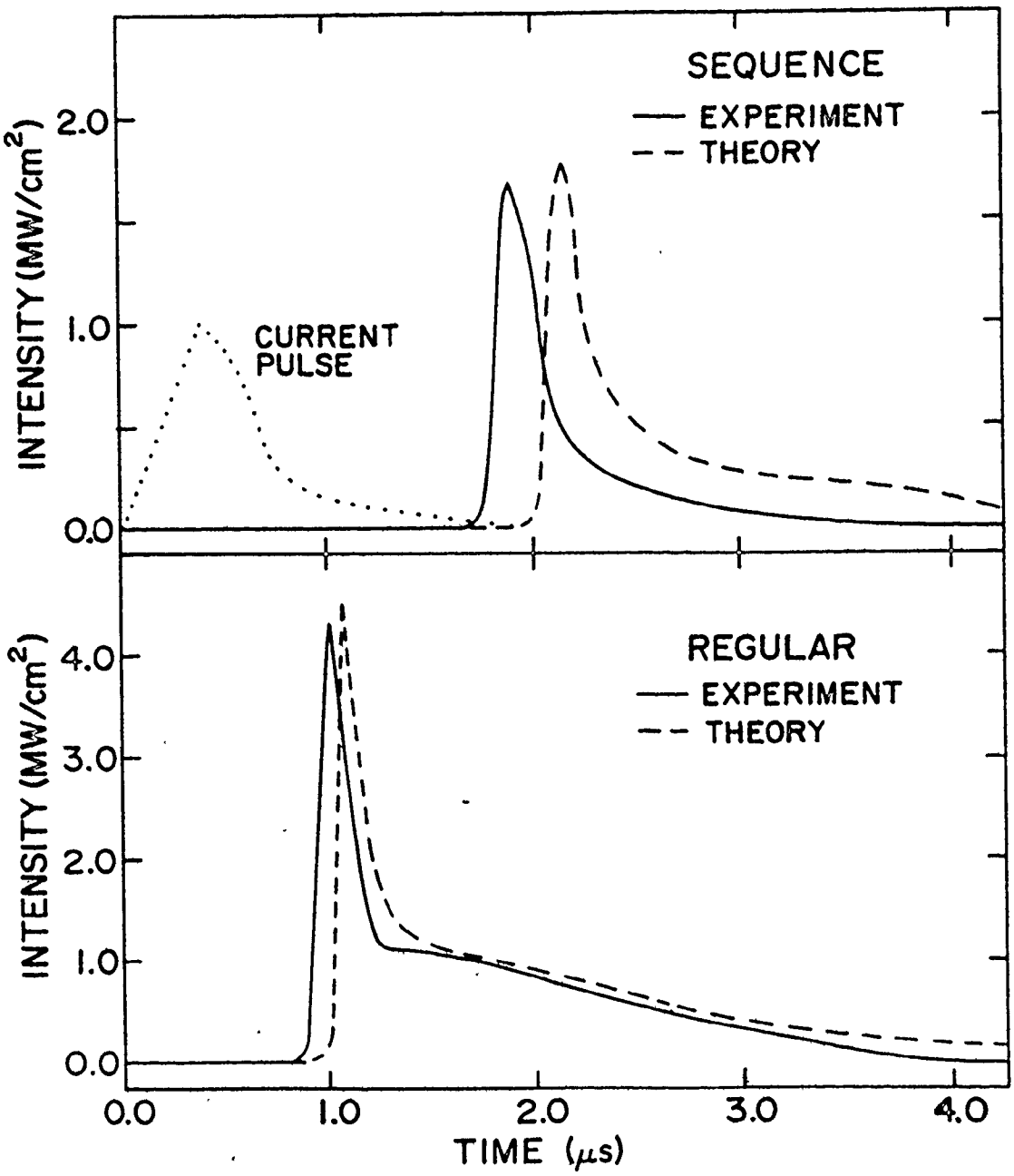
SEQUENCE
EXPERIMENT
THEORY
CURRENT PULSE
INTENSITY (MW/cm²)
2.0
1.0
0.0
REGULAR
EXPERIMENT
THEORY
INTENSITY (MW/cm²)
4.0
3.0
2.0
1.0
0.0
0.0
1.0
2.0
3.0
4.0
TIME (μs)

confirming the validity of the model. It is apparent from the model calculations that there is no fundamental limitation to the extraction of energy on the sequence lines as compared with that on the regular lines. This is a direct consequence of the rapid intra-mode relaxation rates [35]. However, it must again be stressed that proper cavity design is essential if efficient sequence operation is to be achieved. This can best be seen by considering three interrelated factors: hot cell losses, output coupling, and degree of excitation in the discharge.

The origin of the hot cell losses at the sequence frequencies was described above. In order to quantitatively determine the effect of substantial hot cell loss on sequence output, the sequence model calculations were performed for a wide range of hot cell losses well in excess of those occurring in our hot cell. The results are presented in Fig. 6.6. Also shown are the experimental data points corresponding to the range of losses which could be realized using the present apparatus. The calculated loss per pass includes a 4% contribution from optical losses but excludes the 35% transmission of the output coupler. The other experimental conditions are the same as those used in Fig. 6.5 although similar curves were obtained for a wide range of operating conditions. The arrow indicates the point which corresponds to our optimum hot cell conditions and shows that the output energies obtained are within 30% of the maximum energy which could be extracted in the ideal case (i.e., no hot cell loss). This is a considerable improvement over the laser described in Ref. [18] in which the hot

Fig. 6.6

The effect of cavity loss $\bar{L}$ on sequence output energy. $\bar{L} = \bar{L}_{opt} + \alpha_{hot} L_{hot}$ where $\bar{L}_{opt}$ is the optical loss and $\alpha_{hot} L_{hot}$ is the hot cell loss. The data points correspond to the loss introduced on the P(15) sequence transition for hot cell pressures ranging from 400 to 760 Torr. The arrow indicates the position of the P(15) sequence pulse shown in Fig. 6.5.

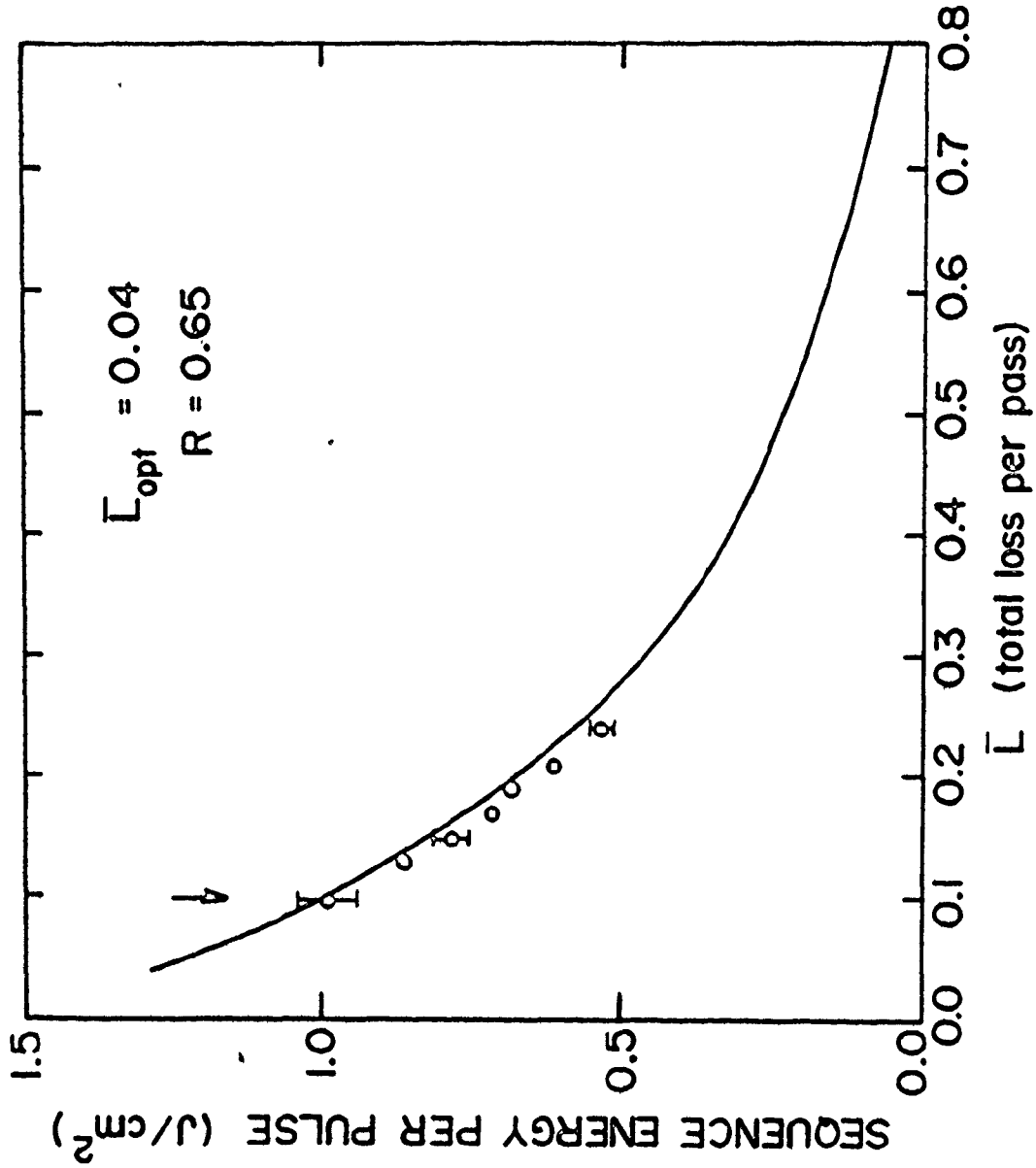
SEQUENCE ENERGY PER PULSE (J/cm²)
1.5
1.0
0.5
0.0
0.0
0.1
0.2
0.3
0.4
0.5
0.6
0.7
0.8
L̄ (total loss per pass)
L̄opt = 0.04
R = 0.65

cell loss was ∿45%/pass. It would certainly be desirable to eliminate hot cell losses altogether, however this is not physically possible. We applied the gain/loss calculations described in Sect. 6.3 and determined that a hot cell loss of 6% per pass is close to the minimum which can be achieved. For a 1-m discharge, the optimum hot cell temperature was found to be ∿600 K, while the optimum length corresponded to an "active" region of ∿1 m also. The loss could be reduced slightly (to ∿4%/pass) by increasing the hot cell length, and thereby employing lower pressures, but at the expense of constructing extremely long cavities. Thus an active hot cell length equal to or slightly greater than the discharge length appears to be the most practical. However, the most critical factor affecting hot cell loss remains that of pressure, and the lowest pressure needed to achieve sequence lasing should always be used.

Another major factor in the design of sequence lasers is that of optimum output coupling. Even in the presence of substantial gain contributions from overlapping bands, the sequence gains will still be only equal to ∿40% of the regular gain. Thus the high transmission output couplers used in regular CO_2 lasers are not suitable for sequence operation. The effect of output coupling on pulse energies and intensities is shown in Fig. 6.7 for both the P(20) regular and P(15) sequence transitions. These curves were obtained using model calculations and confirmed by experiment with selected output couplers. Optimum output coupling for sequence lasers with a 1-m gain section and a 1.2-m hot cell is in the range of 20-40 percent.

Fig. 6.7

Output energy (solid curve) and intensity (dashed curve) as a function of cavity reflectance for both sequence and regular operation. The gas mixture was 73%He:16%N_2:11%CO_2 and the excitation energy was 90 J/ℓ·atm. The optical loss per pass was taken as 4 percent in both cases.

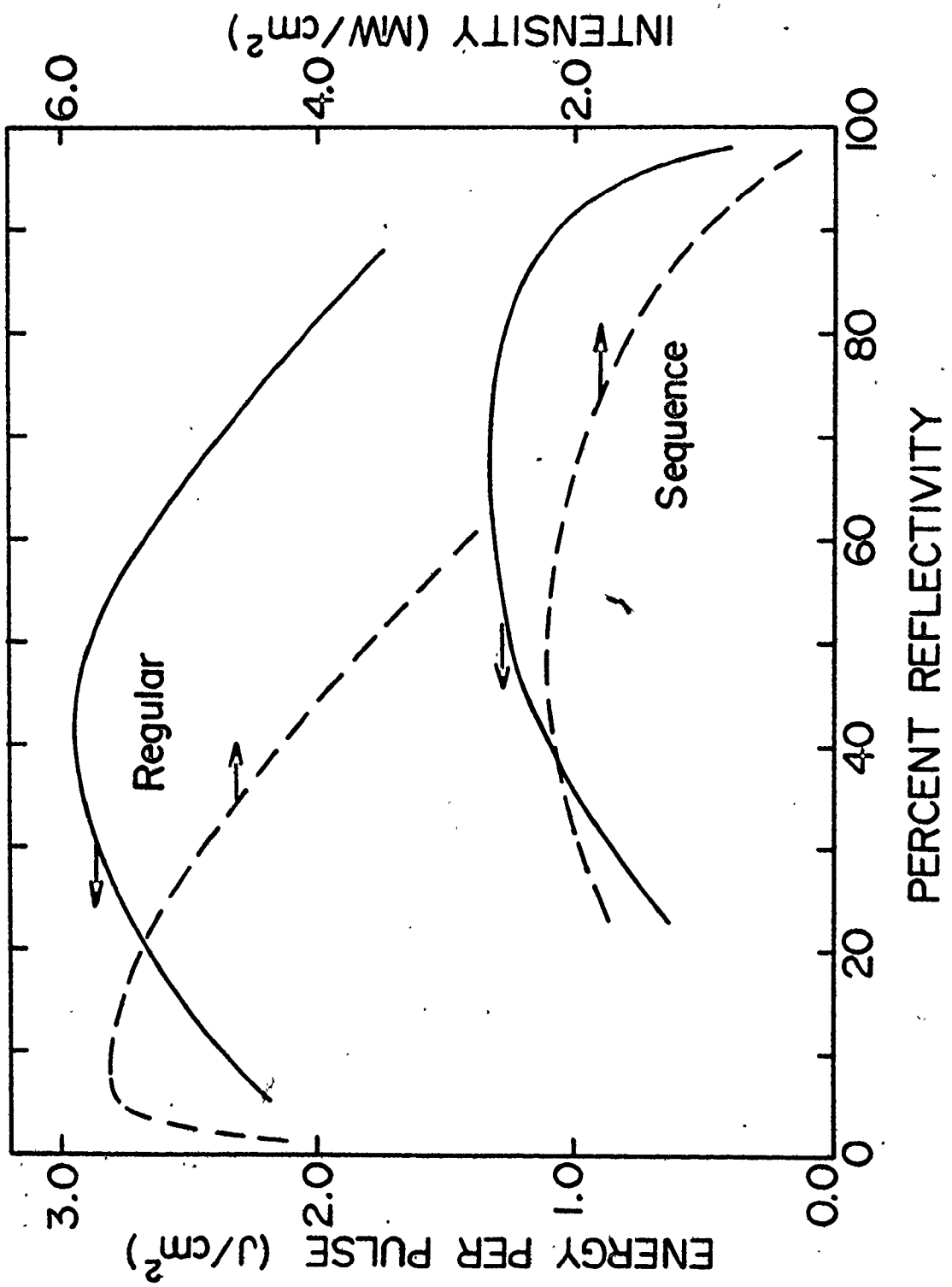
INTENSITY (MW/cm²)
6.0
4.0
2.0
100
80
60
40
20
0
PERCENT REFLECTIVITY
Regular
Sequence
3.0
2.0
1.0
0.0
ENERGY PER PULSE (J/cm²)

The final factor to be considered is that of the degree of excitation in the discharge. In general, the optimum excitation energy for sequence lasers will be greater than for regular lasers. This arises as a result of two factors. First, the small-signal sequence gain is very dependent on the T_3 of the discharge (e.g., sequence gain doubles as the T_3 is increased from 1700 K to 2100 K, whereas the regular gain increases by only 35%). Consequently, use of low excitation causes the sequence laser to operate near threshold resulting in low output energies. Second, the model calculations show that laser action on the sequence transitions will terminate once T_3 is reduced to the point where gain equals cavity loss. For the sequence pulse shown in Fig. 6.5, the final T_3 is 1300 K and as a result a substantial portion of the energy initially stored in the upper laser levels and in the vibrationally excited N_2 cannot be extracted. This is a direct result of the reduced gain values present on the sequence transitions. The effect of this residual energy can only be minimized by ensuring that the initial value of T_3 is as large as possible.

This can be readily seen in the following analysis. The energy stored in the ν_3 mode of CO_2 and in the vibrationally excited N_2 is given, to a good approximation, by [16]

$$E_{stored} = (N_{CO_2} + N_{N_2})h\nu_3 \left[\frac{x_{3i}}{1-x_{3i}}\right] \tag{6.11}$$

where $x_3 = \exp(-h\nu_3/kT_3)$ and the subscript i denotes the initial value before lasing commences. The maximum optical energy which can be extracted is the difference between this quantity (Eq. (6.11)) and

the energy stored at the completion of lasing (denoted by the subscript f), multiplied by the quantum efficiency of the CO_2 laser transition. Hence,

$$E_{optical}^{max} = (0.41)(N_{CO_2}+N_{N_2})h\nu_3 \left[\frac{x_{3i}}{1-x_{3i}} - \frac{x_{3f}}{1-x_{3f}}\right] \quad (6.12)$$

In a lossless cavity (i.e., no losses other than coupling losses), the optical energy extracted $E_{optical}^{ext}$ would be equal to this value. In the more realistic case of a cavity possessing some loss per pass $\bar{L}$, we have

$$E_{optical}^{ext} \simeq \frac{(1-R)}{2\bar{L}+(1-R)} E_{optical}^{max} \quad (6.13)$$

where 1-R represents the output coupling. In Fig. 6.8 we plot percent energy extracted as a function of T_{3i} for both regular and sequence transitions. Percent energy extracted is defined as the ratio of $E_{optical}^{ext}$ to the maximum energy one could theoretically extract from an ideal system (i.e., 0.41 E_{stored}), where 0.41 is the quantum efficiency of the 10-μm transition in CO_2 and E_{stored} is given by Eq. (6.11). The two curves are very similar in that no energy is extracted until the small-signal gain exceeds the cavity loss (T_{3i} = 900 K for regular lasing and 1300 K for sequence lasing). As T_{3i} is further increased the residual energy term in Eq. (6.12) becomes less important and the curves asymptotically approach a final value given by the ratio of useful cavity loss (output coupling) to total cavity loss (including hot cell losses in the sequence case), as given by Eq. (6.13). While Fig. 6.8 gives some indication of the importance of high values of T_{3i},

Fig. 6.8

Percent energy extracted as a function of T_{3i} for both regular and sequence transitions. See text for details.

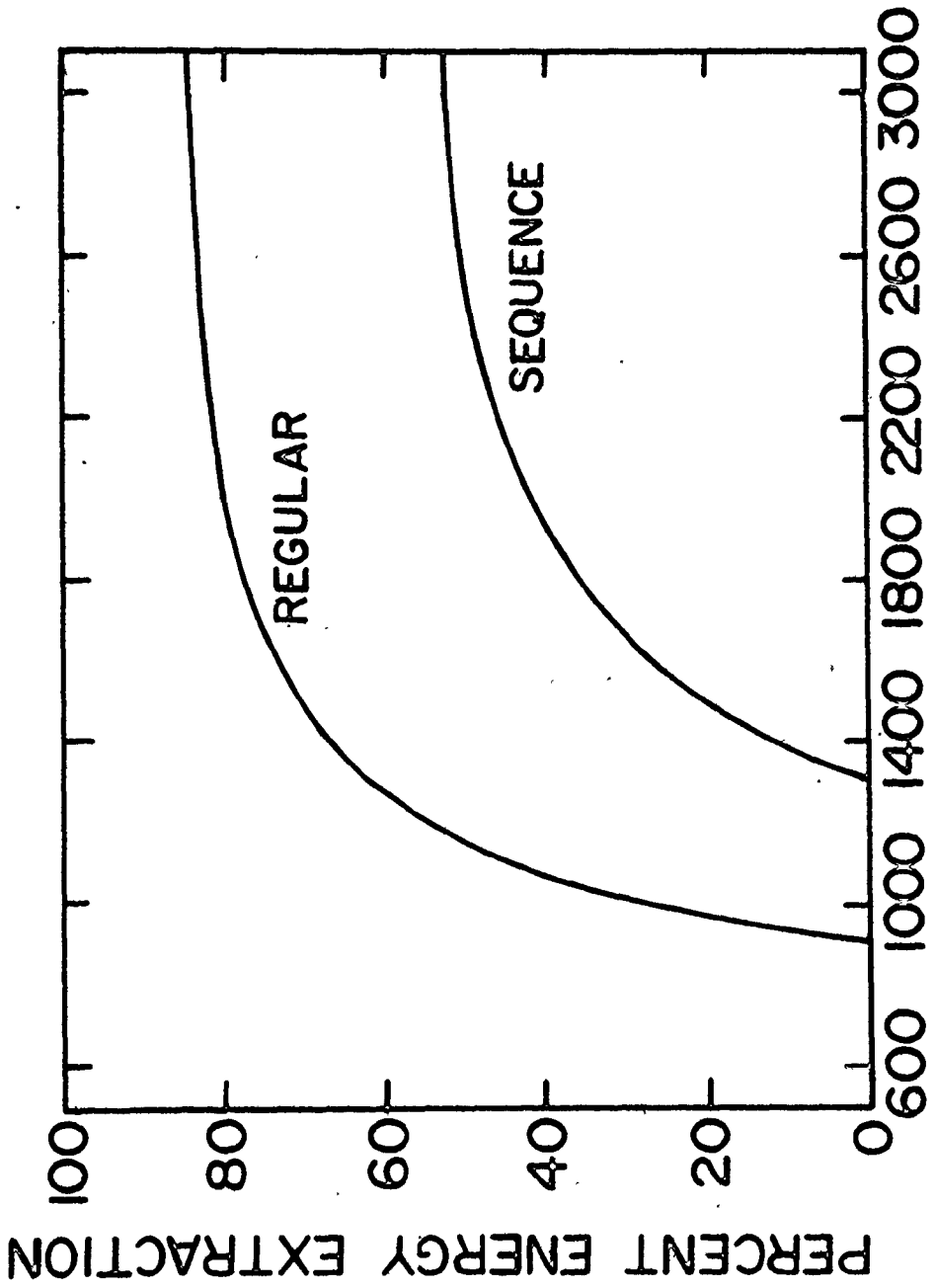
PERCENT ENERGY EXTRACTION
0
20
40
60
80
100
600
1000
1400
1800
2200
2600
3000
T_{3i}
REGULAR
SEQUENCE

one must also remember that the available energy increases dramatically with T_{31}, as can be seen from Eq. (6.11). For these reasons we modified the discharge circuit of the Lumonics module to increase the excitation energy from 90 to 135 J/ℓ·atm [68]. This resulted in an increase in T_{31} from 1750 K* to ∿2050 K, and produced a substantial increase in sequence output energy from 3 to 6 J per pulse. This output energy compares favourably with the maximum 14 J per pulse that can be attained on the regular transitions for a similar level of excitation [73].

6.5 Applications of High Power Sequence Lasers

A convenient means of producing high power sequence pulses is an essential part of the development of a high power 4.3-μm laser employing the pumping scheme described in this thesis. This topic is discussed in detail in the next Chapter. Presently, it is worthwhile to note the overall importance of high power TEA sequence lasers.

Regular CO_2 lasers have excellent output characteristics and high efficiencies and consequently have found widespread use in applications such as laser isotope separation, laser photochemistry and optical pumping of molecular gases. In many of these applications, effective use of the laser is limited to a few chance coincidences between the regular laser frequencies and the absorption lines in the

---

*The T_3 of 1750 K is obtained from small-signal gain measurements provided by Lumonics, Inc., and agrees with the model calculations of Sect. 6.4.

gas under investigation. The use of a hot cell in a grating-tuned cavity results in a near doubling of the number of laser lines which can be obtained from a TEA CO_2 laser [68] and can clearly increase the utility of the TEA CO_2 laser in any frequency dependent application. One example is the recent use of a sequence CO_2 laser to produce 12-μm lasing in NH_3 [74]. The P(7) and P(17) 9.4-μm sequence lines have closer coincidences with NH_3 absorption lines than any of the regular lines. Consequently, for identical pumping powers, higher output powers are obtained when using these sequence lines rather than the R(30) 9.4-μm regular line.

Another application of a high power sequence laser is in the area of atmospheric monitoring. Since the sequence lines experience negligible absorption in atmospheric CO_2, they will have significantly better transmission through the atmosphere than will the regular CO_2 laser lines, particularly under conditions of low humidity [75]. By comparing atmospheric absorption on the sequence and regular lines, one can accurately determine CO_2 concentrations over long path lengths. Similarly, sequence lasers may extend the range of laser Doppler lidar devices currently employing TEA CO_2 lasers to determine wind velocities [76].

6.6 Summary

In this Chapter it was demonstrated that conventional TEA CO_2 lasers can be converted to efficient, high energy operation on the sequence transitions by inclusion of a simple in-cavity hot CO_2 cell.

However, proper design of the laser is essential and factors such as hot cell length and pressure, discharge length and degree of excitation must be considered. Proper implementation of the hot cell technique results in a significant improvement of the line-tunability of TEA CO_2 lasers and the significance of this result to several areas of application has been discussed. The next Chapter deals with the use of TEA sequence lasers in the production of high 4.3-μm output powers.

CHAPTER 7

SCALABILITY OF 4.3-μm CO_2 LASERS

7.1 Introduction

The 4.3-μm lasers described in Chapter 3 employed low pressure pulsed discharges and modest sequence pumping powers, resulting in 4.3-μm output powers in the 1 kW range. Since the output energy from a given laser volume depends on the number of excited molecules present, it is desirable to increase both the CO_2 content and total gas pressure in the 4.3-μm discharge. However, the gain dynamics require that higher sequence pumping powers be employed under these conditions so as to offset the increased collisional losses from the $10^0 1$ level. The TEA sequence laser described in the previous Chapter fulfills the requirements of a high power pump source. This Chapter discusses the scalability of the 4.3-μm laser, based on these increased pump power levels.

As noted above, high 4.3-μm powers can be achieved by increasing the number of CO_2 molecules in the discharge and scaling the sequence pumping power accordingly. Two factors will restrict this type of scalability. Firstly, the increased collisional losses from the $10^0 1$ level, due to the increased CO_2 content will ultimately require prohibitively large sequence pumping powers. Secondly, as the pressure is increased, neighbouring 4.3-μm absorption lines begin to introduce absorption at the 4.3-μm lasing frequencies until the net gain has

been substantially reduced and 4.3-μm output drops. Both factors must be considered to determine the maximum values of CO_2 concentration and total pressure. Section 7.2 discusses the increased absorption which occurs at higher pressures, while the limitations imposed by the gain dynamics are described in Sect. 7.3. Based on these considerations, design criteria for high power 4.3-μm lasers are presented in Sect. 7.4, together with estimates of the anticipated 4.3-μm output power levels.

7.2 4.3-μm Absorption in High Pressure Discharges

The concept of interfering absorptions at the 4.3-μm lasing frequencies was introduced in Chapter 3, where it was noted that certain lines were missing from the 4.3-μm output spectrum. For example, the P(30) ($10^0 1$-$10^0 0$) line is not observed due to the presence of strong absorption arising from the nearly coincident P(52) 4.3-μm line in the ν_3 fundamental band. However, at the low pressures and lean gas mixtures used (e.g. 30 Torr with 1.5% CO_2 concentration) significant absorption is limited to only a few near coincidences between 4.3-μm lasing frequencies and 4.3-μm absorption lines. When the pressure is increased (> 100 Torr) absorptions from many lines can become significant. This is primarily a result of the large value of the 4.3-μm line strength. The problem is aggravated because the CO_2 molecules have been excited in a discharge. This results in significant population in higher lying vibrational levels, particularly those in the ν_3 mode. Consequently large absorptions exist on transitions originating from levels such as $00^0 1$, $00^0 2$ and $00^0 3$, in addition to

the ν_3 fundamental, and these absorption bands overlap with the 4.3-μm lasing transitions. The situation is summarized in Fig. 7.1 which shows the relative positions of the various 4.3-μm absorption bands. Note the presence of numerous hot bands in addition to those absorption lines originating in the ν_3 mode. Clearly, the actual amount of absorption at any particular lasing frequency will depend on the exact positions of the neighbouring absorbing lines. Therefore, a search was performed, using the AFCRL listing of CO_2 absorption lines [69] and the known lasing frequencies (see Chapter 3), to identify the lines which possess the minimum amount of overlapping absorptions. For the ($10^0 1$-$10^0 0$) 4.3-μm band, the P(26), P(22) and P(20) lines were found to be the most promising. Accordingly, it is not surprising that maximum 4.3-μm output was observed on these transitions when the laser was operated at low pressure (see Fig. 3.6).

Next, experiments were performed to measure absorption as a function of pressure on the P(26) 4.3-μm transition, in both an excited and unexcited gas mixture. The experimental apparatus was the same as that used in Sect. 5.5 to determine the V-T relaxation rates. Absorptions were measured at the peak of the sequence gain (approximately four V-T relaxation times after the discharge, based on the data of Sect. 5.5) which is the point where 4.3-μm lasing is produced. Results are shown in Fig. 7.2. The low values of absorption observed for the unexcited gas mixture are expected since the P(26) line is far removed from any 4.3-μm fundamental. Notice however the large absorptions present once the gas mixture has been excited in the

Fig. 7.1

Plot of 4.3-μm absorption bands in the region of the 4.3-μm laser bands. Absorptions at line center of the ($00^{0}0$-$00^{0}1$), ($00^{0}1$-$00^{0}2$), and ($00^{0}2$-$00^{0}3$) bands are in excess of 1.0 cm^{-1}, for a 70%He:20%N_2:10%CO_2 mixture at 100 Torr pressure with $T_1 = T_2 = 350$ K, $T_3 = 2000$ K and $T = 300$ K.

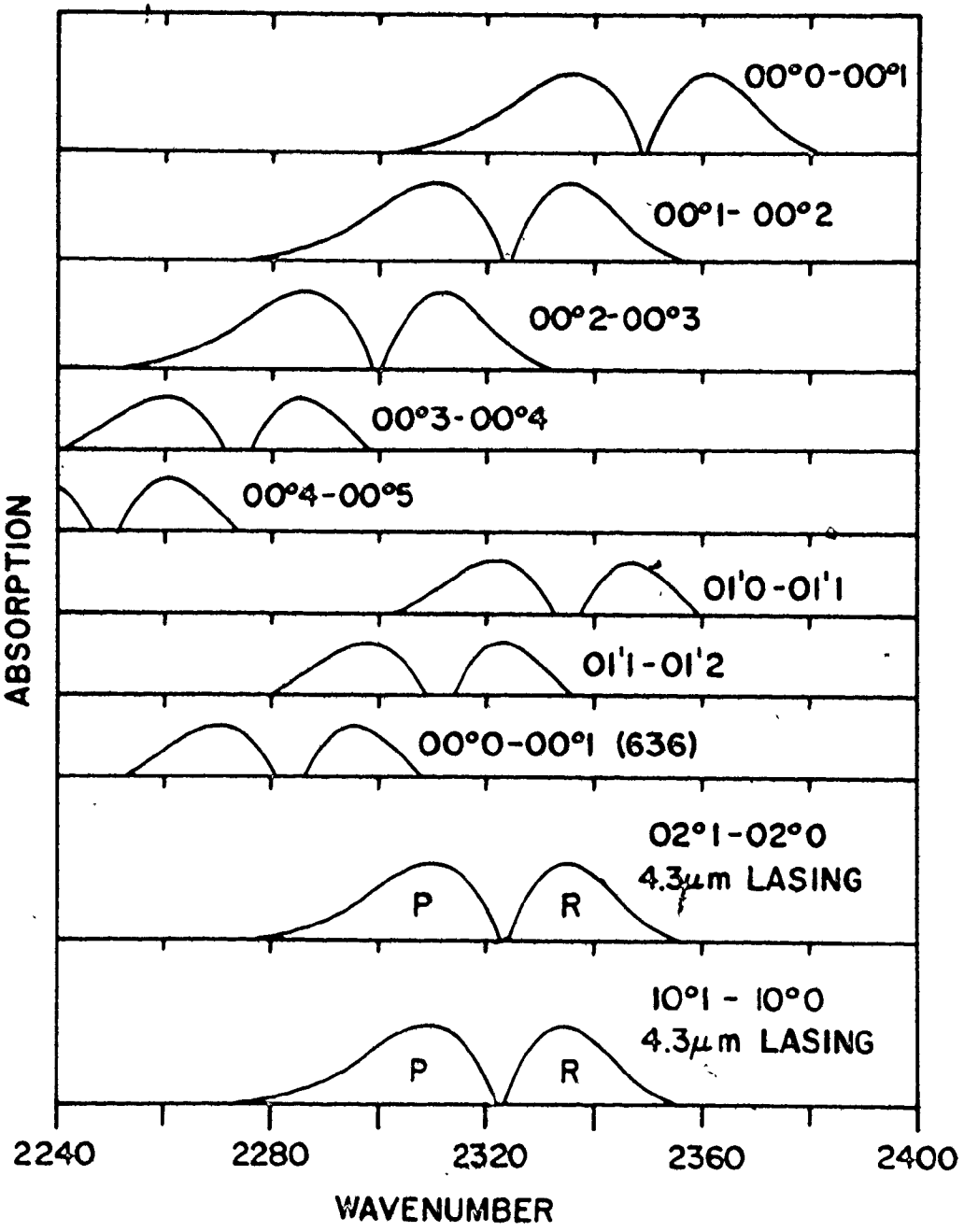
00°0-00°1
00°1- 00°2
00°2-00°3
00°3-00°4
00°4-00°5
01'0-01'1
01'1-01'2
00°0-00°1 (636)
02°1-02°0
4.3μm LASING
P
R
10°1 - 10°0
4.3μm LASING
P
R
ABSORPTION
2240
2280
2320
2360
2400
WAVENUMBER

Fig. 7.2

Measured absorptions on the P(26) ($10^0 1 - 10^0 0$) transition as a function of pressure for both an unexcited and excited gas mixture. The solid curves indicate the results of the calculations described in the text.

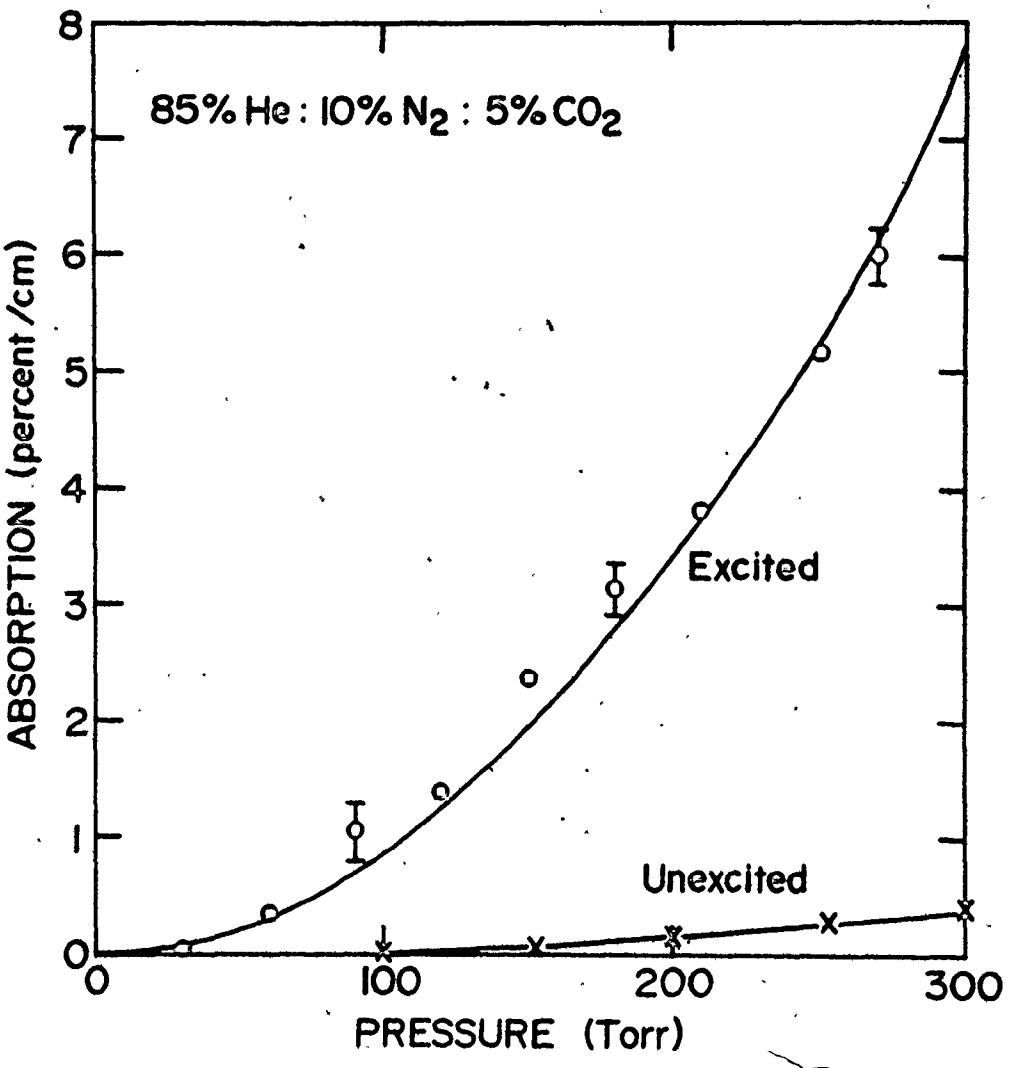
85% He : 10% N_2 : 5% CO_2
ABSORPTION (percent/cm)
PRESSURE (Torr)
Excited
Unexcited
0
1
2
3
4
5
6
7
8
0
100
200
300

discharge. In order to identify the origins of this absorption, calculations were carried out similar to the type described in Sect. 6.3 for 10.6-μm absorption. Using the line strengths and positions given in the AFCRL listing [69], absorption at the P(26) lasing frequency was calculated as a function of pressure and vibrational temperatures. The results are represented by the solid curves in Fig. 7.2. The calculated values for the excited case correspond to a T_3 of 2500 K ($T = T_1 = T_2 = 350$ K) which is in good agreement with the experimentally measured value of ∿2400 K (as derived from small-signal gain measurements, see Sect. 4.3). The good agreement supports the accuracy of the calculated values. Any discrepancies are attributed to variations in the actual T_3 present as the pressure is increased*. In the case of the P(26) laser line most of the observed absorption (> 65%, at 200 Torr) originates from the R(6) ($00^0 2$-$00^0 3$) transition which lies 6.8 GHz from the P(26) laser line, and the remainder is due primarily to the P(23) ($00^0 1$-$00^0 2$) transition. These results are typical, and indicate that substantial absorption at the laser frequencies is present at gas pressures > 100 Torr. The significance of this absorption relative to the scalability of 4.3-μm lasers is discussed in detail in Sect. 7.4.

---

*The experiments were performed under conditions of constant stored energy in the discharge circuit. Consequently, T_3 is not expected to remain constant as pressure is increased.

7.3 4.3-μm Gain in High Pressure Discharges

The other major limiting factor in the scalability of the 4.3-μm laser is related to the gain dynamics. Specifically, the collisional losses from the $10^0 1$ level increase when either the CO_2 concentration or total gas pressure is increased. These increased losses limit the maximum 4.3-μm gain which can be achieved for a given pumping power. In order to acquire a quantitative estimate of this reduction in gain the rate-equation model described in Chapter 4 was used to calculate the small-signal 4.3-μm gain for different gas pressures. The results are shown in Fig. 7.3 as a function of sequence pumping power. Notice that at 1 MW/cm^2 pumping power there is a ten-fold reduction in gain as the pressure is increased from 100 to 300 Torr. Similar results are obtained if the CO_2 content is increased for a constant total pressure, which is expected since the $10^0 1$ de-excitation rate is determined by CO_2-CO_2 collisions [13]. It is shown in the next section that the optimum value of CO_2 concentration and total gas pressure is determined by the combined effect of the gain dynamics discussed here and the overlapping absorptions described in the previous section.

7.4 Optimization

An increase in the number of CO_2 molecules present in the discharge will, under appropriate conditions, result in an increase in 4.3-μm output. However, as shown in the last two sections, there are limits to the CO_2 concentration and total gas pressure that can be employed, due to both the gain dynamics and the interfering absorptions. The optimum operating

Fig. 7.3

Calculated values of the small-signal 4.3-μm gain as a function of sequence pumping power, for the pressures indicated. The initial value of T_3 is 2000 K and the sequence pulse risetime is 100 ns.

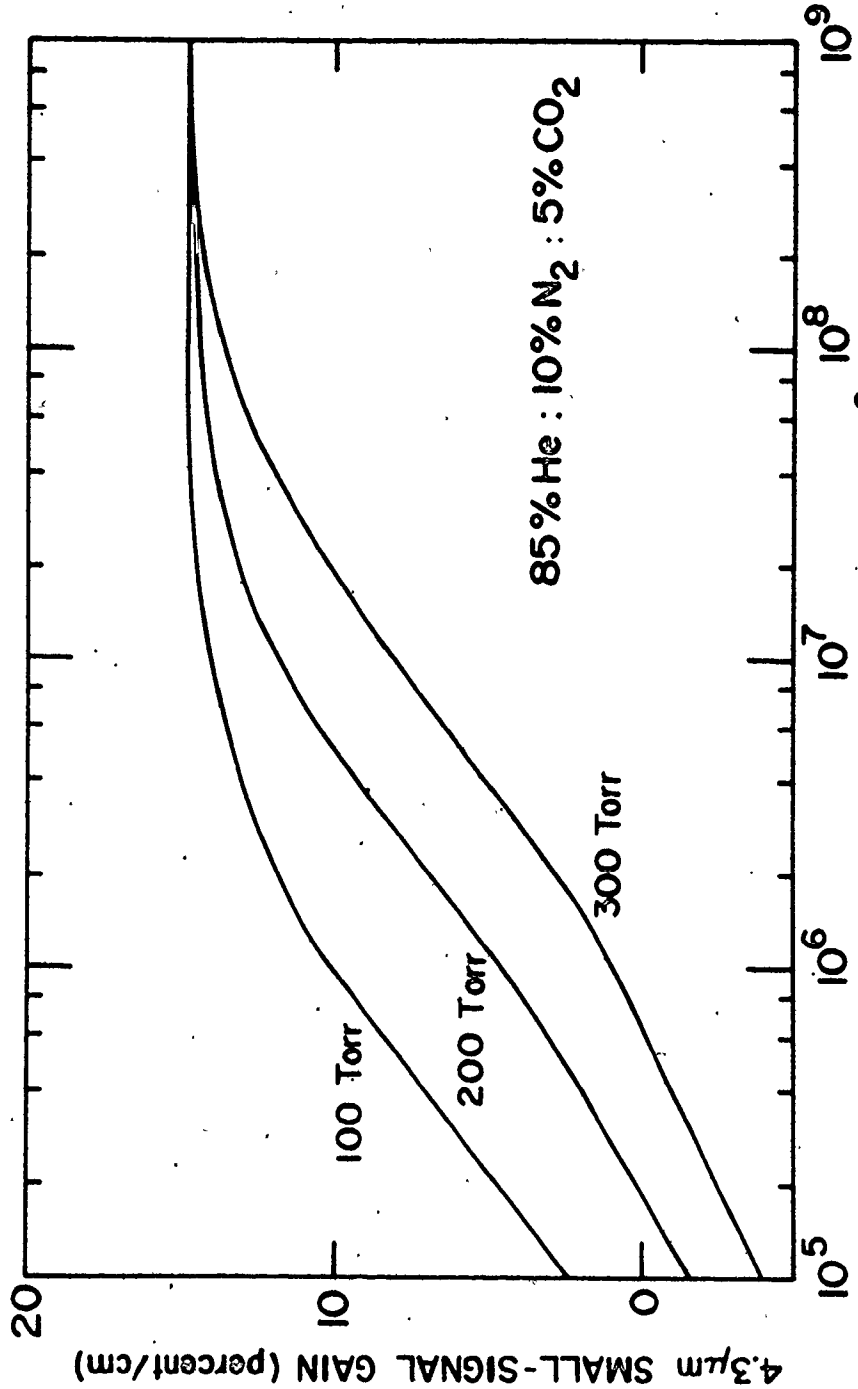
4.3μm SMALL-SIGNAL GAIN (percent/cm)
20
10
0
85% He : 10% N_2 : 5% CO_2
100 Torr
200 Torr
300 Torr
10^5
10^6
10^7
10^8
10^9
PUMPING INTENSITY (W/cm^2)

conditions are determined by the trade-off between these factors. This section identifies optimum operating conditions and estimates the maximum 4.3-μm output which can be obtained from a given volume under these conditions. The principal aim of this section is to present design criteria for high power 4.3-μm laser systems which are currently under investigation.

As noted above, the expected increase in output power due to an increase in the number of CO_2 molecules is offset by a decrease in net gain. This can be seen by referring to Fig. 7.4 which is a plot of net gain and output intensity as a function of pressure for a 85%He:10%N_2:5%CO_2 mixture. A fixed sequence pumping power (1 MW/cm^2) is assumed. Results are presented for two different initial values of T_3 in the discharge, 2000 K and 2500 K. Note the substantial increase in gain in the latter case. This arises since a higher T_3 results in a larger 00^o2 population and ultimately in a higher 4.3-μm net gain. (The increase in gain greatly exceeds the increase in absorption due to the higher T_3 and hence, the net gain increases with T_3 also.) Since the larger initial population in 00^o2 results in a greater number of molecules participating in 4.3-μm lasing, there is also a substantial increase in 4.3-μm output. This can be seen by comparing the dashed curves in Fig. 7.4. These curves correspond to the 4.3-μm output expected from an optical cavity having 36% total reflectance and containing a 1-m discharge. The trade-off between the decrease in net gain and the increase in the number of CO_2 molecules present, as pressure is increased, determines the pressure at which maximum output is expected. In addition, it should be noted that not only does the maximum value of net gain decrease with increasing pressure, but

Fig. 7.4

Calculated values of net gain (absolute gain, see Fig. 7.3, minus absorption, see Fig. 7.2) (solid curve), and output intensity (dashed curve), as a function of total gas pressure. The gas mixture is 85%He:10%N_2:5%CO_2 and the initial values of T_3 are 2000 K and 2500 K, as indicated. The sequence pumping power is 1 MW/cm^2 and the sequence pulse risetime is 100 ns.

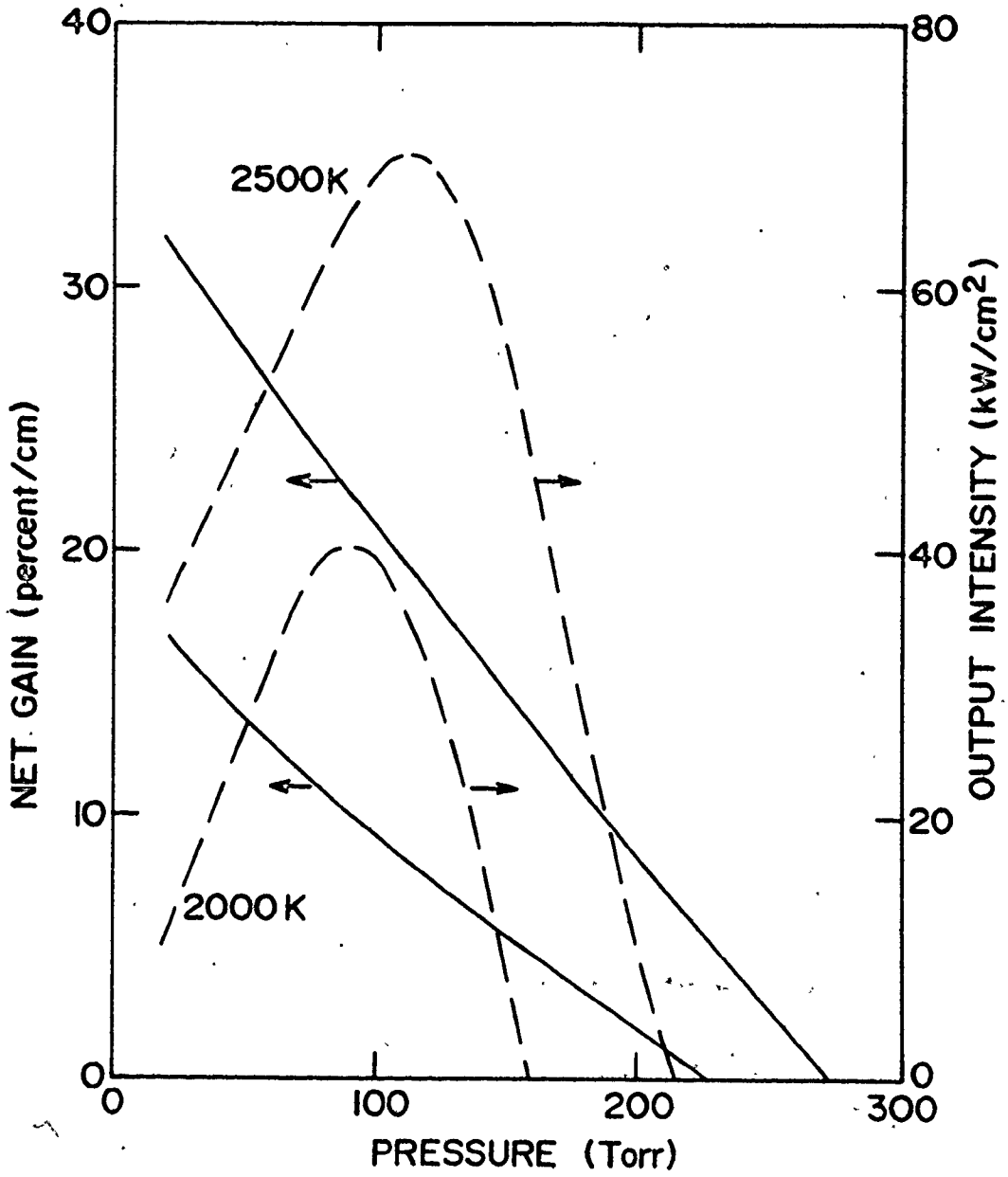
40
30
20
10
0
80
60
40
20
0
0
100
200
300
2500K
2000K
NET GAIN (percent/cm)
OUTPUT INTENSITY (kW/cm²)
PRESSURE (Torr)

there is also a decrease in the gain lifetime (i.e. the lifetime of the $10^0 1$ level). This is significant because a finite time is required for the 4.3-μm radiation to build up inside the cavity, once threshold has been reached. Typically, this time is a few tens of ns, which, for a 100 Torr, 5% CO_2 gas mixture, is similar to the $10^0 1$ level lifetime ($\sim$ 50 ns). Therefore, 4.3-μm output intensity increases nearly linearly with pressure (see Fig. 7.4) until decreasing gain and decreasing gain lifetime become significant. Further increases in pressure result in a reduction in output power and eventual cessation of lasing.

It should be noted that the reduction in the $10^0 1$ lifetime also results in a decrease in output pulse duration. Therefore, maximum output energy per pulse will generally occur at lower pressures than maximum output power. For example, for the 2500 K case in Fig. 7.4, maximum power ($\sim$ 70 kW/cm^2) occurs at $\sim$110 Torr, whereas maximum energy per pulse ($\sim$3 mJ/cm^2) is achieved at a total pressure of $\sim$ 40 Torr. This factor should be taken into account if the laser system is being designed for high output energies rather than for high output powers.

Several conclusions concerning the design of high power 4.3-μm lasers can be drawn from the above discussion. They are as follows:

i) Total gas pressure should be kept low to reduce the effect of overlapping absorptions. Maximum pressures are in the range from 100 to 200 Torr.

ii) To reduce the effect of collisional losses, the total gas pressure and CO_2 concentration should both be kept low, typically 50-150 Torr and a few percent CO_2.

iii) A high degree of excitation (i.e., a high initial value of T_3, typically $\gtrsim$ 2500 K) is desirable for 4.3-μm laser operation because a greater number of molecules are able to participate in the lasing.
iv) The relatively low values of total pressure and CO_2 concentration imply that only moderate sequence pumping powers ($\sim$ 1 MW/cm^2 as opposed to 100 MW/cm^2, see Fig. 7.3).are required to produce 4.3-μm lasing. Therefore, higher output powers can be achieved by increasing the discharge volume, while maintaining optimum discharge conditions (i.e. gas mixture, gas pressure and degree of excitation.)

The maximum 4.3-μm output power which can be obtained from a discharge will ultimately be determined by the level of sequence pumping power present. This can be seen with reference to Fig. 7.5 which is a plot of 4.3-μm output intensity as a function of sequence pumping intensity. The gas mixture is 85%He:10%N_2:5%CO_2 and the total pressure is 100 Torr. As expected, 4.3-μm output increases with increasing pumping intensity until saturation occurs. It is this saturation which determines the level of sequence pumping intensity required for efficient 4.3-μm lasing, and correspondingly, the maximum discharge volume which can be pumped using a particular level of sequence pumping power.

The maximum 4.3-μm output power or output energy expected will be determined through the optimization of the factors listed above. The results shown in Fig. 7.5 are for one such set of conditions, and can be used as an estimate of the operating capabilities of a high power 4.3-μm laser. For example, at 1 MW/cm^2 of sequence pumping power and an initial T_3 of 2500 K, the 4.3-μm output intensity would be $\sim$ 70 kW/cm^2.

Fig. 7.5

Calculated curves of 4.3-μm output intensity as a function of sequence pumping power. The gas mixture is 85%He:10%N_2:5%CO_2 at 100 Torr total pressure. The initial values of T_3 are 2000 K and 2500 K as indicated. The sequence pulse risetime is 100 ns.

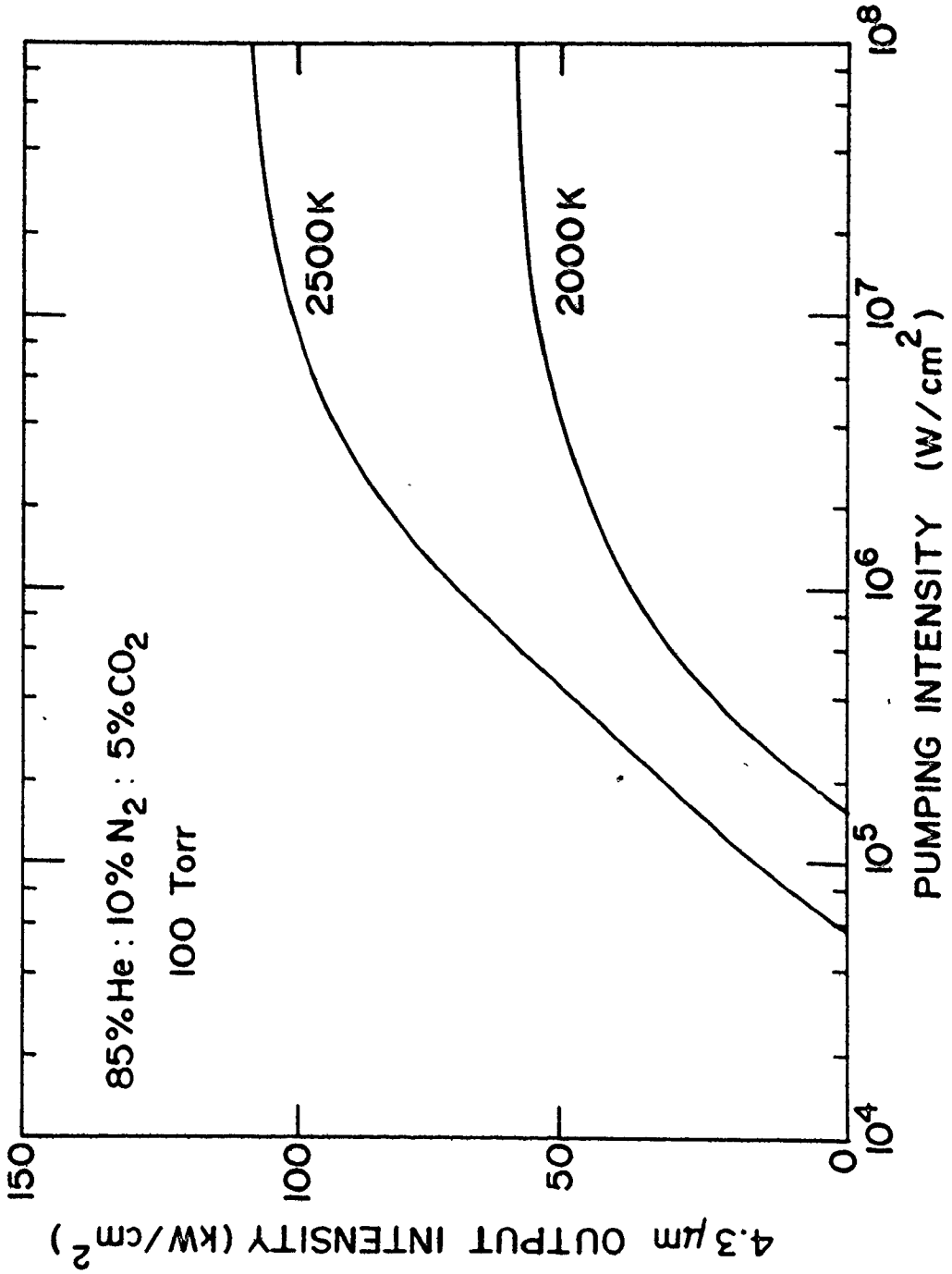
4.3 μm OUTPUT INTENSITY (kW/cm²)
150
100
50
0
10⁴
10⁵
10⁶
10⁷
10⁸
PUMPING INTENSITY (W/cm²)
2500K
2000K
85% He : 10% N₂ : 5% CO₂
100 Torr

Therefore, use of 25 MW of sequence pumping power to pump a 5 cm x 5 cm x 100 cm discharge volume leads to a predicted output power of ∿2 MW. As noted above, maximum output energy is obtained at low pressures, due to the increase in pulse duration. For instance, pumping an 85%He:10%N_2:5%CO_2 mixture at 40 Torr (T_3 = 2500 K) with 0.5 MW/cm^2 of sequence pumping intensity gives a predicted 4.3-μm output energy fluence of ∿2 mJ/cm^2 per pulse. For a 7 cm x 7 cm x 100 cm discharge, this corresponds to an output energy of ∿100 mJ per pulse.

7.5 Summary

This Chapter has dealt with the design criteria for high power 4.3-μm lasers. Two factors are found to limit the maximum pressure and CO_2 content which can be employed in such lasers. The first factor involves the gain dynamics of the system, or specifically, the large collisional losses occurring from the $10^0 1$ level when high CO_2 pressures are used. The second limiting factor is the interfering absorptions arising from overlapping absorption bands in the 4.3-μm region which become significant as the pressure is increased. Based on these considerations, guidelines for the construction of high power 4.3-μm lasers are presented. It is shown that 4.3-μm output powers of ∿2 MW (or output energies of 100 mJ per pulse) should be attainable from large volume, low pressure discharges, using existing TEA sequence lasers as the pump source.

CHAPTER 8

CONCLUSIONS

The work described in this thesis was aimed at developing a basic understanding of the physics of 4.3-μm CO_2 lasers. This Chapter summarizes the results of these investigations. First, a general review of the contents of the thesis is given, followed by a summary of the results of each specific chapter. Lastly, a brief discussion of the applications of 4.3-μm CO_2 lasers is presented.

The order in which the various topics appear in this thesis is essentially chronological. The preliminary experiments reported in Chapter 3 and Ref. [77] correspond to the first use of sequence CO_2 lasers to produce 4.3-μm lasing in CO_2. A low-power helical pin sequence laser was used in conjunction with a standard two-cavity configuration common to many optical pumping experiments. The results demonstrated that sequence lasers were an effective means of producing 4.3-μm lasing and methods were sought by which the laser output could be increased. This led to the development of the intra-cavity configuration described in Sect. 3.4. It became apparent that certain features of the 4.3-μm output, such as the relatively short duration of the pulses, were common to a wide range of experimental conditions. A theoretical model of the laser was then developed in order to investigate better the gain dynamics of the laser. Preliminary comparisons between the model predictions and the experimental results indicated that the model could account for observed 4.3-μm output

characteristics such as pulse duration and peak power. The results of Chapters 3 and 4 identified the basic mechanisms involved in the 4.3-μm lasing process and suggested two possible ways to proceed: i) use of a low pressure continuous discharge and a Q-switched sequence laser to produce high average power at 4.3 μm and, ii) higher pressure, pulsed discharges pumped with a high power sequence laser to produce high peak power at 4.3 μm. The Q-switched 4.3-μm laser was investigated first and the results are presented in Chapter 5. Using the intra-cavity configuration and a passively Q-switched sequence laser, moderately high levels of 4.3-μm average output power were obtained. Operation of the laser in the Q-switched mode was found to be very consistent with the expected gain dynamics. Attention was next given to the scaling of pulsed 4.3-μm lasers to higher output powers. It quickly became apparent that high levels of sequence pumping power would be required to achieve this and therefore, investigations were undertaken to develop a high power sequence laser. The design criteria for efficient, high power TEA sequence lasers are presented in Chapter 6. The scalability of 4.3-μm lasers to higher operating pressures is discussed in Chapter 7 and guidelines for the construction of a high power 4.3-μm laser are given in Sect. 7.4.

The main conclusions of each chapter are summarized below. Chapter 3 describes the basis of the work described in this thesis i.e., the use of sequence lasers to produce 4.3-μm lasing in CO_2. Use of a 30-Torr, 1.5% CO_2 mixture, and a relatively low level of sequence pumping power ($\sim$50 kW/cm^2), led to 4.3-μm output intensities of $\sim$ 1 kW/cm^2 and 4.3-μm small-signal gains of $\sim$3%/cm. The laser was

shown to be line-tunable by using a grating in the optical cavity (while pumping with a single sequence line). In addition, oscillation on the $(02^{0}1\text{-}02^{0}0)$ 4.3-μm band was observed when a 9.4-μm sequence laser was used as the pump source. It was next decided to make use of a unique feature of the present optical pumping scheme, which is that the pump laser experiences gain rather than absorption. Consequently, a means was sought whereby the pump sequence laser could be included in the same optical cavity as the 4.3-μm laser. The result is the intra-cavity arrangement described in Sect. 3.4, which led to a considerable improvement in 4.3-μm output characteristics.

The preliminary calculations described in Chapter 3 indicated that efficient optical pumping was occurring. However, certain features of laser operation could not be completely explained. In particular, observed 4.3-μm pulse durations were always considerably shorter than those of the sequence pump pulses, and 4.3-μm lasing was restricted to relatively low CO_2 content. Therefore, a rate-equation model of the laser was developed in order to gain a better understanding of the lasing process. This model is described in Chapter 4. The good agreement between theory and experiment supports the validity of the model and the model was then used to study the temporal dependence of the level populations during the optical pumping and subsequent 4.3-μm lasing. It was determined that the rapid collisional de-excitation of the $10^{0}1$ level governs the gain dynamics and restricts operation to low CO_2 content. The short pulse durations can be accounted for by considering the short $10^{0}1$ lifetime relative to the longer $10^{0}0$ lifetime. Hence, in order to get additional 4.3-μm

output, the pump laser must be shut off, the $10^{0}0$ level population allowed to decay, and then another pump pulse introduced. This led to the development of the Q-switched 4.3-μm laser reported in Chapter 5 and Ref. [78]. The other possible means of increasing the 4.3-μm output, discussed in Chapter 7, is to increase the CO_2 content and the sequence pumping power and extract as much 4.3-μm output energy as possible before the $10^{0}1$ level can empty by collisions.

Chapter 5 deals with Q-switched operation of the 4.3-μm laser. By Q-switching the sequence pump laser at relatively high repetition rates (> 1 kHz) a corresponding train of 4.3-μm pulses was produced, resulting in moderately high average output powers (120 mW). With improved cavity design, average output powers in excess of 1 W appear feasible. The other major development described in Chapter 5 is the construction of a 4.3-μm laser employing only a single discharge tube. This is significant because the only essential difference between this type of laser and a regular CO_2 laser is the inclusion of a hot cell inside the optical cavity. One application of the Q-switched 4.3-μm laser was presented in Chapter 5, that is the use of the laser to investigate a pulsed CO_2 laser discharge. The 4.3-μm laser was used to measure the V-T relaxation time and it was demonstrated that the $10^{0}0$ level was empty at the peak of the regular (or sequence) gain. Although this fact has been previously discussed in the literature [17], this is the first experimental verification.

Chapter 6 concerns the development of a high power TEA sequence laser. The results showed that the hot cell technique is an efficient means of producing TEA sequence lasing, contrary to the conclusions of

Ref. [18]. However, proper cavity design is essential and the importance of factors such as hot cell loss and degree of excitation in the discharge were discussed. Sequence output energies in excess of 6 J were observed from a commercial one meter discharge module as reported in Ref. [68].

The means by which, and the extent to which, 4.3-μm lasers can be scaled to higher pressures and higher output powers were discussed in Chapter 7. Two important factors were identified. The large collisional losses from the $10^0 1$ level restrict operation to relatively low CO_2 content (since the rate is CO_2 dependent [13]). Similarly, the presence of increased absorption from overlapping absorption bands further limits the operating pressures. The combination of these factors suggests that the optimum conditions for high power 4.3-μm lasing are low CO_2 content (~5%), relatively low pressures (100-200 Torr), large discharge volumes (5 cm x 5 cm x 100 cm) and a high degree of excitation in the discharge ($T_3 \gtrsim 2500$ K). Under these conditions 4.3-μm output energies in excess of 100 mJ per pulse should be attainable. Work is currently proceeding in our laboratory to construct such a laser.

The emphasis of this thesis was on the development of a 4.3-μm CO_2 laser. It is pertinent at this point to outline several possible applications of such a laser. The first area of application is that of monitoring the concentration of CO_2 and its isotopes. There is recent interest in determining C^{13}/C^{12} isotopic ratios as part of a new technique for diagnosing various types of liver disease [79].

Present techniques for measuring such ratios are either very expensive (e.g., mass spectrometers) or of poor reliability (e.g., tunable diode lasers). The use of a sealed-off discharge tube containing the $C^{13}O_2$ molecule would serve as a convenient source of radiation resonant with these molecules and thereby provide a method of measuring their concentration.

Another application is that of atmospheric monitoring. Due to the strong absorption arising from pressure broadened CO_2 absorption lines, atmospheric monitoring with 4.3-μm CO_2 lasers would be restricted to relatively short distances (< 1 km) [80]. However, the absence of any absorption lines in the 4.3-μm region from other atmospheric constituents may lead to applications involving the monitoring of CO_2 itself, or of its isotopic forms. Another interesting possibility is the development of a 4.5-μm N_2O laser employing a sequence N_2O laser [81] and a pumping scheme similar to the one reported here. There is much less atmospheric attenuation in the 4.5-μm region, and consequently, the potential exists for laser monitoring over greater distances.

High power 4.3-μm lasers would find use in many areas of application currently involving high power mid-IR lasers. These include laser isotope separation, laser photochemistry and optical pumping. There is one particularly interesting application in the area of optical pumping. This involves pumping high pressure (~30 atm) CO_2 so as to invert the $(00^01\text{-}10^00)$ and $(00^01\text{-}02^00)$ transitions and thereby produce tunable lasing in the 9-11-μm region. Such a scheme has been demonstrated by Chang and Wood [52,82] using an HBr laser. However, one principal limitation in their experiments was the low output power

of the HBr laser in the 4.3-μm region (∿100 kW). A high power 4.3-μm laser would greatly help to overcome this difficulty.

Lastly, there is the use of 4.3-μm CO_2 lasers in the investigation of CO_2 laser dynamics. It was shown in Sect. 4.4 that a study of 4.3-μm output itself could result in measurements of vibrational relaxation rates, in particular, that of the $10^0 1$ level. Alternatively, following the work reported in Sect. 5.5, 4.3-μm lasers could be used to probe a 10.6-μm CO_2 laser since they share a common lower level. The determination of the $10^0 0$ relaxation rate is one interesting possibility.

In conclusion, this thesis has described a new type of CO_2 laser operating in the 4.3-μm region. The physical processes responsible for laser action were discussed and different operating regimes were described. The 4.3-μm laser is shown to possess good output characteristics and is scalable using existing CO_2 laser technology. It is hoped that the results described here will be of value in the future development of this laser and its applications, and provide a better understanding of CO_2 laser dynamics in general.

APPENDIX A

CALCULATION OF CO_2 LASER GAIN

In a gas, the gain coefficient between a lower level, ℓ, and an upper level, u, can be written as [83]

$$\alpha(\nu) = \frac{\lambda_o^2}{8\pi} A_{u\ell} \left[N_u - \frac{g_u}{g_\ell} N_\ell\right] g(\nu) \qquad (A.1)$$

where λ_o is the wavelength at line center, $A_{u\ell}$ is the spontaneous transition probability, N_u and N_ℓ are the population densities of the upper and lower levels (having statistical weights g_u and g_ℓ), respectively, and $g(\nu)$ is the normalized lineshape function evaluated at the frequency ν.

The spontaneous transition probability is given by [83]

$$A_{u\ell} = \frac{64\pi^4}{3h\lambda_o^3} \frac{|R_{\ell u}|^2 S_J F_J}{g_u} \qquad (A.2)$$

where $|R_{\ell u}|^2$ is the vibrational contribution to the transition moment, S_J is the rotational contribution, F_J is the interaction factor and h is Planck's constant. For Σ transitions, $S_J(P) = J$ and $S_J(R) = J + 1$ [84]. The interaction factor differs little from unity; it is set to this value for all transitions. The most recent value of $|R_{\ell u}|^2$ for 10.4-μm regular transitions is 1.61×10^{-39} erg-cm^3 [85]. The value for the 10.4-μm sequence transitions should be a factor of 2 greater, based on the harmonic oscillator approximation, and the experimentally measured value is 1.89 [86]. For the 4.3-μm ($10^0 1$-$10^0 0$) transition $|R_{\ell u}|^2 = 1.103 \times 10^{-37}$ erg-cm^3 [87]. Substituting the above values

into Eq. (A.2) yields the following values for the spontaneous transition probability:

$A_{u\ell}$ = 0.219 for P(20) 10.4-μm regular
= 0.413 for P(19) 10.4-μm sequence
= 208 for P(20) 4.3-μm

At line center, the normalized lineshape function can be expressed as [88]

$$g(\nu_o) = \frac{1}{\pi^{1/2}\,\Delta\nu_c}\, a e^{a^2} \operatorname{erfc} a \qquad (A.3)$$

where $a = (\ell n\ 2)^{1/2}\ \Delta\nu_c/\Delta\nu_D$, $\Delta\nu_c$ is the pressure broadened half-width and $\Delta\nu_D$ is the Doppler broadened half-width. The Doppler broadened half-width is given by

$$\Delta\nu_D = \frac{\nu_o}{c}\left(2\,\frac{kT}{m}\,\ell n 2\right)^{1/2}$$

where T is the translational temperature, m is the mass of the CO_2 molecule and the constants have their standard meaning. At 350 K, $\Delta\nu_D$ is equal to 29 MHz for 10.4-μm transitions and 70 MHz for 4.3-μm transitions. The pressure broadened half-width has been measured by several researchers, and can be expressed as [83]

$$\Delta\nu_c(\text{Hz}) = 11.40 \times 10^6\ (7.52\text{-}0.059\ J)\ P_T\ (\text{Torr})$$
$$\times\ (\psi_{CO_2} + 0.64\psi_{He} + 0.73\psi_{N_2})\ T^{-1/2}$$

where ψ_i is the fractional content of gas i in the mixture and P_T is the total pressure. In the pressure broadened regime (i.e.,

$\Delta\nu_c >> \Delta\nu_\Delta$), $g(\nu_o)$ can be reduced to

$$g(\nu_o) = \frac{1}{\pi\ \Delta\nu_c} \tag{A.4}$$

Using the above results, and the expressions for level populations (see Sects. 2.3 and 2.5), the gain coefficient can be calculated via Eq. (A.1).

APPENDIX B

REGULAR CO_2 LASER MODEL

The model describing operation on the regular CO_2 laser bands is similar to the one described in Sect. 6.2 for sequence operation, except that the equations are adjusted to account for the different levels involved.

The seven differential equations governing regular operation of a TEA CO_2 laser are as follows:

$$\frac{dN_{001}}{dt} = -fgc\delta\rho - \frac{N_{001}}{\tau_3} - \frac{N_{001} - N^e_{001}(T_3)}{\tau_{v_3}} \tag{B.1}$$

$$\frac{dN_{100}}{dt} = fgc\delta\rho - \frac{N_{100} - N^e_{100}(T_1)}{\tau_{100}} \tag{B.2}$$

$$\frac{dE_{BS}}{dt} = \frac{E_{001}}{\tau_3} + \frac{E_{100} - E^e_{100}(T_1)}{\tau_{100}} - \frac{E_{BS} - E^e_{BS}(T)}{\tau_{VT}} \tag{B.3}$$

$$\frac{dE_3}{dt} = \frac{E_{001} - E^e_{001}(T_3)}{\tau_{v_3}} + \frac{E_4 - E^e_4(T_3)}{\tau_{N_2}} \tag{B.4}$$

$$\frac{dE_4}{dt} = -\frac{E_4 - E^e_4(T_3)}{\tau_{N_2}} \tag{B.5}$$

$$\frac{d\delta}{dt} = -2fgc\delta\rho - \frac{\delta - K(J)(N_{001} - N_{100})}{\tau_R} \tag{B.6}$$

$$\frac{d\rho}{dt} = fgc\delta\rho - ac\rho - \frac{\rho}{\tau_c} + \gamma K(J)\, N_{001} \tag{B.7}$$

The variables and constants are analogous to those described in Sect. 6.2 for sequence operation, e.g., E_3 is the energy stored in the ν_3 mode, excluding the $00^{\circ}1$ level.

REFERENCES

1. C.K.N. Patel, W.L. Faust, and R.A. McFarlane, Bull. Am. Phys. Soc. 9, 500 (1964), and Phys. Rev. Lett. 12, 588 (1964).
2. C.K.N. Patel, Phys. Rev. 136A, 1187 (1964).
3. "Laser Photochemistry and Diagnostics", Report on a National Science Foundation/Department of Energy Seminar, June 4-5, 1979.
4. C.R. Jones, Laser Focus, August (1978), pg. 68.
5. D.T. Hodges, Infrared Phys. 18, 375 (1978).
6. D.C. Hanna, M.A. Yuratich, and D. Cotter, Nonlinear Optics of Free Atoms and Molecules (Springer-Verlag, New York, 1979), Chapter 7.
7. J. Reid and K.J. Siemsen, Appl. Phys. Lett. 29, 250 (1976).
8. J. Reid and K.J. Siemsen, J. Appl. Phys. 48, 2712 (1977).
9. K.J. Siemsen and B.G. Whitford, Opt. Commun. 22, 11 (1977).
10. A.B. Petersen, C. Wittig and S.R. Leone, J. Appl. Phys. 47, 1051 (1976).
11. A.B. Petersen and C. Wittig, J. Appl. Phys. 48, 3665 (1977).
12. M.I. Buchwald, C.R. Jones, H.R. Fetterman and H.R. Schlossberg, Appl. Phys. Lett. 29, 300 (1976).
13. J. Finzi and C.B. Moore, J. Chem. Phys. 63, 2285 (1975).
14. L.O. Hocker, M.A. Kovacs, C.K. Rhodes, G.W. Flynn, and A. Javan, Phys. Rev. Lett. 17, 233 (1966).
15. K.R. Manes and H.J. Seguin, J. Appl. Phys. 43, 5073 (1972).
16. K. Smith and R.M. Thomson, Computer Modeling of Gas Lasers (Plenum Press, New York, 1978).

17. B.K. Garside, J. Reid and E.A. Ballik, IEEE J. Quantum Electron. QE-11, 583 (1975).

18. P. Lavigne, J.-L. Lachambre and G. Otis, Opt. Lett. 2, 127 (1978).

19. B.J. Feldman, R.A. Fisher, C.R. Pollock, S.W. Simons, and R.G. Tercovich, Opt. Lett. 2, 16 (1978).

20. I.M. Bertel, B.F. Kuntsevich, V.O. Petukhov, B.I. Stepanov, S.A. Trushin, and V.V. Churakov, Sov. Tech. Phys. Lett. 4, 532 (1978).

21. E. Fermi, Z. Phys. 71, 250 (1931).

22. P.K. Cheo, "CO_2 Lasers" in Lasers, Vol. 3, edited by A.K. Levine and A.J. DeMaria (Marcel Dekker, New York, 1971).

23. G. Herzberg, Infrared and Raman Spectra of Polyatomic Molecules, (Van Nostrand Reinhold, New York, 1945).

24. B. Hartmann and B. Kleman, Can. J. Phys. 44, 1609 (1966).

25. J.A. Howe and R.A. McFarlane, J. Mol. Spectrosc. 19, 224 (1966).

26. C.K.N. Patel, Phys. Rev. Lett. 13, 617 (1964).

27. W.L. Nighan, Phys. Rev. A 2, 1989 (1970).

28. J.J. Lowke, A.V. Phelps, and B.W. Irwin, J. Appl. Phys. 44, 4664 (1973).

29. L.J. Denes and J.J. Lowke, Appl. Phys. Lett. 23, 130 (1973).

30. O.P. Judd, J. Appl. Phys. 45, 4572 (1974).

31. C.B. Moore, R.E. Wood, B. Hu and J.T. Yardley, J. Chem. Phys. 46, 4222 (1967).

32. G.J. Schulz, Phys. Rev. 125A, 229 (1962).

33. G.J. Schulz, Phys. Rev. 135A, 988 (1964).

34. H. Statz, C.L. Tang and G.F. Koster, J. Appl. Phys. 37, 4278 (1966).

35. I. Burak, Y. Noter and A. Szöke, IEEE J. Quantum Electron. QE-9, 541 (1973).

36. R.T. Pack, J. Chem. Phys. 72, 6140 (1980).

37. K. Bulthuis, J. Chem. Phys. 58, 5786 (1973).

38. W.A. Rosser, E. Hoag, and E.T. Gerry, J. Chem. Phys. 57, 4153 (1972).

39. C.K. Rhodes, M.J. Kelly, and A. Javan, J. Chem. Phys. 48, 5730 (1968).

40. T.A. DeTemple, D.R. Suhre, and P.D. Coleman, Appl. Phys. Lett. 22, 349 (1973).

41. E.E. Stark, Jr., Appl. Phys. Lett. 23, 335 (1973).

42. R.R. Jacobs, K.J. Pettipiece, and S.J. Thomas, Phys. Rev. A 11, 54 (1975).

43. K.N. Seeber, J. Chem. Phys. 55, 5077 (1971).

44. R.D. Sharma, J. Chem. Phys. 49, 5195 (1968).

45. R.L. Taylor and S. Bitterman, Rev. Mod. Phys. 41, 26 (1969).

46. D.C. Allen, T. Scragg, and C.J.S.M. Simpson, Chem. Phys. 51, 279 (1980).

47. R.L. Abrams and P.K. Cheo, Appl. Phys. Lett. 15, 177 (1969).

48. E.A. Ballik, B.K. Garside, and J. Reid, Appl. Phys. Lett. 26, 380 (1975).

49. B.F. Gordietz, N.N. Sobolev, V.V. Sokovikov, and L.A. Shelepin, IEEE J. Quantum Electron. QE-4, 796 (1968).

50. C. Dang, J. Reid, and B.K. Garside, submitted for publication, Appl. Phys.

51. J. Reid, Ph.D. thesis, McMaster University, 1974.

52. T.Y. Chang and O.R. Wood, Appl. Phys. Lett. 23, 370 (1973).

53. K.J. Siemsen, J. Reid, and C. Dang, IEEE J. Quantum Electron. QE-16, 668 (1980).

54. R. Fortin, M. Gravel and R. Tremblay, Can. J. Phys. 49, 1783 (1971).

55. W. Berger, K. Siemsen, and J. Reid, Rev. Sci. Instrum. 48, 1031 (1977).

56. C. Dang, J. Reid, and B.K. Garside, IEEE J. Quantum Electron. QE-16, 1097 (1980).

57. L.S. Rothman and W.S. Benedict, Appl. Opt. 17, 2605 (1978).

58. A. Gondhalekar, E. Holzhauer and N.R. Heckenberg, Phys. Lett. 46A, 229 (1973).

59. R.W. Hamming, Numerical Methods for Scientists and Engineers, 2nd ed. (McGraw-Hill, 1973).

60. H. Kogelnik and T. Li, Proc. IEEE 54, 1312 (1966).

61. O.R. Wood and S.E. Schwarz, Appl. Phys. Lett. 11, 88 (1967).

62. I. Burak, P.L. Houston, D.G. Sutton, and J.I. Steinfeld, IEEE J. Quantum Electron. QE-7, 73 (1971).

63. U.P. Oppenheim and Y.J. Kaufman, IEEE J. Quantum Electron. QE-10, 533 (1974).

64. T.A. Znotins, M.Sc. thesis, McMaster University, 1978.

65. K.J. Siemsen, Appl. Opt. 19, 818 (1980).

66. R.R. Jacobs, Rev. Sci. Instrum. 44, 1146 (1973).

67. C.O. Weiss, M. Grinda and K. Siemsen, IEEE J. Quantum Electron. QE-13, 892 (1977).

68. R.K. Brimacombe, J. Reid and T.A. Znotins, to be published, Appl. Phys. Lett., August 15, 1981.

69. R.A. McClatchey, W.S. Benedict, S.A. Clough, D.E. Burch, R.F. Calfee, K. Fox, L.S. Rothman and J.S. Garing, "AFCRL Atmospheric Absorption Line Parameters Compilation", AFCRL Report 73-0096 (1973).

70. T. Stamatakis and J.M. Green, Opt. Commun. 30, 413 (1979).

71. J. Reid and K.J. Siemsen, IEEE J. Quantum Electron. QE-14, 217 (1978).

72. P. Lavigne, J.-L. Lachambre and G. Otis, J. Appl. Phys. 49, 3714 (1978).

73. Lumonics Inc., private communication.

74. T.A. Znotins, J. Reid, B.K. Garside, and E.A. Ballik, Opt. Lett. 5, 528 (1980).

75. P.L. Kelley, R.A. McClatchey, R.K. Long and A. Snelson, Opt. and Quantum Electron. 8, 117 (1976).

76. T.R. Lawrence, M.J. Post, R.M. Hardesty, R.J. Keeler, R.A. Richter, R.M. Huffaker and F.F. Hall, Conference on Lasers and Electro-Optics, Washington, D.C., June 1981, paper WD3.

77. T.A. Znotins, J. Reid, B.K. Garside, and E.A. Ballik, Opt. Lett. 4, 253 (1979).

78. T.A. Znotins, J. Reid, B.K. Garside and E.A. Ballik, Appl. Phys. Lett. 39, 199 (1981).

79. Laser Focus, May (1981), pg. 28.

80. R.A. McClatchey, J.E. Selby, "AFCRL Atmospheric Attenuation of Laser Radiation from 0.76 to 31.25 μm", AFCRL Report 74-0003 (1974).

81. K. Siemsen and J. Reid, Opt. Commun. 20, 284 (1977).

82. T.Y. Chang and O.R. Wood, II, IEEE J. Quantum Electron. QE-13, 907 (1977).

83. A.M. Robinson and N. Sutton, Appl. Opt. 18, 378 (1979).

84. G. Herzberg, Spectra of Diatomic Molecules, (Van Nostrand Reinhold, New York, 1950).

85. E. Arié, N. Lacome, and C. Rossetti, Can. J. Phys. 50, 1800 (1972).

86. J. Reid, J. Shewchun, and B.K. Garside, Appl. Phys. 17, 349 (1978).

87. B. Fridovich, W.C. Braun, G.R. Smith and E.E. Champion, J. Mol. Spectrosc. 81, 248 (1980).

88. A.M. Robinson, "Computed Absorption Coefficient for CO_2 Laser Transitions", DREV Report TN-1989/71 (1971).